AD-A040 021 CALIFORNIA UNIV BERKELEY HYDRAULIC ENGINEERING LAB F/G 8/3
LABORATORY INVESTIGATION OF TIDAL INLETS ON SANDY COASTS.(U)
APR 77 R E MAYOR-MORA DACW72-71-C-0005
UNCLASSIFIED WES-GITI-11 NL

1 OF 2
AD A040021

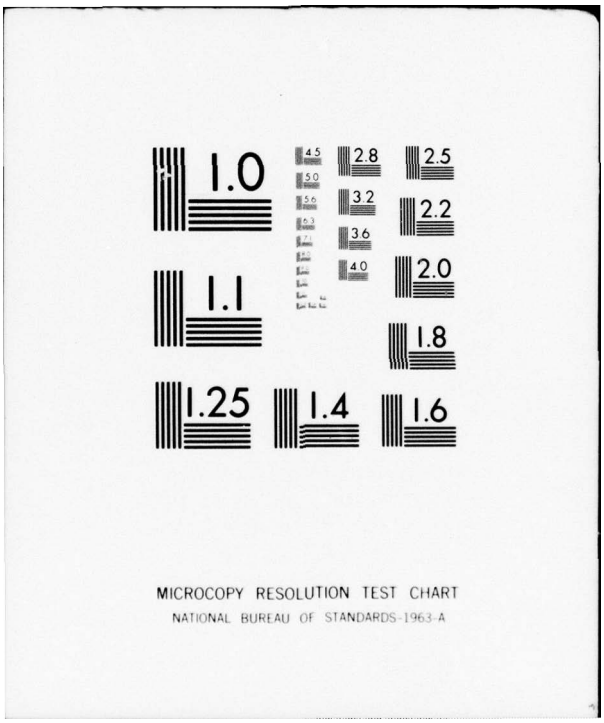
1.0
1.1
1.25
1.4
1.6
1.8
2.0
2.2
2.5
2.8
3.2
3.6
4.0
4.5
5.0
5.6
6.3
MICROCOPY RESOLUTION TEST CHART
NATIONAL BUREAU OF STANDARDS-1963-A

Laboratory Investigation of Tidal Inlets on Sandy Coasts

by

Ramiro E. Mayor-Mora

GITI REPORT 11

April 1977

Prepared for
U.S. Army Coastal Engineering Research Center
under
Contract DACW72-71-C-0005
by
University of California
Hydraulic Engineering Laboratory
Berkeley, California 94720

GENERAL INVESTIGATION OF TIDAL INLETS

A Program of Research Conducted Jointly by
U.S. Army Coastal Engineering Research Center, Fort Belvoir, Virginia
U.S. Army Engineer Waterways Experiment Station, Vicksburg, Mississippi

Department of the Army
Corps of Engineers

Reprint or republication of any of this material shall give appropriate credit to the U.S. Army Coastal Engineering Research Center.

Limited free distribution within the United States of single copies of this publication has been made by this Center. Additional copies are available from:

National Technical Information Service
ATTN: Operations Division
5285 Port Royal Road
Springfield, Virginia 22151

Contents of this report are not to be used for advertising, publication, or promotional purposes. Citation of trade names does not constitute an official endorsement or approval of the use of such commercial products.

The findings in this report are not to be construed as an official Department of the Army position unless so designated by other authorized documents.

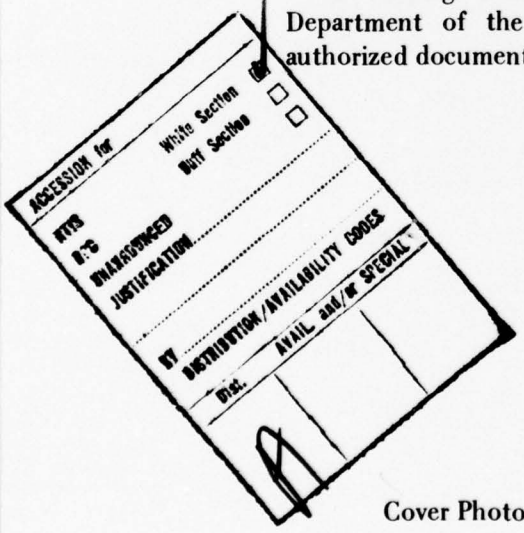

Cover Photo: Drum Inlet, North Carolina, March 1962
Courtesy of the U.S. Geological Survey

UNCLASSIFIED
SECURITY CLASSIFICATION OF THIS PAGE (When Data Entered)

REPORT DOCUMENTATION PAGE	READ INSTRUCTIONS BEFORE COMPLETING FORM
1. REPORT NUMBER: GITI ~~Report~~ 11	2. GOVT ACCESSION NO.
3. RECIPIENT'S CATALOG NUMBER	
4. TITLE (and Subtitle): LABORATORY INVESTIGATION OF TIDAL INLETS ON SANDY COASTS,	5. TYPE OF REPORT & PERIOD COVERED: Final Report.
6. PERFORMING ORG. REPORT NUMBER	
7. AUTHOR(s): Ramiro E. Mayor-Mora	8. CONTRACT OR GRANT NUMBER(s): DACW72-71-C-0005
9. PERFORMING ORGANIZATION NAME AND ADDRESS: University of California, College of Engineering, Hydraulic Engineering Laboratory, Berkeley, California 94720	10. PROGRAM ELEMENT, PROJECT, TASK AREA & WORK UNIT NUMBERS: F31019
11. CONTROLLING OFFICE NAME AND ADDRESS: Department of Army, Coastal Engineering Research Center, Kingman Building, Fort Belvoir, Virginia 22060	12. REPORT DATE: April 1977
	13. NUMBER OF PAGES: 106
14. MONITORING AGENCY NAME & ADDRESS (if different from Controlling Office)	15. SECURITY CLASS. (of this report): Unclassified
	15a. DECLASSIFICATION/DOWNGRADING SCHEDULE

16. DISTRIBUTION STATEMENT (of this Report)
Approved for public release; distribution unlimited.

17. DISTRIBUTION STATEMENT (of the abstract entered in Block 20, if different from Report)

18. SUPPLEMENTARY NOTES

19. KEY WORDS (Continue on reverse side if necessary and identify by block number)
Tidal inlets
Lumped parameter approach
Hydraulic models
Sandy shores
Model basins

20. ABSTRACT (Continue on reverse side if necessary and identify by block number)
Experiments were conducted on a fine sand barrier separating two 1-foot-deep basins representing an ocean and a 94- by 64-foot bay. Pilot channels with varying geometric characteristics were cut through the barrier to communicate the basins and thus create an ocean-inlet-bay system subsequently subjected to ocean tide and wave action. Measurements were made of cross-sectional areas, water surface elevations at ocean, bay, and inlet, and inlet current velocities for a number of cycles (sinusoidal tides) until
(continued)

DD FORM 1 JAN 73 1473 EDITION OF 1 NOV 65 IS OBSOLETE

UNCLASSIFIED
SECURITY CLASSIFICATION OF THIS PAGE (When Data Entered)

(cont fr p1473A)

the water surface fluctuations in the bay became periodic for each run. Exploratory studies included runs with jettied inlets, a run with "fresh-water" inflow into the bay, inlets under mild and steep ocean waves, and runs to determine the effect of model bed ripple orientation on the friction coefficient of the inlet channel. Experimental data are presented in tabular and photographic form, and as plots correlating the various dimensionless hydraulic parameters (e.g., tidal range damping coefficient, bay superelevation, mean current velocity timelag between maxima and minima, duration of ebbtide) to the repletion coefficient, K, and to a proposed parameter, $K\sqrt{F}$. These results are then compared to the basic theoretical solution of the problem by Keulegan (1967) and to an extension of the Keulegan theory (the lumped parameter approach), developed by Huval and Wintergerst (in preparation, 1977). Comparison of tidal prisms and minimum flow areas are made between the laboratory results and available field data. An appendix includes plots summarizing the inlet channel's geometrical properties for the experiments.

K (square root F).

FOREWORD

This report is based on a series of experiments conducted at the Hydraulic Engineering Laboratory (HEL), College of Engineering, University of California, Berkeley, in 1972-73. The research was supported by the U.S. Army Coastal Engineering Research Center (CERC) under contract DACW72-71-C-0005 as part of the General Investigation of Tidal Inlets (GITI) program. The GITI research program is under the technical surveillance of CERC, and is conducted by CERC, the U.S. Army Waterways Experiment Station (WES), other Government agencies, and by private organizations.

The report was prepared by Ramiro E. Mayor-Mora, who conducted the experiments, under the supervision of Professor J.W. Johnson and assistance of Dean M.P. O'Brien, and the late Professor H.A. Einstein. W.N. Seelig of CERC provided technical review for the report. Members of the HEL contributing to the laboratory work were J. Allison, W. Hewitt, W. Matthew, E. Parscale, and E. Caine; G. Chalon, J. Moore, and W. Bishop helped in the data reduction. The Quebec Ministry of Education and SNC, Inc. (consultants) of Montreal, Canada, supported the author during the investigation.

CERC contract technical monitor was C. Mason, under the general supervision of Dr. R.M. Sorensen, Chief, Coastal Structures Branch, Research Division.

Technical Directors of CERC and WES were T. Saville, Jr., and F.R. Brown, respectively.

Comments on this publication are invited.

Approved for publication in accordance with Public Law 166, 70th Congress, approved 31 July 1945, as supplemented by Public Law 172, 88th Congress, approved 7 November 1963:

JOHN L. CANNON
Colonel, Corps of Engineers
Commander and Director
Waterways Experiment Station

JOHN H. COUSINS
Colonel, Corps of Engineers
Commander and Director
Coastal Engineering Research Center

PREFACE

1. The Corps of Engineers, through its Civil Works program, has sponsored, over the past 23 years, research into the behavior and characteristics of tidal inlets. The Corps' interest in tidal inlet research stems from its responsibilities for navigation, beach erosion prevention and control, and flood control. Tasked with the creation and maintenance of navigable U.S. waterways, the Corps routinely dredges millions of cubic yards of material each year from tidal inlets that connect the ocean with bays, estuaries, and lagoons. Design and construction of navigation improvements to existing tidal inlets are an important part of the work of many Corps' offices. In some cases, design and construction of new inlets are required. Development of information concerning the hydraulic characteristics of inlets is important not only for navigation and inlet stability, but also because inlets, by allowing for the ingress of storm surges and egress of flood waters, play an important role in the flushing of bays and lagoons.

2. A research program, General Investigation of Tidal Inlets (GITI), was developed to provide quantitative data for use in design of inlets and inlet improvements. It is designed to meet the following objectives:

> To determine the effects of wave action, tidal flow, and related phenomena on inlet stability and on the hydraulic, geometric, and sedimentary characteristics of tidal inlets; to develop the knowledge necessary to design effective navigation improvements, new inlets, and sand transfer systems at existing tidal inlets; to evaluate the water transfer and flushing capability of tidal inlets; and to define the processes controlling inlet stability.

3. The GITI is divided into three major study areas: (a) inlet classification, (b) inlet hydraulics, and (c) inlet dynamics.

a. Inlet Classification. The objectives of the inlet classification study are to classify inlets according to their geometry, hydraulics, and stability, and to determine the relationships that exist among the geometric and dynamic characteristics and the environmental factors that control these characteristics. The classification study keeps the general investigation closely related to real inlets and produces an important inlet data base useful in documenting the characteristics of inlets.

b. Inlet Hydraulics. The objectives of the inlet hydraulics study are to define the tide-generated flow regime and water level fluctuations in the vicinity of coastal inlets and to develop techniques for predicting these phenomena. The inlet hydraulics study is divided into three areas: (1) idealized inlet model study, (2) evaluation of state-of-the-art physical and numerical models, and (3) prototype inlet hydraulics.

(1) The Idealized Inlet Model. The objectives of this model study are to determine the effect of inlet configurations and structures on discharge, head loss and velocity distribution for a number of realistic inlet shapes and tide conditions. An initial set of tests in a trapezoidal inlet was conducted between 1967 and 1970. However, in order that subsequent inlet models are more representative of real inlets, a number of "idealized" models representing various inlet morphological classes are being developed and tested. The effects of jetties and wave action on the hydraulics are included in the study.

(2) Evaluation of State-of-the-Art Modeling Techniques. The objectives of this part of the inlet hydraulics study are to determine the usefulness and reliability of existing physical and numerical modeling techniques in predicting the hydraulic characteristics of inlet-bay systems, and to determine whether simple tests, performed rapidly and economically, are useful in the evaluation of proposed inlet improvements. Masonboro Inlet, North Carolina, was selected as the prototype inlet which would be used along with hydraulic and numerical models in the evaluation of existing techniques. In September 1969 a complete set of hydraulic and bathymetric data was collected at Masonboro Inlet. Construction of the fixed-bed physical model was initiated in 1969, and extensive tests have been performed since then. In addition, three existing numerical models were applied to predict the inlet's hydraulics. Extensive field data were collected at Masonboro Inlet in August 1974 for use in evaluating the capabilities of the physical and numerical models.

(3) Prototype Inlet Hydraulics. Field studies at a number of inlets are providing information on prototype inlet-bay tidal hydraulic relationships and the effects of friction, waves, tides, and inlet morphology on these relationships.

c. *Inlet Dynamics.* The basic objective of the inlet dynamics study is to investigate the interactions of tidal flow, inlet configuration, and wave action at tidal inlets as a guide to improvement of inlet channels and nearby shore protection works. The study is subdivided into four specific areas: (1) model materials evaluation, (2) movable-bed modeling evaluation, (3) reanalysis of a previous inlet model study, and (4) prototype inlet studies.

(1) Model Materials Evaluation. This evaluation was initiated in 1969 to provide data on the response of movable-bed model materials to waves and flow to allow selection of the optimum bed materials for inlet models.

(2) Movable-Bed Model Evaluation. The objective of this study is to evaluate the state-of-the-art of modeling techniques, in this case movable-bed inlet modeling. Since, in many cases, movable-bed modeling is the only tool available for predicting the response of an inlet to improvements, the capabilities and limitations of these models must be established.

(3) Reanalysis of an Earlier Inlet Model Study. In 1975, a report entitled, "Preliminary Report: Laboratory Study of the Effect of an Uncontrolled Inlet on the Adjacent Beaches," was published by the Beach Erosion Board (now CERC). A reanalysis of the original data is being performed to aid in planning of additional GITI efforts.

(4) Prototype Dynamics. Field and office studies of a number of inlets are providing information on the effects of physical forces and artificial improvements on inlet morphology. Of particular importance are studies to define the mechanisms of natural sand bypassing at inlets, the response of inlet navigation channels to dredging and natural forces, and the effects of inlets on adjacent beaches.

4. This study supports the goals of the General Investigation of Tidal Inlets by using a movable-bed inlet model to study inlet hydraulics for a variety of inlet configurations and for various conditions, including wave steepness with and without jetties, freshwater inflow, and bed rippling. The study also suggests parameters useful to classify inlet hydraulics and briefly discusses inlet stability by re-examining the inlet cross-sectional area versus prism relationship.

CONTENTS

		Page
	CONVERSION FACTORS, U.S. CUSTOMARY TO METRIC (SI)	11
	SYMBOLS AND DEFINITIONS	12
I	INTRODUCTION	17
II	THEORETICAL ANALYSES	18
	1. Simplified Tidal Inlet Hydraulics	18
	2. Gradually Varied Unsteady Flow in Open Channels	19
	3. Principal Theoretical Approaches to the Problem	19
III	THE EXPERIMENTAL PROGRAM	25
	1. Experimental Conditions	25
	2. Testing Facilities and Equipment	27
	3. Instrumentation, Controls, and Data Recording Units	32
	4. Testing Program and Procedures	39
IV	EXPERIMENTAL DATA	55
	1. Measurements	55
	2. Measurement Problems	57
	3. Reduction and Presentation of Data	62
V	CORRELATION OF HYDRAULIC VARIABLES	67
	1. Summary of Computations	67
	2. Computations of Parameters from Experimental Data	67
	3. Computation of Theoretical Parameters by the Lumped Parameter Approach	72
	4. Comparison of Measured and Theoretical Tides and Currents	73
	5. Dimensionless Parameters as Functions of K_e	79
	6. Effect of Ripple Orientation on Friction Coefficients	88
	7. Tidal Inlet Prism versus Area Relationships	88
VI	SUMMARY AND CONCLUSIONS	93
	LITERATURE CITED	95
	APPENDIX - MODEL GEOMETRIC DATA	97

TABLES

1	Ocean experimental variables	28
2	Inlet experimental variables	29
3	Bay experimental variables	65
4	Experimental and computed parameters for tide-only runs	66

CONTENTS

TABLES--Continued

		Page
5	Experimental and computed parameters for simultaneous wave and tide runs.	68
6	Experimental and computed parameters for special runs, and simultaneous wave and tidal action	69
7	Samples of program "DATATHE" output (lumped parameter approach).	74
8	Experimental relations between inlet prisms and areas	93

FIGURES

1	An inlet-bay system with the Keulegan (1967) assumptions. . . .	21
2	Sample tides and currents for an ocean-inlet-bay system which satisfy the Keulegan (1967) assumptions.	22
3	Variation of dimensionless parameters with Keulegan repletion coefficient, K	23
4	Sieve analysis of the sand used in the testing program.	26
5	Plan view of testing facilities showing water circulation between basins	30
6	Overall view of testing facilities.	31
7	Tide-generating mechanism; ocean basin in background.	33
8	Instrument carriage over sand barrier and platform for overhead photography.	34
9	Schematic layout of testing facilities showing relative locations of instruments, controls, and recording units.	35
10	Resistance-type water level gage (1) inside stilling well (2) .	36
11	Recording and control units	36
12	Float-type water level recorder mounted on stilling well. . . .	37
13	Instruments mounted on carriage	37
14	Propeller current velocity meter.	38
15	Reproduction of inlet cross sections on paper	38

CONTENTS

FIGURES--Continued

		Page
16	Time-lapse photos showing evolution of a long channel bed under tidal action	43
17	Time-lapse photos showing a short inlet under tidal and wave actions	46
18	Time-lapse photos showing an inlet controlled by smooth vertical jetties	49
19	Photos showing a short inlet bed after last ebbtide in a bay with "freshwater" discharge and before start of run 16C	53
20	Photos showing short and deep inlet beds "fixed" with plaster after last ebbtide and after last floodtide, under tidal action only	54
21	Samples of current velocity and ocean, inlet, and bay tide recordings by resistance gages	56
22	Sample recordings of water surface slopes at midchannel and at the throat	58
23	Sample flow cross-sectional records showing the pilot channel and sections at end of runs under tidal action and under tidal and wave actions	59
24	Photos taken after end of runs with tidal action with tidal and wave actions and a run extension	60
25	Sample records of vertical profiles along channel centerline.	61
26	Schematic representation of simultaneous water elevations in the ocean, inlet, and bay.	63
27	Diagrams identifying the main parameters of the sand barrier profiles and the flow cross'sections	64
28	Tidal elevations, mean current velocity at midchannel, and discharge as functions of time computed by the lumped parameter approach	75
29	Lumped parameter prediction of bay tide levels for run 8.	76
30	Tidal elevations, mean current velocity and midchannel, and discharge as functions of time (no waves).	77
31	Tidal elevations, mean current velocity at inlet throat, and discharge as functions of time (with waves)	78

FIGURES--Continued

		Page
32	Tidal elevations, mean current velocity at midinlet, and discharge as functions of time (no waves)	80
33	Tidal elevations, mean current velocity at inlet throat, and discharge as functions of time (with waves)	81
34	Tidal damping as a function of Keulegan's repletion coefficient for ebbtide	82
35	Tidal damping as a function of $K_e\sqrt{F}$	83
36	Dimensionless timelag between high waters as a function of K_e	84
37	Dimensionless timelag between low waters as a function of K_e	85
38	Dimensionless maximum inlet velocity as a function of K_e	86
39	Dimensionless bay superelevation as a function of K_e	87
40	Typical rippled beds after ebbtide flow for high (F) inlets	89
41	Examples of typical rippled beds after ebbtide flow for low (F) model inlets	90
42	Fixed ripple beds and estimated friction coefficients at maximum discharge	91
43	Model inlet tidal prism versus area	92

CONVERSION FACTORS, U. S. CUSTOMARY TO METRIC (SI) UNITS OF MEASUREMENT

U.S. customary units of measurement used in this report can be converted to metric (SI) units as follows:

Multiply	by	To obtain
inches	25.4	millimeters
	2.54	centimeters
square inches	6.452	square centimeters
cubic inches	16.39	cubic centimeters
feet	30.48	centimeters
	0.3048	meters
square feet	0.0929	square meters
cubic feet	0.0283	cubic meters
yards	0.9144	meters
square yards	0.836	square meters
cubic yards	0.7646	cubic meters
miles	1.6093	kilometers
square miles	259.0	hectares
acres	0.4047	hectares
foot-pounds	1.3558	newton meters
ounces	28.35	grams
pounds	453.6	grams
	0.4536	kilograms
ton, long	1.0160	metric tons
ton, short	0.9072	metric tons
degrees (angle)	0.1745	radians
Fahrenheit degrees	5/9	Celsius degrees or Kelvins[1]

[1] To obtain Celsius (C) temperature readings from Fahrenheit (F) readings, use formula: $C = (5/9)(F - 32)$. To obtain Kelvin (K) readings, use formula: $K = (5/9)(F - 32) + 273.15$.

SYMBOLS AND DEFINITIONS

A_b	bay surface area (constant for vertical walls) in square feet
A_c	inlet channel cross-sectional area at any time (generally at mean sea level, MSL) in square feet
A_{ce} A_{cf}	mean channel cross-sectional area (runs A) or cross-sectional area at throat (runs B and C) below MSL at maximum ebbtide and floodtide discharges (square feet)
A_{pilot}	pilot channel cross-sectional area below MSL (runs A) or average area of preceding run below MSL for relevant runs (runs B and C), in square feet
a_o	ocean tide amplitude, equal to one-half the ocean range
a_b	bay tide amplitude, equal to one-half the bay range
C	celerity of surface waves (feet per second)
CD	velocity coefficient at maximum discharge (dimensionless)
CD_1	discharge coefficient of maximum discharge (dimensionless)
C_f	Chezy friction coefficient; $(\text{feet})^{\frac{1}{2}}$ per second
C_g	wave group velocity (feet per second)
c	a subscript meaning channel
D	water depth (feet)
D_c	water depth below MSL near the current meter
D_H	hydraulic depth at MSL (feet)
d	diameter of sand grain (millimeters)
E	total energy in one wavelength to permit crest width (foot-pound per foot)
F	inlet energy loss coefficient (dimensionless)
f	Darcy-Weisbach friction coefficient (dimensionless)
g	acceleration of gravity (feet per second squared)
H	average wave height at ocean beach toe (feet)
HBL HIL HOL	highest bay, inlet, and ocean water levels referred to MSL (feet)

SYMBOLS AND DEFINITIONS--Continued

H_o	average wave height in deep water (feet)
H_r	average height of highest ripples along channel centerline (feet)
h_b	instantaneous water surface elevation at center of bay (feet)
h_o	instantaneous water surface elevation in ocean at toe of beach (feet)
h_{be} h_{bf}	bay elevations at maximum ebbtide and floodtide discharges (feet)
h_{ce} h_{cf}	water surface elevations at midchannel (runs A) or at channel throat (runs B and C) at maximum ebbtide and floodtide discharges (feet)
h_{oe} h_{of}	ocean elevation at maximum ebbtide and floodtide discharges (feet)
h_{ie} h_{if}	inlet water level at maximum ebbtide and floodtide discharges (feet)
K	Keulegan repletion coefficient, dimensionless (subscript e for ebbtide, f for floodtide)
k_{en}	coefficient of energy losses due to channel entrance (dimensionless)
k_{ex}	coefficient of energy losses due to channel exit (dimensionless)
L	length of channel: distance along centerline from start of ripples in ocean beach to crest of bay delta; used for estimation of friction coefficients (feet)
L_o	average wavelength in deep water (feet)
MBL	mean bay elevation above MSL over a tidal cycle (feet)
MIL	mean inlet water level at throat (runs B and C) or at midchannel (runs A) over a tidal cycle (feet)
MSL	mean ocean level over a tidal cycle. The horizontal plane at this elevation is the datum to which all vertical distances are referred. The value of MSL in Table 1 is the location of MSL below the stillwater level (feet)
n	Manning's roughness coefficient

SYMBOLS AND DEFINITIONS--Continued

p	average wetted perimeter (runs A) or wetted perimeter at throat (runs B and C) at MSL (feet)
P_o	average wave power in deep water (pound-foot per second per foot of wave crest)
Q	discharge through inlet at time t (cubic foot per second)
Q_w	"freshwater" discharge into bay (cubic foot per second)
Q_{max}	maximum discharge through inlet (cubic foot per second)
R	hydraulic radius at time t (feet)
R_b	range of tide at center of bay (feet)
R_{MSL}	hydraulic radius at MSL (feet)
R_o	range of tide at toe of ocean beach (feet)
S	slope
S_{be} S_{bf}	rate of emptying of bay at maximum ebbtide discharge and of filling of bay at maximum floodtide discharge (0.00001 foot per second)
STAT	station at which throat is located according to reference scale along model inlet; equal to zero for runs A
SWL	stillwater level common to ocean, channel, and bay at the end of each run
T	tidal period: duration of tidal cycle (seconds)
TE	approximate duration of ocean drop (seconds)
T_o	average wave period (seconds)
t	elapsed time (seconds)
V	velocity of current (feet per second)
V_{max}	measured maximum velocities at channel centerline (midchannel for runs A and at throat for runs B and C) at maximum discharge (feet per second)
V^T_{max}	computed maximum average velocity across the average cross section (runs A) or across the throat (runs B and C) (foot per second)
V'_{max}	dimensionless mean maximum velocity (equation 5) across the average channel cross section (rus A) or across the throat (runs B and C)

SYMBOLS AND DEFINITIONS--Continued

W_{MSL}	average channel width (runs A) or channel width at throat (runs B and C) at MSL (feet)
w	width of inlet channel at a given location at time t (feet)
max or *m*	subscript; maximum
min	subscript; minimum
b	subscript; bay condition
e	subscript; at maximum ebbtide flow
f	subscript; at maximum floodtide flow
T	superscript; theoretical
o	subscript; deepwater condition (ocean) or MSL condition
α	velocity distribution coefficient (dimensionless)
β	coefficient for linear variation of horizontal bay surface area (dimensionless)
γ	unit weight of water (pounds per cubic foot)
Δ	superelevation of bay over ocean defined as the difference in elevations between MBL and MSL over a tidal cycle (feet)
ζ	average channel bank slope (runs A) or bank slope at throat (runs B and C); horizontal distance per unit of vertical raise
ε_h ε_l	dimensionless timelags between ocean and bay high or low waters = timelag per tidal period
η	water surface elevation at inlet taken as the average of instantaneous bay and ocean levels (feet)
Ω	tidal prism equal to R_b times A_b for all runs (cubic feet)

LABORATORY INVESTIGATION OF TIDAL INLETS ON SANDY COASTS

by
Ramiro E. Mayor-Mora

I. INTRODUCTION

Sandy beaches are a common feature along the coast and often act as barriers between the ocean and inland bodies of water (i.e., bays, lagoons, estuaries). Such barriers may have one or more relatively narrow channels (inlets) that connect the two bodies of water and control the amount and the manner in which the energy of ocean tides, waves, and currents is exchanged within the ocean-inlet-bay system.

Meteorological, hydrographical, geographical, and wave conditions may force inlets to migrate, change their orientation or shape, and at times, close completely. Man's intervention in the natural process of an inlet, bay, or on the neighboring coast may affect an inlet's migrational tendency to close.

A study of the hydrodynamic phenomena involved is complicated by the many factors that act upon the system and by the unpredictable nature of most of these factors. This study is designed to provide a better understanding of the factors influencing inlet behavior which may affect navigation, water quality, the ecology, recreation, and marine life. Both the dynamic changes in the inlet bed and the nearby beaches and the hydraulic characteristics of the system are major aspects of the problem that many investigators have studied in recent years.

Since the collection of field data presents many problems, completely controlled model studies are needed to examine basic inlet processes and parameters. In response to this need for additional understanding of general inlet processes, this study includes:

(a) Laboratory testing of a movable-bed inlet with varying geometric characteristics subjected to combinations of ocean tides and waves;

(b) measurement of the temporal and spatial variation in water levels, current velocities, and channel geometry;

(c) investigation of the effects of tide, wave, runoff, and geometric parameters on the inlet channel hydrography and the flushing ability of the system;

(d) correlation between dimensionless hydraulic parameters; and

(e) comparison of model results to theoretical hydraulic solutions.

This laboratory study uses several simplifications to reduce the complexity of the inlet characteristics, processes, and data analysis. These include: A fixed inlet location; no study of the stability of the channel nor the sediment transport rates through it; no consideration of saltwater effects or flow patterns at the entrance and vicinity; and no investigation of longshore transport.

The report presents a brief review of the principal theoretical approaches developed for predicting the hydraulic characteristics of the system, a summary of field and other laboratory data, and a description of the experimental program. The collected data are given in reduced form and the various dimensionless parameters discussed, correlated, and compared to theoretical approximations. Comparisons of laboratory and field data are included. Conclusions, comments, and suggestions for further use of the empirical data are also presented.

II. THEORETICAL ANALYSES

1. Simplified Tidal Inlet Hydraulics.

A complete study of the hydraulics of a bay-inlet-ocean system would require consideration of the numerous time-dependent factors acting upon such a system, including:

(a) Ocean climate (wind waves, storm surge, tide);

(b) nearshore conditions (longshore currents, manmade modifications to the shore);

(c) hydrologic conditions in the basins draining into the bay;

(d) geometric characteristics of the bay (shape, depth, irregularity, slope of sides) and the inlet channel (location relative to the bay, depth, orientation, length, shape, and ability to shift location);

(e) inlet sediment characteristics; and

(f) ocean-freshwater density wedge effects.

Since these factors are beyond the scope of this investigation, the study has been simplified to the determination of water level fluctuations in the bay and flow through the inlet channel (average current velocity, discharge) in response to a defined periodic ocean tide. Therefore, the approaches found in the literature and discussed in this section involve some simplifying assumptions common to all of these analyses: relatively small and deep bays; constant water density throughout the system; fixed sediment characteristics and behavior; and a fixed inlet channel orientation, location, and shape.

2. Gradually Varied Unsteady Flow in Open Channels.

The simplified equations governing gradually varied unsteady flow of water in an open prismatic channel are the continuity equation:

$$D \frac{\partial V}{\partial x} + V \frac{\partial y}{\partial x} + \frac{\partial y}{\partial t} = 0 \ , \tag{1}$$

and the general dynamic equation:

$$\frac{\partial y}{\partial x} + \alpha \frac{V}{g} \frac{\partial V}{\partial x} + \frac{1}{g} \frac{\partial V}{\partial t} - S_c + S = 0 \ , \tag{2}$$

where x and y define, respectively, a horizontal axis along the channel and a vertical axis along which heights above a datum are measured; D is the hydraulic depth (A_c/w), where A_c is the cross-sectional area and w is channel width; g is the acceleration due to gravity; $\partial y/\partial x$ and $\partial y/\partial t$, the variation of the water surface with distance and with time, respectively; S_c is the slope of the channel bottom along its longitudinal axis; S is the slope of the energy line; and α is the coefficient resulting from the velocity distribution (Chow, 1959).

The change in total head for the channel depends on friction, acceleration, and eddy (turbulence) losses.

3. Principal Theoretical Approaches to the Problem.

The application of equations (1) and (2) to an ocean-inlet-bay system has occupied the attention of several investigators (Chapman, 1923; Brown, 1928; O'Brien, 1937; Keulegan, 1967; Van de Kreeke, 1967; Shemdin and Forney, 1970; Mota Oliveira, 1971; Huval and Wintergerst, in preparation, 1977). The main differences among these studies are the assumptions regarding the physical phenomena and the relative importance given to the basic terms included in these equations. The principal theoretical approaches are summarized below.

a. The Keulegan Solution. Keulegan (1967) obtained a mathematical method of describing inlet hydraulics with these assumptions:

(a) Walls of the bay are vertical;

(b) there is no inflow from streams;

(c) no density currents are present;

(d) tidal fluctuations are sinusoidal;

(e) the bay water level rises uniformly;

(f) length of the bay is less than the tidal wavelength;

(g) the inlet channel flow area is constant; and

(h) the inertia of the mass of the water in the channel is negligible.

An ocean-inlet-bay system which satisfies the Keulegan assumptions is shown in Figures 1 and 2.

The Keulegan solution describes the water surface fluctuation in the bay by the differential equation:

$$\frac{dh_b}{dt} = K \frac{\pi}{T} \sqrt{2R_o|h_o - h_b|} , \tag{3}$$

where h_b is the water level in the bay; h_o is the water level of the ocean; T is the tidal period; R_o is the tidal range in the ocean; and K is the coefficient of repletion, a dimensionless number defined as:

$$K = \frac{T}{\pi\sqrt{R_o}} \frac{A_c}{A_b} \sqrt{\frac{g}{k_{en} + k_{ex} + fL/4R}} , \tag{4}$$

where A_c is the inlet cross-sectional area; A_b is the area of the bay; k_{en} is the entrance loss coefficient; k_{ex} is the exit loss coefficient; f is the Darcy-Weisbach friction coefficient of the channel; L is the channel length; and R is the hydraulic radius of the channel.

O'Brien and Dean (1972) presented Keulegan's solution in dimensionless bay tidal range and phase lag plotted against the coefficient of repletion, K (Fig. 3). Note in the figure that for low values of K, the tide amplitude in the bay, a_b, is smaller than the ocean amplitude, a_o (a_b/a_o is less than 1). As K increases, the amplitude in the bay increases, so that for values of K greater than 2, the ocean and bay tide amplitudes are the same.

Similarly, the lag between the ocean and bay water levels ε, approaches 90° for small values of K and drops to zero for values of K greater than 10 (Fig. 3).

Dimensionless maximum velocity, V'_{max}, is also given as a function of K with maximum velocity increasing for higher values of K (Fig. 3). Maximum inlet velocity, V_{max}, is related to dimensionless maximum velocity by the equation:

$$V_{max} = V'_{max} \frac{2\pi}{T} a_o \frac{A_b}{A_c} . \tag{5}$$

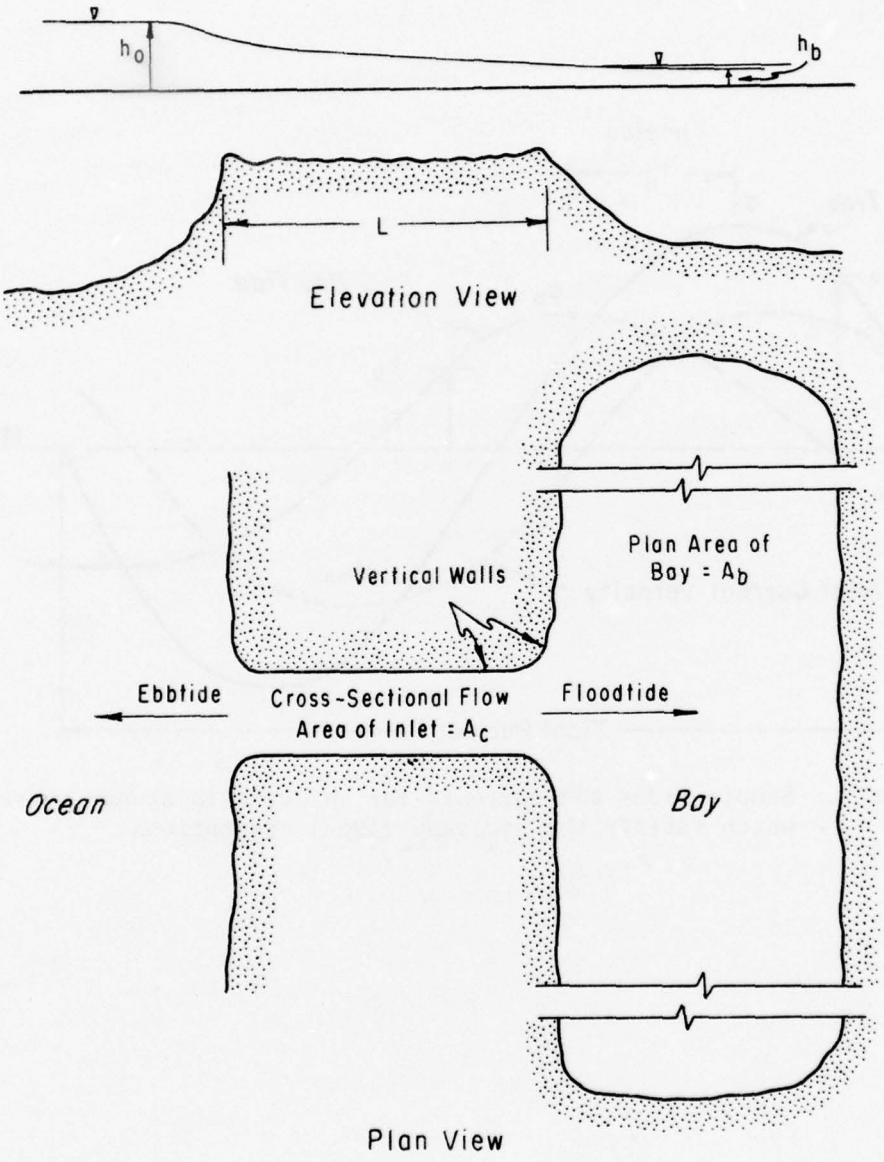

Figure 1. An inlet-bay system with the Keulegan (1967) assumptions.

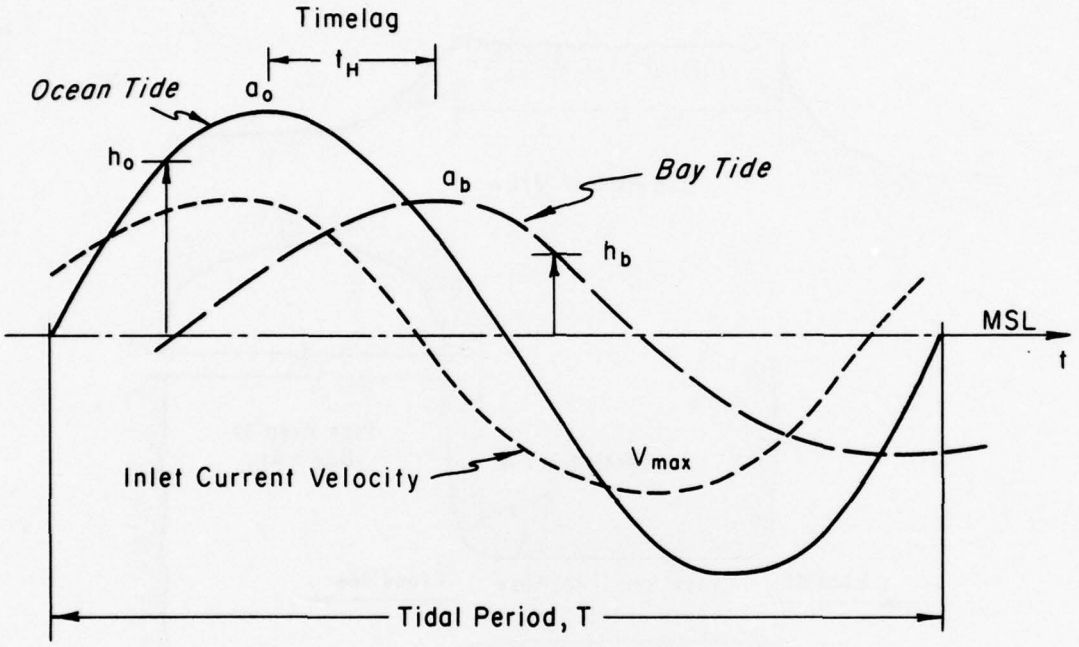

Figure 2. Sample tides and currents for an ocean-inlet-bay system which satisfy the Keulegan (1967) assumptions.

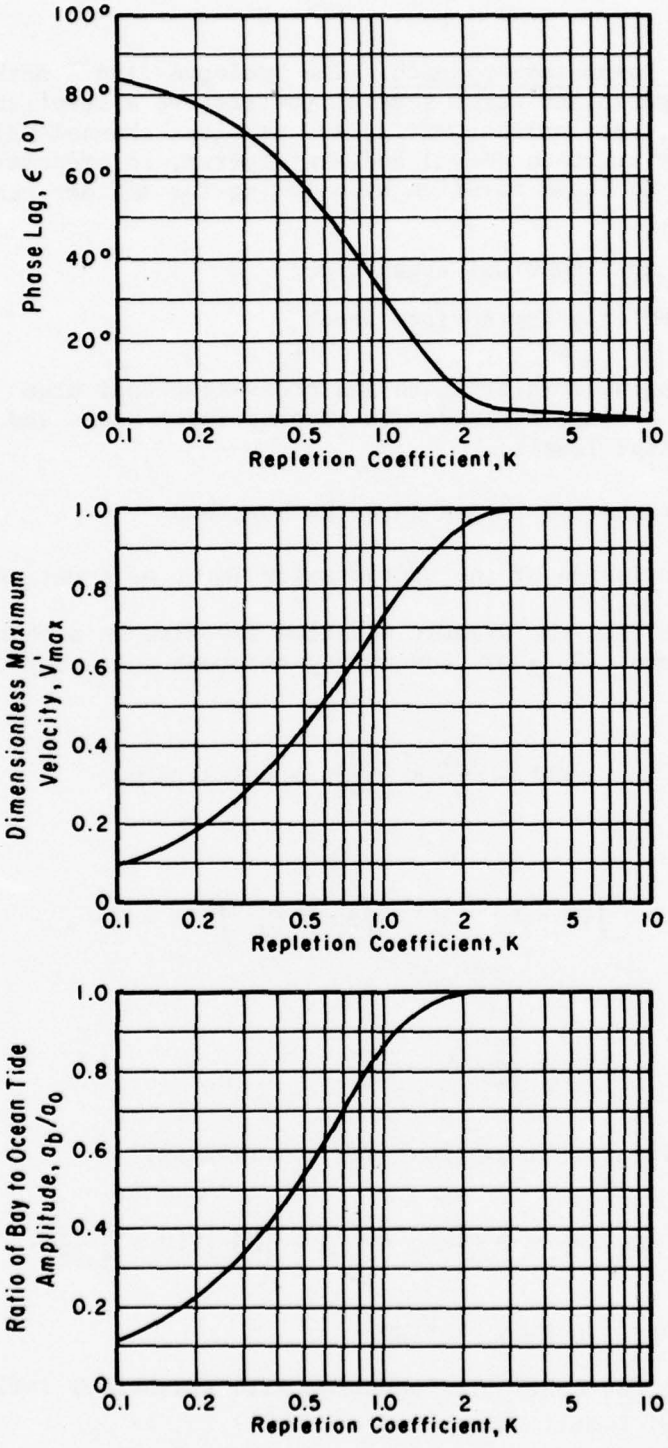

Figure 3. Variation of dimensionless parameters with Keulegan's repletion coefficient, K.

b Lumped Parameter Approach. The Keulegan (1967) method of predicting inlet hydraulics makes several restrictive assumptions, i.e., a sinusoidal tide, vertical bay walls, and vertical channel walls. The lumped parameter approach (Huval and Wintergerst, in preparation, 1977) generalizes the Keulegan solution by allowing for a wider range of conditions:

(a) A nonsinusoidal ocean tide;

(b) variable bay surface area;

(c) variable inlet depth and cross-sectional area throughout a tidal cycle due to sloping inlet banks and variable water levels;

(d) freshwater inflow into the bay; and

(e) inclusion of the acceleration terms of equation (2).

In equation (2), the dynamic equation for flow in a channel with a bed slope of zero ($S_c = 0$) connecting an ocean and a bay can be simplified to:

$$\partial y + \alpha \frac{V \partial V}{g} + \frac{1}{g} \frac{\partial V}{\partial t} \partial x + S \partial x = 0 . \tag{6}$$

Taking

$$\int \partial y = h_b - h_o, \quad \int \partial x = L, \quad \int V \partial V = \frac{V^2}{2} ,$$

and

$$S = \frac{fV^2}{8gR}$$

(quadratic resistance assumption) and rearranging,

$$h_o - h_b = \frac{1}{2g} \left(k_{en} + k_{ex} + \frac{fL}{4R} \right) |V| V + \frac{L}{g} \frac{\partial V}{\partial t} , \tag{7}$$

where h_o is any function of time.

Introducing the continuity equation with freshwater inflow, Q_w (any function of time):

$$\frac{\partial h_b}{\partial t} = \frac{A_c V + Q_w}{A_b} . \tag{8}$$

Equations (7) and (8) are nonlinear. Since the hydraulic radius, R, varies approximately with the water level $R \simeq R_{MSL} + \eta$, and because of the term $|V|V$, both A_b and A_c are also functions of time. Let:

$$A_b = A_{bo}\left(1 + 2\beta \frac{h_b}{R_o}\right). \tag{9}$$

and

$$A_c = A_{co} + W_o \eta + \zeta \eta^2 , \tag{10}$$

where $\eta = (h_b + h_o)/2$, A_{bo} is the bay surface area at mean sea level (MSL), β is a dimensionless parameter of bay slope, and ζ is the channel wall slope. Furthermore, the friction factor, f, is expressed by the Manning coefficient, n, and the hydraulic radius (Chow, 1959) as:

$$f = \frac{8\ g\ n^2}{2.208 R^{1/3}} = \frac{116.7 n^2}{R^{1/3}} \tag{11}$$

A Runge-Kutta-Gill numerical method for integration of the two simultaneous ordinary differential equations (7) and (8) was programed for the digital computer, taking $k_{en} + k_{ex} = 1$. Starting with initial boundary conditions, the program integrates the equations over several tidal cycles until bay tide and velocity become periodic.

The original computer program (Huval and Wintergerst, 1977) computes instantaneous bay tide, average inlet current velocity, and inlet discharge for given values of Manning's n. This program was modified so that the expression $(k_{en} + k_{ex} + fL/4R)$ in equation (7) is substituted by F, a factor determined from experimental results, thus avoiding the necessity of assuming values of k_{en}, k_{ex}, and f.

III. THE EXPERIMENTAL PROGRAM

1. Experimental Conditions.

A systematic series of 36 laboratory experiments was carried out on an idealized ocean-inlet-bay system involving reversing flows (tidal action) and wave action. Del Monte white sand, 60 mesh with a median diameter of 0.34 millimeter, was used to model the barrier in all tests (Fig. 4). Freshwater was used.

Other parameters constant throughout the tests were:

(a) The surface area of the bay (vertical tank walls);

(b) the water depth at MSL in the ocean basin;

(c) the sand barrier slope on the bay side and the bank slopes of the pilot channels;

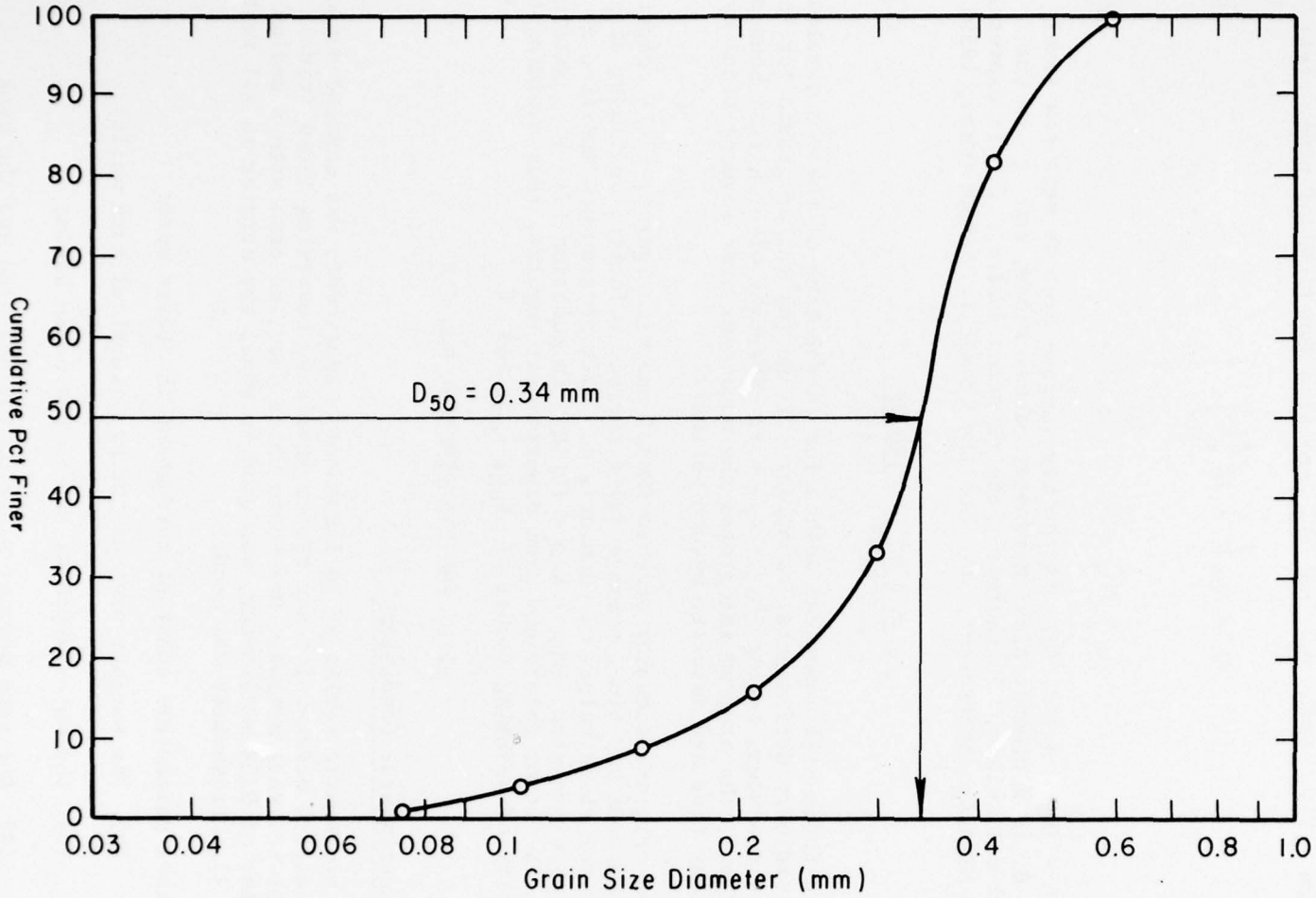

Figure 4. Sieve analysis of the sand used in the testing program.

(d) the location and orientation of the wave generator;

(e) the ocean beach slope (1:30);

(f) the alinement of the pilot channels (parallel to the direction of wave propagation); and

(g) the relative location of the walls defining the ocean basin, the sand barrier section, and the bay basin.

The independent variables (ocean tidal range, pilot channel area and length, wave characteristics, tidal cycle amplitude and duration) were selected so that the range of repletion coefficients, K, varied from 0.04 to 1.30 to provide a wide range of a_b/a_o ratios (0.025 to 0.95). Experimental conditions tested are shown in Tables 1 and 2.

In addition to a series of tests with an unimproved inlet, two runs were conducted to study the response of an inlet improved by parallel vertical-wall jetties. Further studies included a run with "freshwater" discharge into the bay, runs with a "fixed-bed" prismatic channel, and a run with the bed form "fixed" in plaster.

This study does not include a systematic account of water circulation patterns in the ocean, channel or bay, or any measurement of sediment transport rates or size composition of the bed; it concentrates more on measurements of water surface elevations and current velocities as a function of time, timelags, and the size and shape of the inlet at the end of each run. Temperature effects were not investigated, although at times the water temperatures in the ocean and in the bay differed by 8° Fahrenheit.

2. Testing Facilities and Equipment.

The experiments were conducted at the Richmond Engineering Field Station, University of California, Berkeley. A 2.5-foot-deep, 94.3-foot-long, and 63.7-foot-wide basin was divided into three subbasins by concrete block walls covered with plastic sheets on both sides to prevent any leakage through the walls (Fig. 5). The larger subbasin represented the bay and was separated from the smaller basin (the ocean) by a sand barrier contained between two guide walls (Fig. 6). This 8-foot-wide sand barrier extended into the ocean with a slope of 1:30; on either side, 8-foot-wide cement barriers formed the ocean beach. The third basin collected the water outflow from the ocean where it drained into the outside storage basin.

The storage basin, located outside of the building, was equipped with a filter and a pump. The circulating system operated as shown in Figure 5.

A 24-foot flap-type wave generator was always at the position shown in Figures 5 and 6, so that the periodic waves traveled with their crests

Table 1. Ocean experimental variables.

Run	Duration	Water temperature	Ocean tide								Wave characteristics[1]						Remarks
			T	R_O	High	Low	MSL	T_e/T	Water levels at maximum discharge		T	H	H_O	L_O	H_O/L_O	P_O	
	(h)	(°F)	(s)	(ft)	(ft)	(ft)			Ebb	Flood	(s)	(ft)	(ft)	(ft)			
2	4.5	----[2]	1200	0.0930	-------	-------	-------	0.473	-------	-------	0.00	0.000	0.000	0.00	0.000	0.000	Preliminary; no beach
3	8.1	----[2]	1200	0.1335	0.0665	-0.0670	0.0030	0.478	-0.0660	0.0660	0.00	0.000	0.000	0.00	0.000	0.000	Preliminary; no beach
4	13.7	58.0	1200	0.1365	0.0690	-0.0675	0.0045	0.477	-0.0675	0.0690	0.95	0.105	0.114	4.63	0.024	0.250	Mild waves; long run
5	15.3	51.0	1200	0.1375	0.0670	-0.0705	0.0045	0.486	-0.0705	0.0670	0.75	0.176	0.185	2.88	0.064	0.513	Steep waves; long run
6A	5.7	73.0	1204	0.1460	-------	-------	0.0005	0.492	-------	-------	0.00	0.000	0.000	0.00	0.000	0.000	Tide record disturbed
6B	16.0	64.0	1188	0.1380	0.0670	-0.0710	0.0010	0.477	-0.0710	0.0670	0.95	0.089	0.096	4.63	0.021	0.175	Mild waves; long run
7A	7.5	69.0	1800	0.1500	0.0755	-0.0745	0.0005	0.492	-0.0735	0.0775	0.00	0.000	0.000	0.00	0.000	0.000	
7B	25.0	74.0	1800	0.1360	0.0665	-0.0695	0.0015	0.473	-0.0685	0.0630	0.95	0.091	0.099	4.63	0.021	0.186	Overnight run
7C	24.0	66.0	1800	0.1370	0.0685	-0.0685	0.0010	0.478	-0.0670	0.0655	0.95	0.084	0.092	4.63	0.020	0.161	Jetty; overnight run
8A	7.0	71.0	1806	0.1370	0.0675	-0.0695	0.0005	0.478	-0.0675	0.0595	0.00	0.000	0.000	0.00	0.000	0.000	
8B	24.5	68.0	1800	0.1345	0.0670	-0.0675	0.0020	0.481	-0.0670	0.0625	0.95	0.087	0.095	4.63	0.021	0.172	Overnight run
8C	18.0	68.0	1808	0.1330	0.0655	-0.0675	0.0015	0.489	-0.0660	0.0610	0.95	0.087	0.095	4.63	0.020	0.172	Extension of R8B
9A	7.0	69.0	1808	0.1390	0.0690	-0.0700	0.0050	0.487	-0.0685	0.0650	0.00	0.000	0.000	0.00	0.000	0.000	Repetition of R8A
9B	24.0	69.0	1804	0.1300	0.0845	-0.0655	0.0025	0.487	-0.0650	0.0575	0.75	0.120	0.126	2.88	0.044	0.238	Steeper waves than R8B
10A	5.0	69.0	3600	0.1250	0.0600	-0.0650	0.0020	0.465	-0.0560	0.0450	0.00	0.000	0.000	0.00	0.000	0.000	Not at equilibrium
10B	6.0	68.0	3600	0.1235	0.0600	-0.0635	0.0020	0.450	-0.0570	0.0405	0.95	0.068	0.074	4.63	0.016	0.103	Not at equilibrium
11A[3]	3.0	66.0	3600	0.0590	0.0280	-0.0310	0.0175	0.436	-0.0265	0.0235	0.00	0.000	0.000	0.00	0.000	0.000	Prismatic fixed bed
11B[3]	4.0	66.5	3600	0.0605	0.0280	-0.0325	0.0040	0.510	-0.0290	0.0270	0.75	0.030	0.031	2.88	0.011	0.015	Mild waves
11C[3]	2.0	67.0	3600	0.0605	0.0280	-0.0325	0.0040	0.000	-0.0290	0.0240	0.75	0.063	0.066	2.88	0.023	0.065	Steeper waves
12A	5.0	67.0	3600	0.0605	0.0295	-0.0310	0.0035	0.442	-0.0215	0.0115	0.00	0.000	0.000	0.00	0.000	0.000	
12E[3]	4.0	66.0	3600	0.0590	0.0290	-0.0300	0.0050	0.434	-0.0190	0.0135	0.00	0.000	0.000	0.00	0.000	0.000	Fixed beach, channel
12A	5.5	68.0	3612	0.0560	0.0270	-0.0290	0.0050	0.412	-0.0155	0.0085	0.00	0.000	0.000	0.00	0.000	0.000	Repetition of R12A
12F[3]	4.0	67.0	3618	0.0565	0.0270	-0.0295	0.0045	0.423	-0.0195	0.0075	0.00	0.000	0.000	0.00	0.000	0.000	Fixed beach, channel
12B	5.0	63.0	3612	0.0595	0.0290	-0.0305	0.0045	0.445	-0.0215	0.0140	0.75	0.042	0.044	2.88	0.015	0.029	Follows R12F
12C	4.5	61.0	3612	0.0575	-------	-------	0.0045	-------	-------	-------	0.75	0.042	0.044	2.88	0.015	0.029	Extension of R12B
14A	4.5	58.0	1806	0.0550	0.0270	-0.0280	0.0030	0.485	-0.0265	0.0240	0.00	0.000	0.000	0.00	0.000	0.000	
14B	5.0	58.0	1806	0.0570	0.0270	-0.0300	0.0033	0.496	-0.0280	0.0245	0.75	0.047	0.049	2.88	0.017	0.036	
15A	4.5	58.0	2700	0.0545	0.0265	-0.0280	0.0040	0.465	-0.0250	0.0225	0.00	0.000	0.000	0.00	0.000	0.000	
15B	5.3	58.0	2700	0.0600	0.0285	-0.0315	0.0035	0.475	-0.0265	0.0225	0.75	0.038	0.040	2.88	0.014	0.024	
16A	4.5	56.0	2700	0.0530	0.0260	-0.0260	0.0055	0.462	-0.0215	0.0160	0.00	0.000	0.000	0.00	0.000	0.000	
16B	5.0	56.5	2700	0.0570	0.0280	-0.0290	0.0035	0.460	-0.0235	0.0180	0.75	0.038	0.039	2.88	0.014	0.023	
16C	4.5	55.5	2700	0.0565	0.0275	-0.0290	0.0020	0.470	-0.0220	0.0180	0.75	0.036	0.038	2.88	0.013	0.022	Freshwater inflow
17A	4.0	52.0	1800	0.0720	0.0310	-0.0380	0.0045	0.510	-0.0370	0.0425	0.00	0.000	0.000	0.00	0.000	0.000	
17B	5.5	52.0	1800	0.0720	0.0310	-0.0380	0.0060	0.495	-0.0370	0.0320	0.75	0.051	0.053	2.88	0.018	0.042	
18B	5.3	46.5	2712	0.0715	0.0335	-0.0380	0.0065	0.503	-0.0375	0.0310	0.75	0.042	0.044	2.88	0.015	0.029	Follows R17B
18C	6.8	47.0	2700	0.0735	0.0350	-0.0385	0.0060	0.507	-0.0390	0.0310	0.75	0.042	0.043	2.88	0.015	0.028	Jetty

[1]Linear theory used for deepwater characteristics.
[2]Not determined.
[3]Fixed bed.

Table 2. Inlet experimental variables.

Run	Tides: Duration/T Ebb	Tides: Duration/T Flood	Tides: Lags/T ϵ_e Ebb	Tides: Lags/T ϵ_f Flood	Inlet length L (ft)	Parameters at maximum discharges: Water level Ebb (ft)	Water level Flood (ft)	Inlet area Ebb (ft^2)	Inlet area Flood (ft^2)	Pilot A_c (ft^2)	Parameters at throat measured at MSL: A_c (ft^2)	p (ft)	W (ft)	Bank slope (ft/ft)	Station (ft)	Maximum velocity Ebb (ft/s)	Maximum velocity Flood (ft/s)	Remarks
2	0.506	0.494	0.157	0.183	------[1]	------	------	------	------	------	------	------	------	1.0	0.0	1.27	1.26	Preliminary, short, deep channel
3	0.600	0.400	0.179	0.288	10.50	0.0090	0.0400[2]	0.180	0.277	0.400	0.197	2.05	1.93	2.0	0.0	1.24	1.15	Preliminary, longer channel
4	0.607	0.393	0.188	0.313	17.50	0.0510[2]	0.0615[2]	0.190	0.216	0.191	0.089	1.62	1.57	8.0	11.55	0.71	1.01	Long, shallow channel
5	0.609	0.391	0.189	0.314	18.50	0.0125	0.0745[2]	0.096	0.232	0.191	0.076	1.58	1.53	7.5	10.70	0.77	0.97	Long, shallow channel
6A	0.633	0.370	0.184	0.315	16.00	0.0135	0.0540	0.155	0.239	0.099	0.128	2.10	2.00	1.0	0.0	0.71	0.94	Cross sections after floodtide
6B	0.578	0.412	0.177	0.287	16.50	0.0180	0.0550	0.160	0.248	0.127	0.124	1.97	1.89	6.5	13.00	0.91	1.04	
7A	0.616	0.385	0.167	0.296	16.50	0.0075	0.0530	0.196	0.305	0.099	0.179	2.42	2.30	1.5	0.0	0.93	1.31	
7B	0.576	0.424	0.165	0.260	19.50	0.0160	0.0380	0.289	0.354	0.177	0.246	2.70	2.60	6.5	10.50	1.03	1.44	
7C	0.558	0.442	0.169	0.248	20.60	0.0150	0.0340	0.253	0.350	0.237	0.283	2.28	1.97	0.0	9.00	0.90	0.99	12-foot parallel jetties
8A	0.581	0.422	0.157	0.262	18.50	−0.0170	0.0350	0.287	0.424	0.302	0.331	2.77	2.60	1.5	0.0	0.98	1.18	
8B	0.571	0.429	0.162	0.259	20.50	0.0180	0.0370[2]	0.316	0.363	0.327	0.276	2.20	2.07	7.5	8.25	1.02	1.36	
8C	0.577	0.437	0.166	0.244	22.50	0.0140	0.0260	0.376	0.408	0.276	0.341	2.52	2.36	8.5	7.75	0.84	1.22	
9A	0.585	0.420	0.168	0.260	18.50	−0.0075	0.0320	0.299	0.402	0.292	0.318	2.75	2.58	1.5	0.0	1.10	1.20	No cross-sectioning
9B	0.573	0.429	0.157	0.242	21.00	0.0080	0.0400	0.428	0.577	0.312	0.392	4.50	4.43	5.0	9.00	0.86	0.90	Wide channel; after floodtide
10A	0.562	0.438	0.082[2]	0.182	13.75	−0.0150[2]	0.0040[2]	0.372	0.423	0.334	0.412	2.90	2.67	1.5	0.0	1.06	1.49	
10B	0.552	0.448	0.061[2]	0.160	13.50	−0.0070[2]	0.0330[2]	0.432	0.611	0.412	0.462	4.54	4.34	5.0	14.50	0.92	1.25	Wide channel
11A[3]	0.530	0.470	0.137[2]	0.175	7.00	−0.0230[2]	0.0010[2]	0.141	0.189	0.187	0.187	2.10	2.04	1.7	0.0	1.18	1.15	Fixed prismatic bed
11B[3]	0.527	0.473	0.129[2]	0.156	7.00	−0.0060[2]	0.0120[2]	0.171	0.208	0.183	0.183	2.10	2.04	1.7	14.00	1.21	1.07	Fixed prismatic bed
11C[3]	0.500	0.500	0.133[2]	0.165	7.00	−0.0020[2]	0.0160[2]	0.179	0.216	0.183	0.183	2.10	2.04	1.7	14.00	1.17	1.10	
12A	0.502	0.498	0.030[2]	0.095[2]	11.15	−0.0155	0.0000	0.378	0.415	0.434	0.415	2.61	2.41	1.7	0.0	0.75	0.79	Sections after ebbtide
12E[3]	0.506	0.494	0.025[2]	0.103[2]	11.15	−0.0115	0.0000	0.375	0.402	0.402	0.402	2.60	2.40	1.7	0.0	0.92	0.72	Fixed rippled bed (ebbtide)
−12A	0.502	0.498	0.017[2]	0.095[2]	11.30	−0.0150	−0.0050	0.382	0.405	0.430	0.417	2.58	2.38	1.7	0.0	0.88	0.88	Sections after floodtide
12F[3]	0.501	0.499	0.033[2]	0.108[2]	11.30	−0.0136	0.0000	0.374	0.406	0.406	0.406	2.57	2.37	1.7	0.0	0.90	0.86	Fixed rippled bed (floodtide)
12B	0.517	0.483	0.025[2]	0.103[2]	11.00	−0.0110	0.0000	0.330	0.356	0.406	0.356	2.54	2.41	6.0	14.50	0.88	0.90	
12C	0.503	0.497	------	0.125[2]	11.50	------	------	0.336	0.336	0.356	0.336	2.42	2.27	8.0	14.00	------	------	Sections after floodtide
14A	0.535	0.465	0.100[2]	0.200[2]	9.90	−0.0200	0.0085	0.279	0.344	0.304	0.324	2.50	2.29	1.4	0.0	1.02	1.04	Short channel
14B	0.538	0.462	0.138[2]	0.190[2]	10.25	−0.0150	0.0155	0.252	0.325	0.323	0.286	2.52	2.37	8.0	14.25	1.06	1.00	
15A	0.526	0.474	0.100[2]	0.164[2]	8.40	−0.0170	0.0075	0.291	0.349	0.317	0.331	2.51	2.35	1.4	0.0	1.02	1.00	Short channel
15B	0.527	0.473	0.111[2]	0.156[2]	9.50	−0.0160	0.0090	0.229	0.285	0.332	0.264	2.38	2.27	6.5	13.75	1.04	0.94	
16A	0.512	0.488	0.081[2]	0.130[2]	10.90	−0.0190	0.0020	0.383	0.435	0.420	0.430	2.67	2.48	1.5	0.0	0.88	0.84	Short, deep channel
16B	0.513	0.487	0.080[2]	0.149[2]	11.00	−0.0180	0.0040[2]	0.330	0.384	0.435	0.374	2.72	2.57	7.0	14.50	0.92	0.88	
16C	0.548	0.452	0.073[2]	0.149[2]	11.00	−0.0120	0.0100	0.346	0.401	0.378	0.375	2.62	2.48	8.0	14.25	0.92	0.86	
17A	0.595	0.405	0.197[2]	0.300[2]	10.50	−0.0060	0.0190	0.091	0.139	0.082	0.102	1.97	1.89	1.6	0.0	0.56	0.64	Long, shallow channel
17B	0.558	0.442	0.182[2]	0.247[2]	11.00	0.0000	0.0255	0.083	0.127	0.098	0.083	1.65	1.59	5.5	13.50	0.54	0.60	
18B	0.564	0.436	0.199[2]	0.263[2]	11.00	−0.0050	0.0240[2]	0.067	0.112	0.082	0.074	1.47	1.38	8.0	12.50	0.60	0.54	Velocities doubtful
18C	0.564	0.436	0.200[2]	0.248[2]	10.00	−0.0035[2]	0.0245	0.079	0.122	0.074	0.084	1.67	1.56	0.0	12.50	0.66	0.62	

[1]Not measured.
[2]Approximate.
[3]Fixed bed.

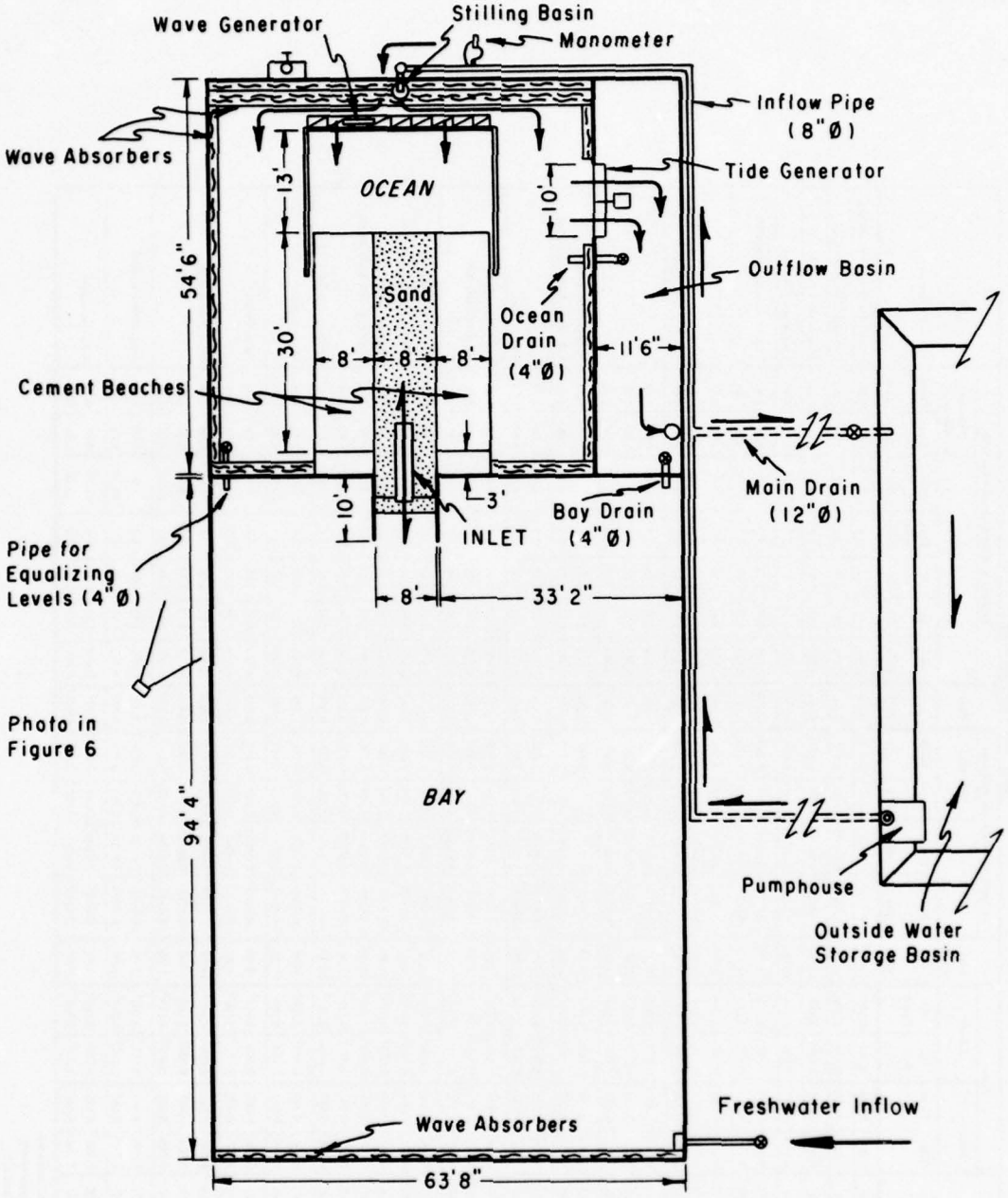

Figure 5. Plan view of testing facilities showing water circulation between basins. Thick arrows indicate direction of flow.

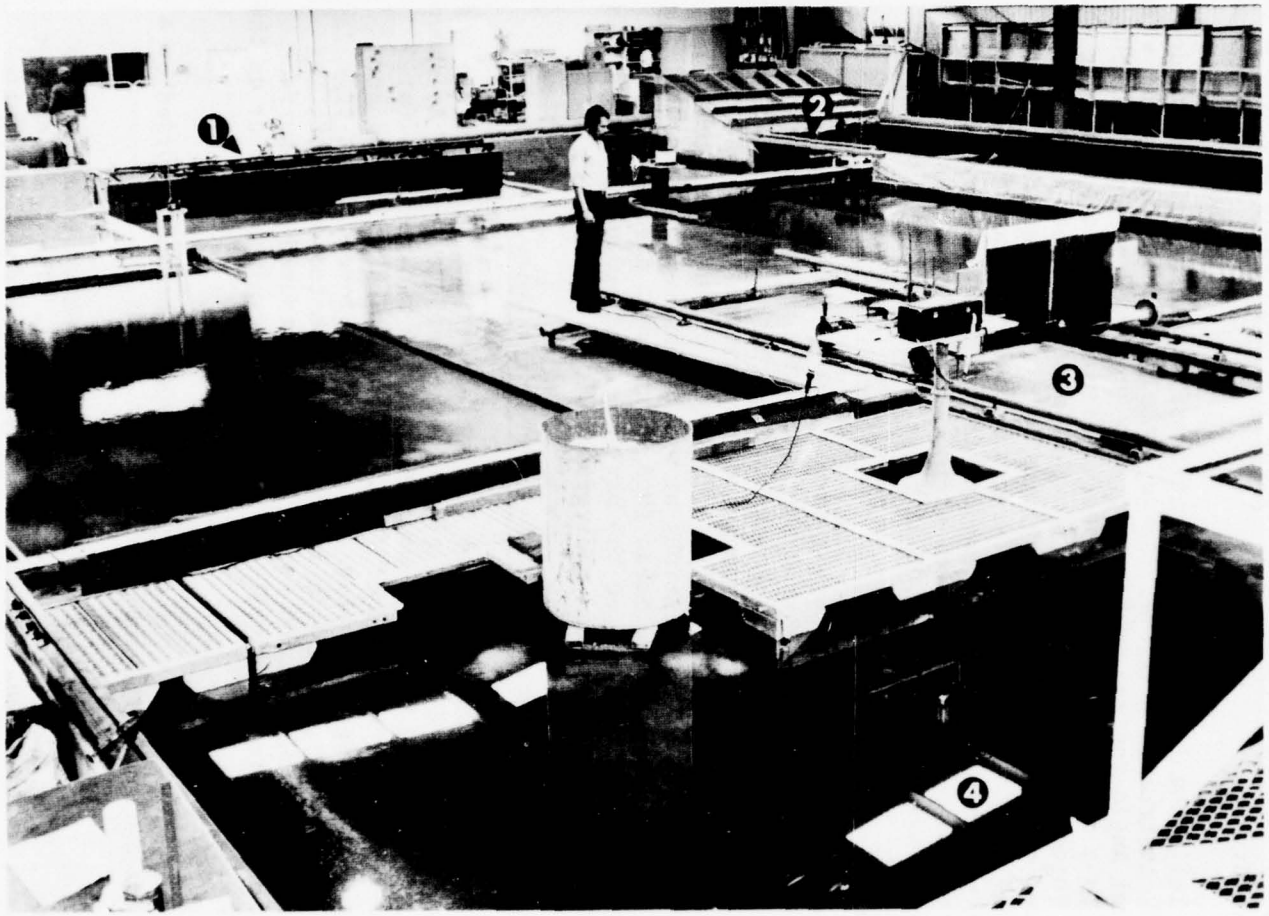

Figure 6. Overall view of testing facilities. Numbers are: (1) wave generator; (2) tide generator; (3) sand barrier and inlet channel; (4) bay basin.

perpendicular to the beach. Two parallel 18-foot-long steel barriers, raised about 6 inches above the basin bottom to allow water circulation, helped prevent spreading of wave energy caused by diffraction and refraction. Wave absorbers were installed along the outer walls and behind the wave generator.

A special mechanism for the generation of sinusoidal tides was designed and constructed (Fig. 7). An adjustable 10-foot-long wooden weir, with a steel angle top and rubber ends, was supported by three turnbuckles connected to a common shaft. This shaft was connected to a rotating wheel through a wooden Pitman arm and driven by a motor equipped with a gearbox that allowed control of the tidal periods by varying the number of revolutions per minute (RPM). The driving arm could be fixed to the wheel at several eccentric positions according to the tidal range desired (about equal to the vertical travel of the weir). The turnbuckles allowed further adjustment of the tidal range, the mean water depth, and leveling of the weir crest.

The inlet region and the moving carriage supported by 30-foot-long rails are shown in Figure 8. Instruments mounted on the carriage reached any point on the sand barrier. Points within this area were located by perpendicular scales (in feet) mounted on a carriage and on one of the steel channels supporting the rails. The scale on the steel channel defined the location of the stations at which measurements were made. Station 10 was located at the ocean face of the wall dividing the two main basins and station 0 was on the bay side. A bridge over the width of the basin permitted overhead photography (Fig. 8).

3. Instrumentation, Controls, and Data Recording Units.

Simultaneous recording of water surface elevations in the ocean and current velocities in the channel aided control of the tests. As shown in Figure 9, ocean and bay tides were recorded by two systems: (a) Resistance-type water level gages (Fig. 10) connected to two Sanborn four-channel recording units (Fig. 11); and (b) Stevens float-type water level recorders, each with its own chart mounted on a rotating drum (Fig. 12). Each gage and each float was protected from surface disturbances by appropriate stilling wells with openings near or on the basin floor.

Waves were measured by the resistance-type gages and recorded by a separate two-channel unit with varying chart speeds.

A special resistance gage was used to detect water levels at the inlet channel because of its relative shallowness. The L-shaped gage (mounted on the carriage as shown in Fig. 13) was made of thin wires spaced 0.25 inch apart. Three other special gages were installed along the channel axis to measure the water surface slope. A standard point gage and a small current meter (Kent Miniflow, 265-3, propeller diameter 0.95 centimeter; Fig. 14) were also mounted on the carriage. The current

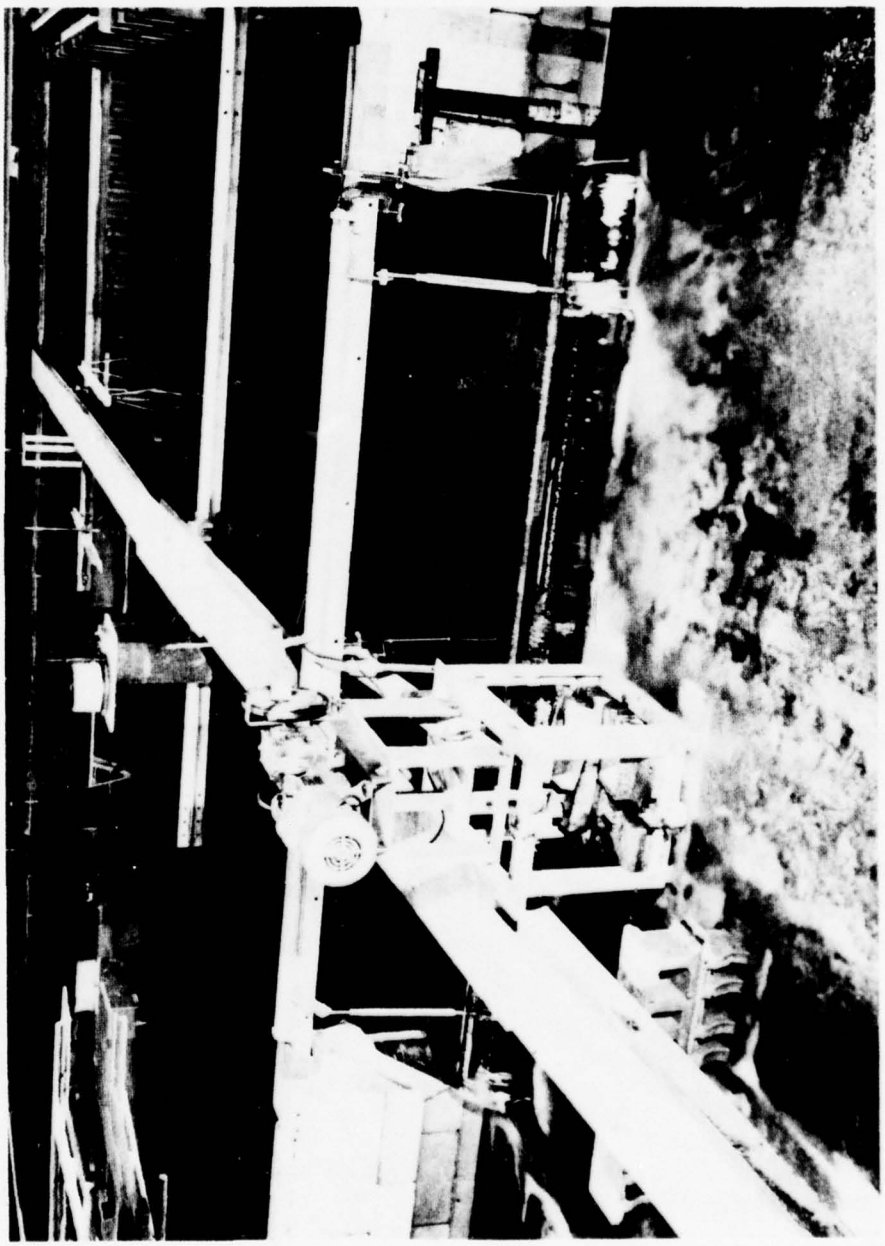

Figure 7. Tide-generating mechanism; ocean basin in background.

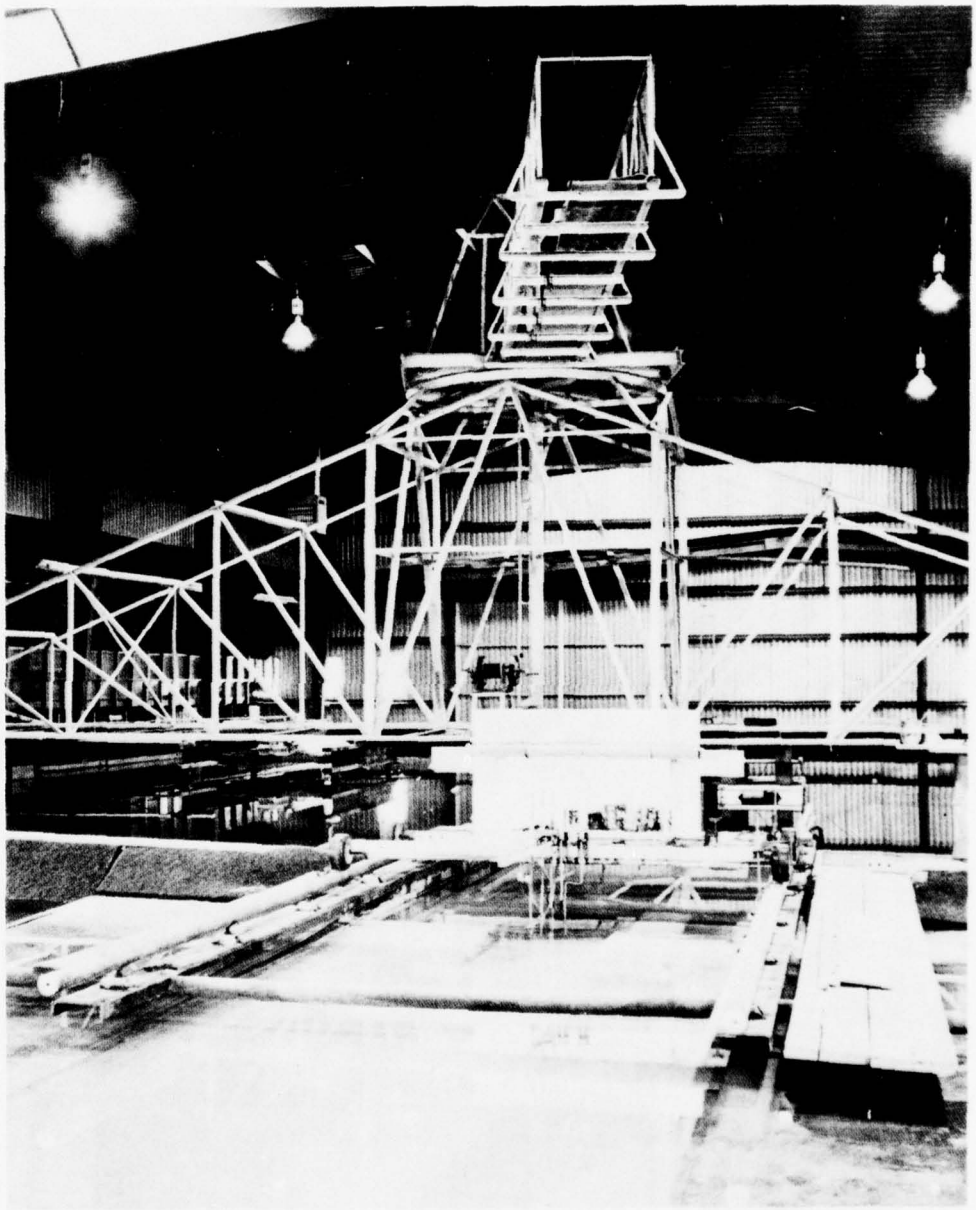

Figure 8. Instrument carriage over sand barrier and platform for overhead photography.

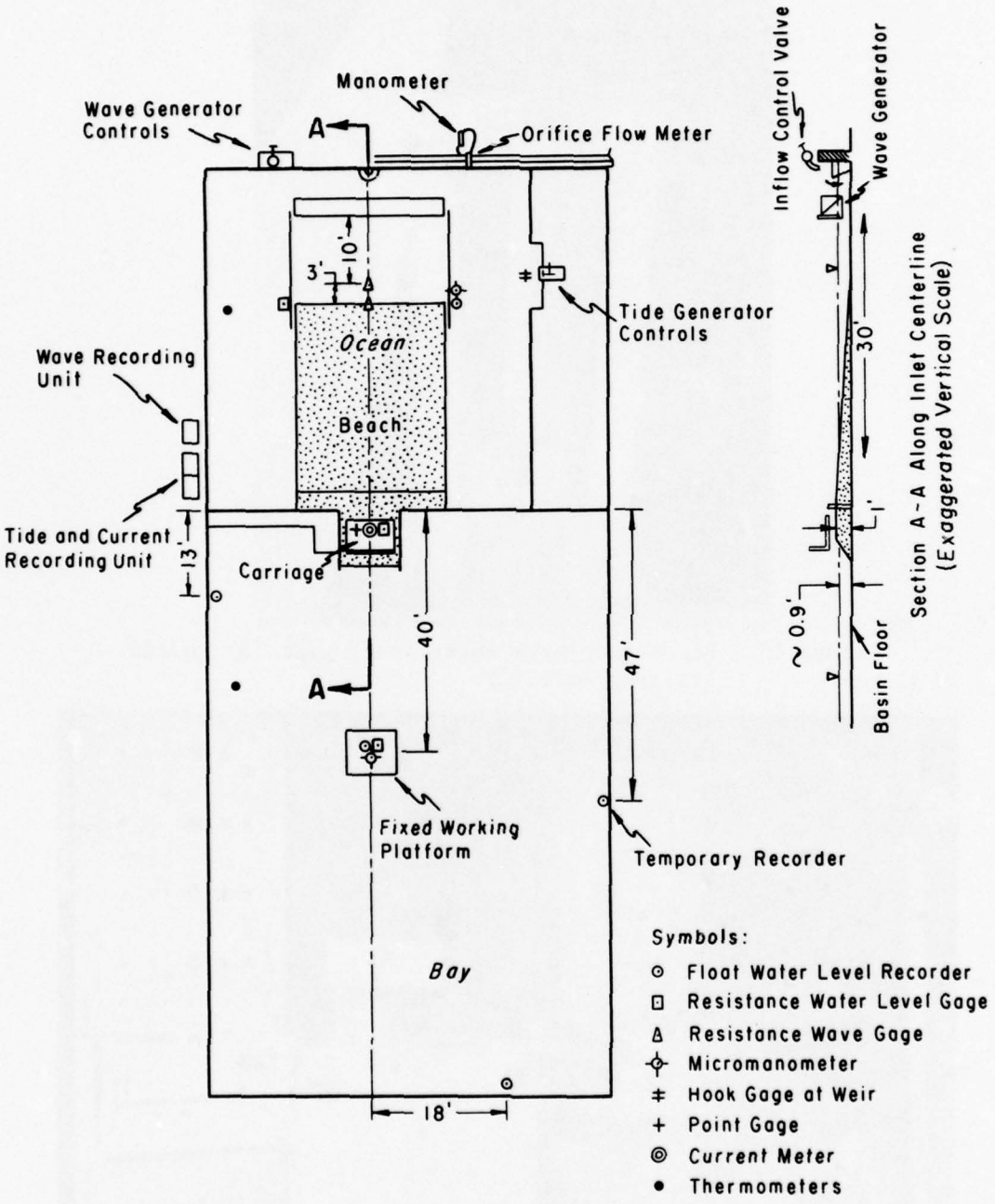

Figure 9. Schematic layout of testing facilities showing relative locations of instruments, controls, and recording units.

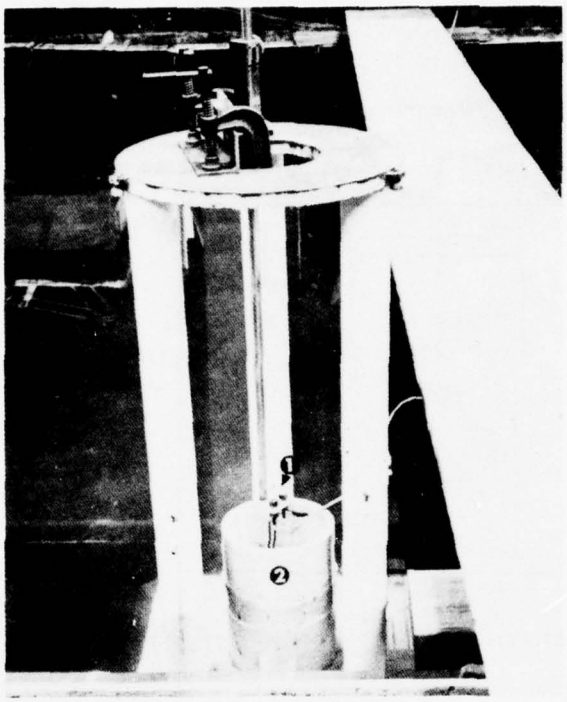

Figure 10. Resistance-type water level gage (1) inside stilling well (2).

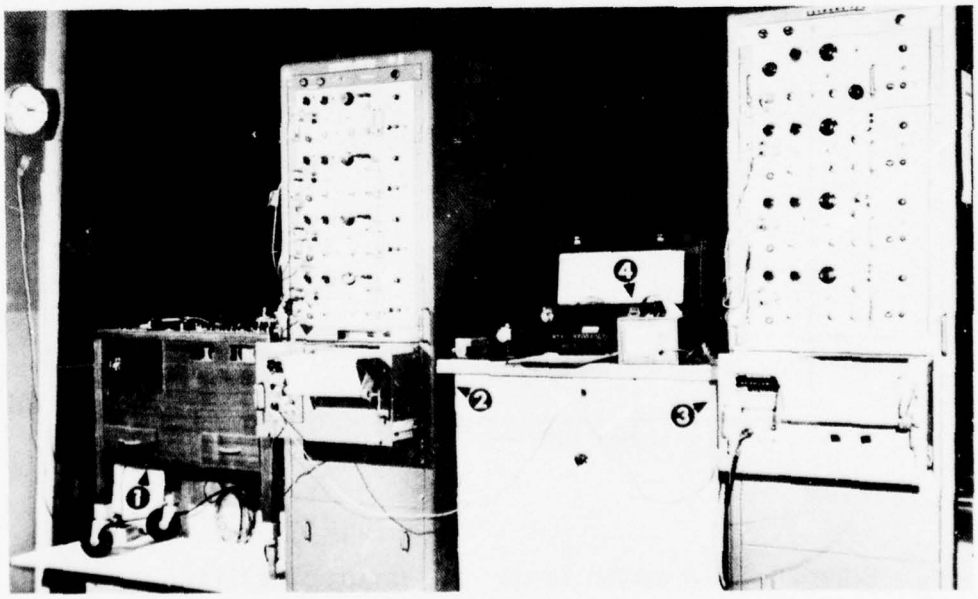

Figure 11. Recording and control units. Numbers are: (1) surface wave recorder; (2) water surface slope recorder: (3) current velocity and tides recorder; (4) current meter dial (for calibration).

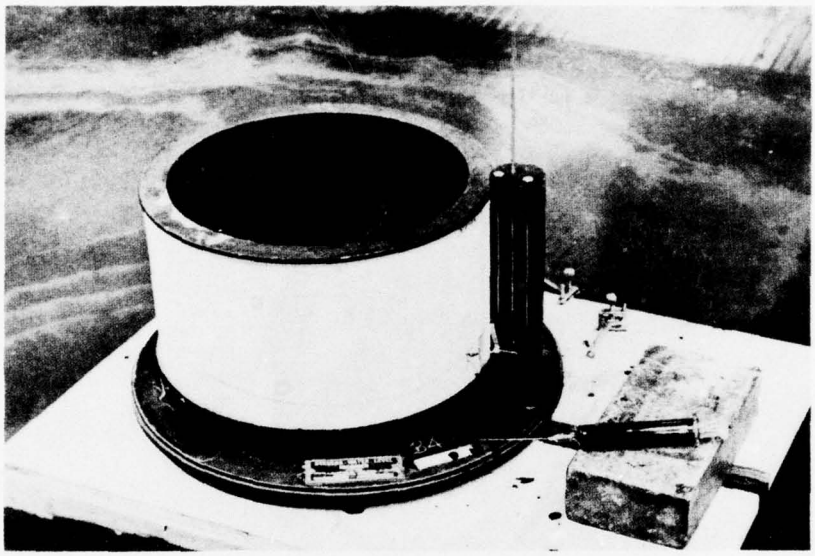

Figure 12. Float-type water level recorder mounted on stilling well.

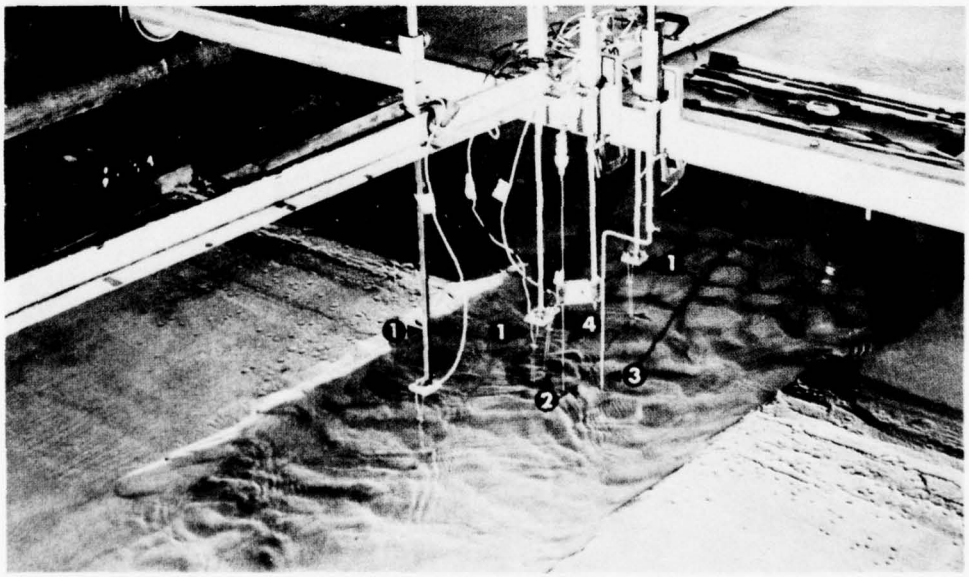

Figure 13. Instruments mounted on carriage. Numbers are: (1) water surface slope gages; (2) water level resistance gage; (3) water level point gage; (4) current velocity meter.

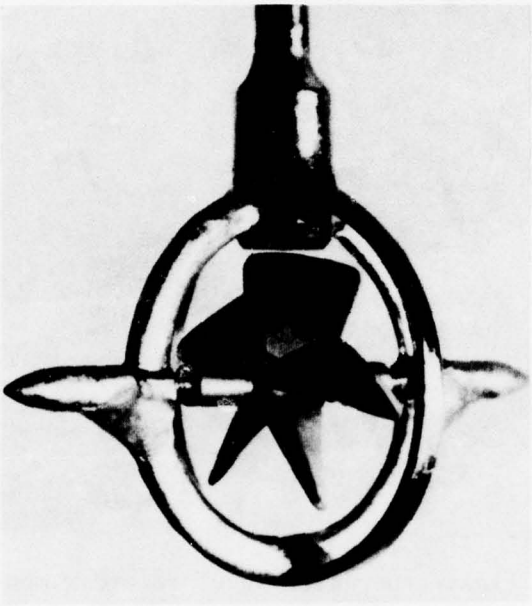

Figure 14. Propeller current velocity meter.

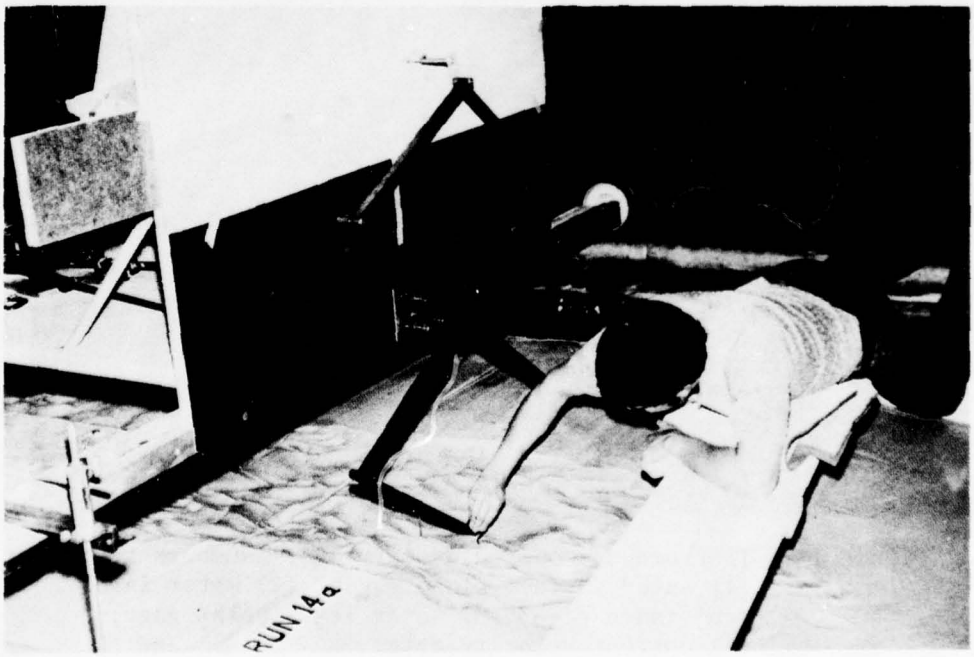

Figure 15. Reproduction of inlet cross sections on paper.

meter and the shallow-water gages were connected to the four-channel recorder units to record ocean tide, bay tide, inlet tide, and current velocity on the same chart.

Two micromanometers (readings to 0.02 millimeter) were installed close to the float recorders in the ocean and at the center of the bay. Readings at high and low tides were made during the last cycles of a run and the ranges compared with those from the float charts. These readings proved invaluable when water level data were reduced.

The two temporary float recorders (Fig. 9) were used in conjunction with the recorders at the center and the back of the bay to check the propagation of the tidal wave in the bay.

The method of cross-sectioning the inlet channel after the end of a run is illustrated in Figure 15. A vertical planigraph mounted on the bay side of the carriage was used to reproduce the sand surface elevation on tracing paper.

4. Testing Program and Procedures.

The main objective of the tests was to measure the hydraulic response of the bay and movable-bed inlet to tides and waves in the ocean, and to the initial inlet conditions.

Since the development of equilibrium in a tidal inlet model requires a long testing time several parameters were kept constant to reduce the number of tests. The constant parameters were: (a) The slope of the ocean beach (1:30); (b) the beach material (d_{50} = 0.34-millimeter sand); (c) the geometry and surface area of the bay; and (d) the water depth in the ocean below MSL (0.91 to 0.94 foot).

a. Character of Studies and Range of Independent Variables. Most tests were conducted on the uncontrolled (natural) condition of the beach and inlet, first run with tidal action, then re-run with simultaneous tidal and wave actions.

Other runs provided data for the following studies:

(a) Inlet under controlled conditions (jetties);

(b) effect of duration of run;

(c) propagation of the ocean tide in the bay (simultaneous vertical movement of water surface at different locations);

(d) effect of initial conditions (pilot channel area and water level in bay);

(e) effect of wave steepness;

(f) development and movement of bed ripples;

(g) effect of a fixed prismatic channel; and

(h) effects of fixed rippled beds.

The channel centerline profile and inlet cross-sectional area were measured after the end of the last ebbtide flow and, in a few, after floodtide.

The independent variables with selected ranges were:

(a) Period of ocean tidal cycle (20 to 60 minutes),

(b) range of ocean tide (0.054 to 0.150 foot),

(c) pilot channel area (0.082 to 0.434 square foot),

(d) length of inlet channel (7 to 22.5 feet),

(e) wave period (0.75 to 0.95 second),

(f) wave height at beach toe (0.030 to 0.176 feet),

(g) wave steepness (0.011 to 0.064),

(h) duration of run (4 to 25 hours),

(i) water temperature (45° to 76° Fahrenheit) uncontrolled,

(j) freshwater inflow discharge (0.0 to 10.2 gallons per minute), and

(k) slope of bay side of barrier (1:3 to 1:12).

b. Preliminary Runs. Runs 2 and 3 were devoted to preliminary checks of the facilities, i.e., testing procedure, equipment, and instruments. In these runs the inlet barrier was formed by loosely placing just enough dry sand to separate the two basins (run 2) and form a 7-foot-wide barrier (run 3). The runs helped define the magnitude of the independent variables used in subsequent runs.

c. Preparations for a Typical Run. The first step was the formation of the ocean beach, the sand barrier crest, and the bay-side beach. The basins were filled with freshwater, about 2 inches below the barrier crest, to saturate the sand. A wooden straightedge supported on the interior cement beach walls was then progressively moved to obtain a flat beach with a 1:30 slope. The same procedure was followed for the crest and the bay beach, taking care not to cause any compaction of the material. Excess sand was subsequently removed.

Cutting of the pilot channel followed. A trapezoid-shaped board was attached to the front of the carriage and pushed along the inlet's

longitudinal axis to obtain a centered horizontal prismatic channel with a base 1.70 feet wide and 30° bank slopes. This cutting was done slowly to avoid accidental wave generation and resulting bank erosion. Excess sand was removed during the channel cutting.

Next a uniform stillwater level (SWL) was established over the entire basin using care to avoid flow in the inlet.

All recording units were balanced, the instruments calibrated, and the SWL recorded on charts and floats for a short time. The SWL was also read from micromanometers and point gages. The instrument carriage was fixed at midchannel before the actual start of the run.

Three series of test conditions used during the investigation were (prefix n is the run number):

Series A (run nA); tidal action only.

Series B (run nB); tidal and wave action.

Series C (run nC); tidal and wave action with special conditions.

d. Tidal Action Only (Runs nA). The resistance gage recording units and the float recorders were syncronized (before start of run) by turning on the tide generator. Normally, the weir was initially at the mean position and started its upswing movement thus creating a floodtide current into the bay. Where a superelevation in the bay was expected (depending on barrier and inlet characteristics, tidal cycle and tidal range), the bay water level was maintained at an elevation higher than the ocean before the start of the run. This was done by temporarily placing a thin metal blade (Fig. 8) across the channel which helped to prevent exaggerated erosion in the channel during the first floodtide flow into the bay.

High rates of sediment transport were visually observed during the first cycles, most of it as bedload. Ripples were formed and reversed orientation and movement according to the current direction.

Recording of water stages was continuous throughout the run. Slack waters were marked on the charts by manually operating a remote-control marker when reversal of the flow in the channel was observed. The manometer deflection at the orifice meter in the inflow pipe was constantly checked to ensure that the discharge was constant throughout the run.

During the last tidal cycles, readings of high and low water elevations were taken from the micromanometers, current velocities were recorded, and the temperatures of the bay and ocean waters were recorded at 1-hour intervals.

After periodic bay tide motion was attained, the metal blade was dropped vertically on the sand inlet at the slack following the ebbtide flow, to isolate the bay from the tidal action. The tide generator operated until the weir returned to the initial position; then the circulation was from ocean to storage basin back to the ocean. The pipe between the bay and ocean was opened to obtain a common water level in the two basins to prevent any further flow through the inlet.

All recorders continued to register the new common level (final SWL, below the initial level in all runs) obtained when the blade was removed and no flow was observed through the inlet channel. The resistance gages were recalibrated and the SWL read from the micromanometers and the point gages.

Finally, the pump was stopped and the ocean and bay drains opened to allow the slow drainage of the basins into the storage basin until a water level a few inches below the deepest point in the channel bed was attained. In this procedure, the sand bed was wet at all times and the sand grains at the surface layers were held together by surface tension and capillary forces, an ideal condition for the reproduction of the cross sections by the planigraph (Fig. 15). Normally, this cross-sectioning was made at stations spaced at 0.5 foot on the day following the run.

The last step was to profile the channel bottom along its centerline extending from the bay delta to a point oceanward of the original beach unmodified by the currents. Vertical photos of the inlet channel area were taken from the overhead platform.

Durations of runs A ranged from 4 to 7.5 hours, depending on the time required to obtain periodic motion of the bay tides.

Time-lapse photos in Figure 16 illustrate the channel bed development (movement of sand ripples) for a long inlet subjected to tidal action only.

e. Simultaneous Tidal and Wave Action (Runs B and C). Runs B were carried out after part A measurements were completed, the rippled channel becoming the initial condition for the new run. The magnitude of the other independent variables in A remained unchanged; the only difference was the introduction of periodic waves.

Filling of the basins and preparations for the run were similar to those described previously. If bay superelevations were detected in previous runs, the bay level was initially set at that elevation and the metal blade removed only when the level in the ocean was high enough to initiate flooding of the bay. The run was then started, and the selected waves were introduced at mean ocean level only after one or two cycles of tidal action. This procedure was changed for runs 4 and 5 where waves were introduced simultaneously with the start of the tide, i.e., part A was eliminated.

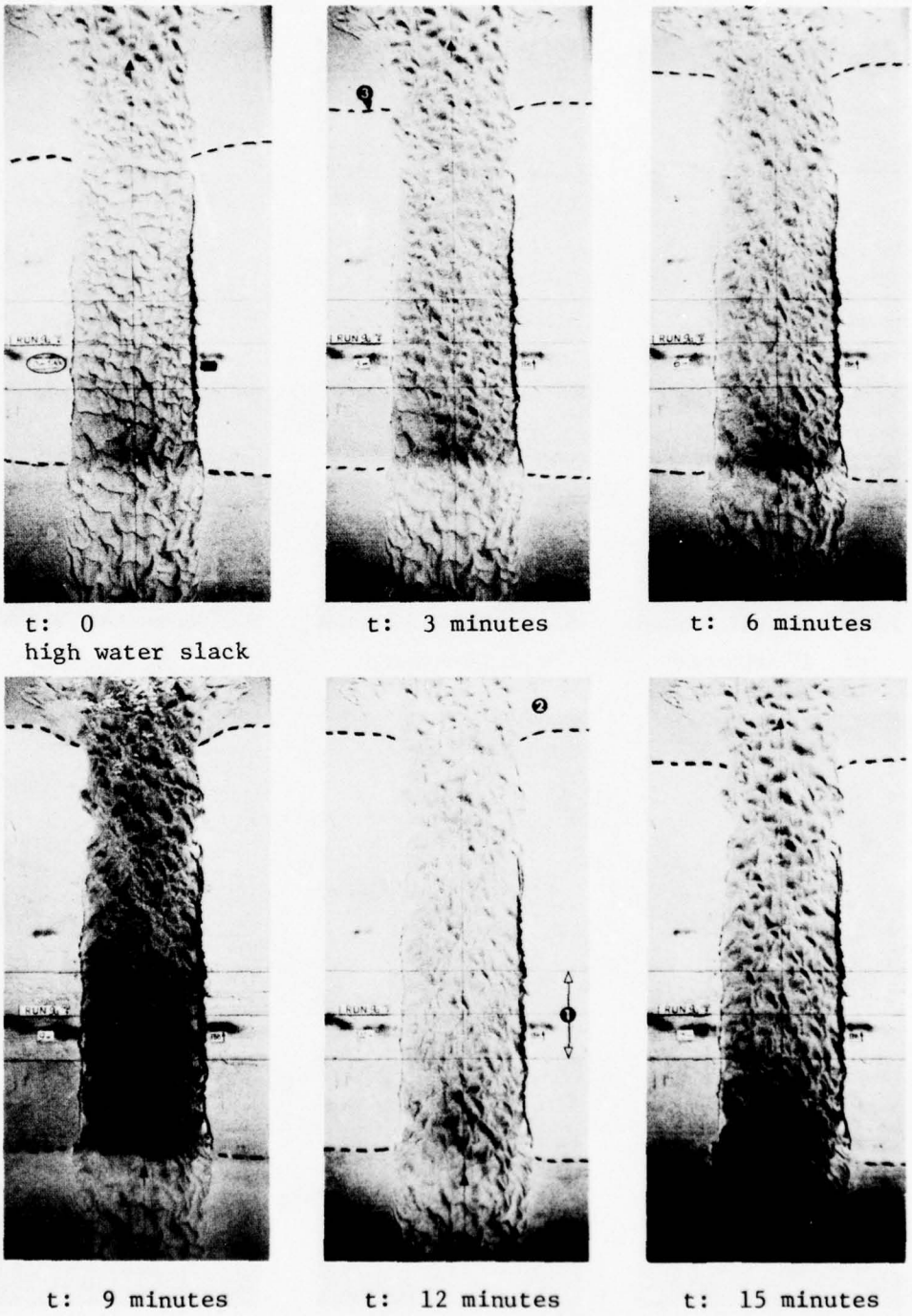

Figure 16. Time-lapse photos showing evolution of a long channel bed (run 9A, cycle 9) under tidal action (ebbtide). Tidal period is 30 minutes. Numbers are: (1) 2-foot barrier crest; (2) ocean: (3) waterline.

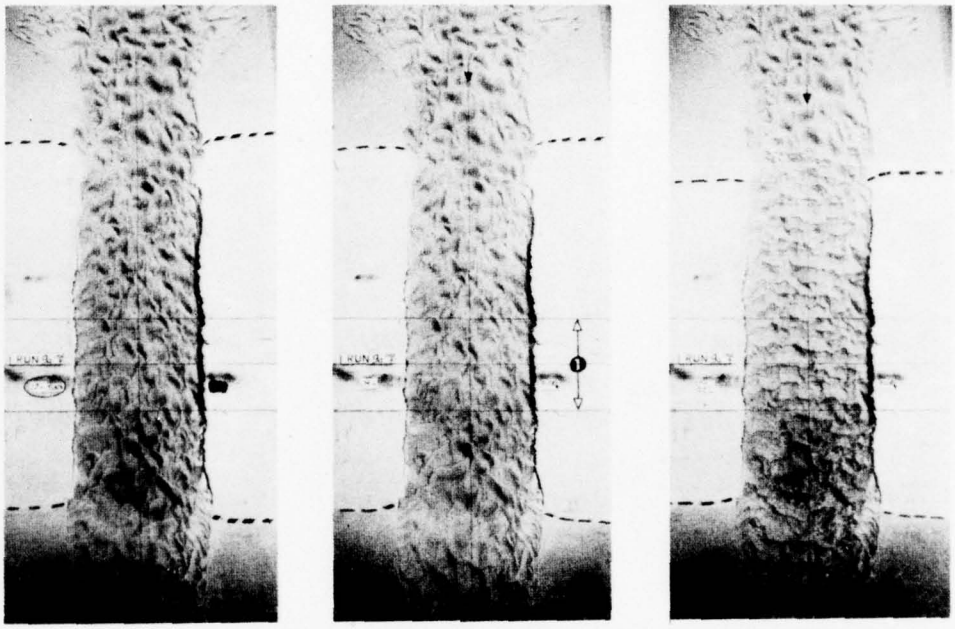

t: 17 minutes
low water slack

t: 18 minutes

t: 21 minutes

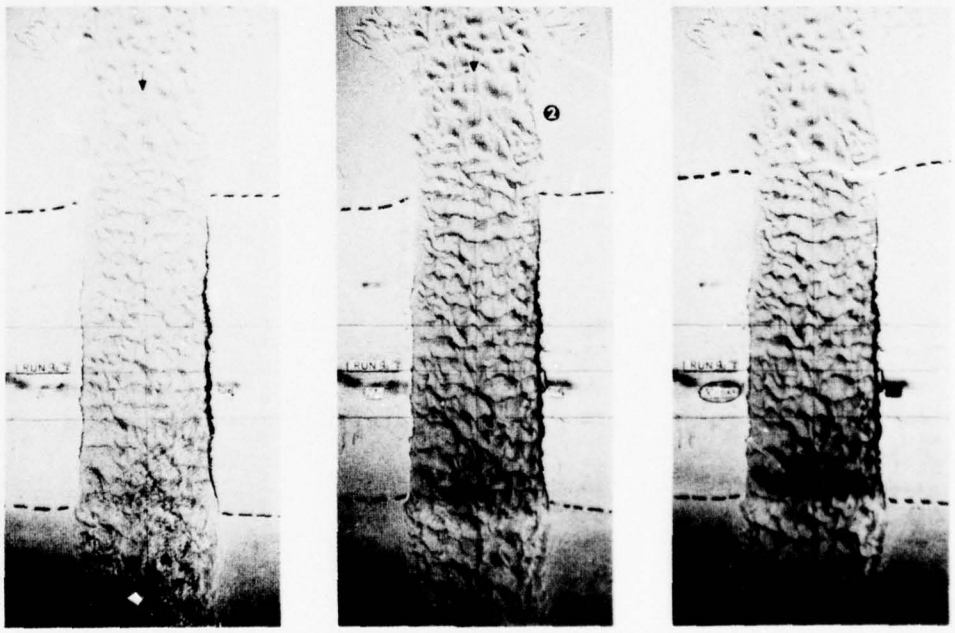

t: 24 minutes

t: 27 minutes

t: 30 minutes
high water slack

Figure 16. Time-lapse photos showing evolution of a long channel bed under tidal action (floodtide).--Continued

Period and height (flap stroke) were constantly checked at regular intervals throughout the run to ensure uniform wave conditions. Wave heights varied slightly because of the varying water depth (submergence of flap) and the presence of currents from or into the inlet. Mild waves (deepwater steepnesses smaller than 0.0215) were selected for most runs; only a few steep waves were studied because of time limitations.

The evolution of the beach and inlet channel was different from that observed under tidal action. The beach geometry adjacent to the inlet was shaped in response to the waves and currents, the sand transport towards the bay increased, the channel banks became flatter, and ebbtide channels became more defined. The inlet region (short channels) presented the funnellike shape commonly observed in natural inlets, with the narrowest section (throat) on the bay side. This region initially advanced towards the bay at a fast rate, until it reached a position when the bay tide became periodic; some long channels tended to meander.

A series of photos in Figure 17 show the inlet configuration and the current and wave patterns for a run with a short channel; note the sandspits, the geometry of the inlet region, and the wave action in the bay during floodtide.

Water levels were usually recorded continuously from the start to end of a run. Current velocities at the inlet and extreme water levels in the bay were recorded during the last few cycles. The carriage supporting the instruments was positioned so that the gages and the current meter were at the throat region at all times. The run was usually completed on the same day; however, in a few instances the run was halted and resumed the following day. Halting the run was necessary for long inlet channels (wide barrier) that required long run times. The duration of runs nB ranged from 4 to 25 hours.

As in part A, most runs ended at slack water following the ebbtide flow, and the final procedures discussed previously were repeated. Inlet cross sections were spaced at 0.25- to 0.20-foot intervals.

After the final measurements were taken, some of runs B were extended from 2 to 18 hours and subjected to the same environment (run C) to detect further evolution and movement of the throat region (run 8C), hydraulic changes due to steeper waves (run 11C), or both the effect of time and of ending the run after the floodtide flow on the cross-sectional area of the throat (run 12C). Two exceptions to the standard procedure were: (a) Run 18B, for which the channel from run 17B was used as a pilot channel, and (b) tidal period increased from 30 to 45 minutes and waves were introduced immediately after the start of the run. Run 9B followed run 9A without interruption.

f. Inlet Controlled by Jetties (Runs 7C and 18C). Tests with jetties followed runs 7B and 18B with the wave conditions and ocean tide unchanged. Idealized jetties were formed using two long thin aluminum sheets riveted to a reinforced frame (Fig. 18) which was installed in

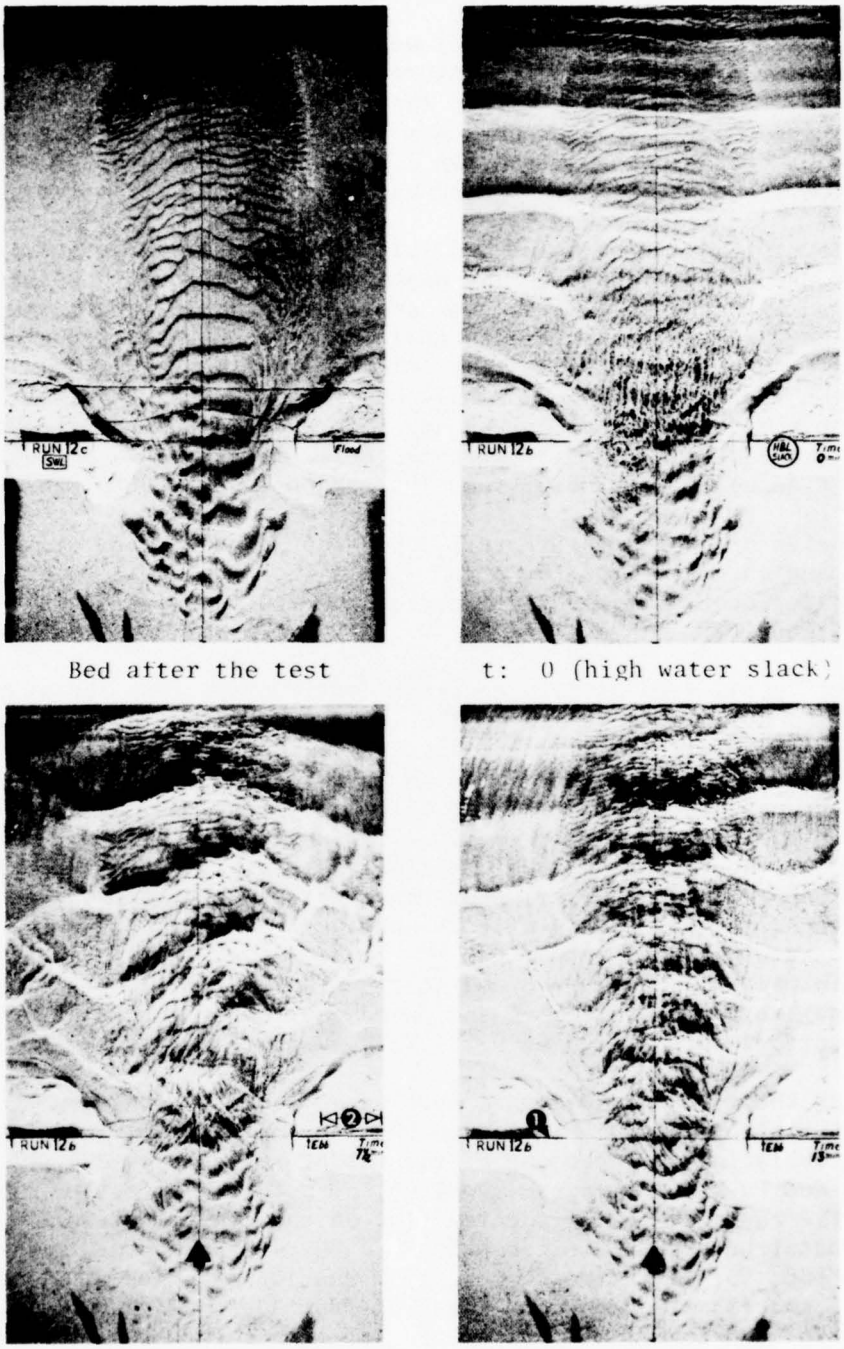

Bed after the test

t: 0 (high water slack)

t: 7.5 minutes

t: 13 minutes

Figure 17. Time-lapse photos showing a short inlet (run 12B, cycle 8) under tidal and wave actions. Tidal period is 60 minutes; wave period 0.75 second. Numbers are: (1) sand barrier crest; (2) 1 foot.

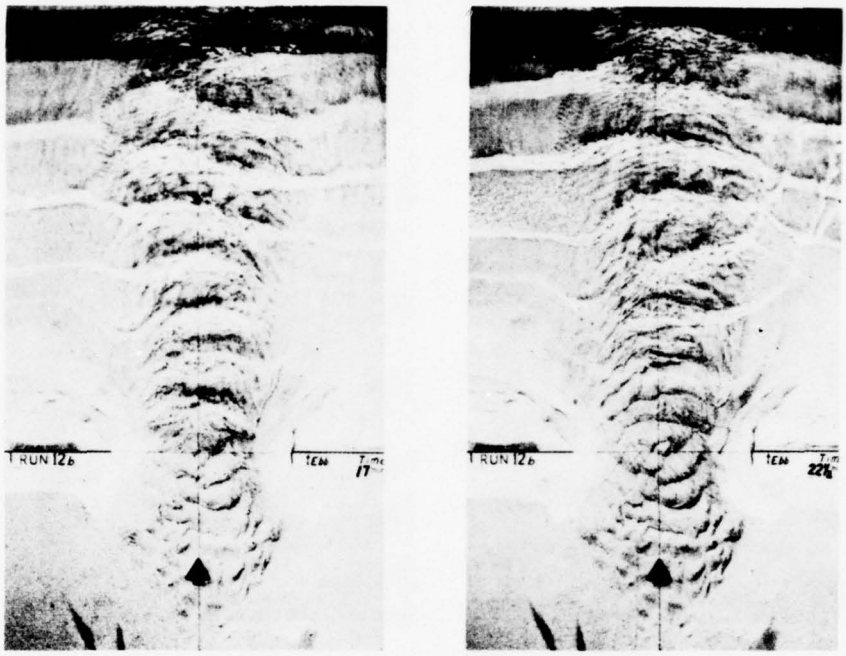

t: 17 minutes

t: 22.5 minutes

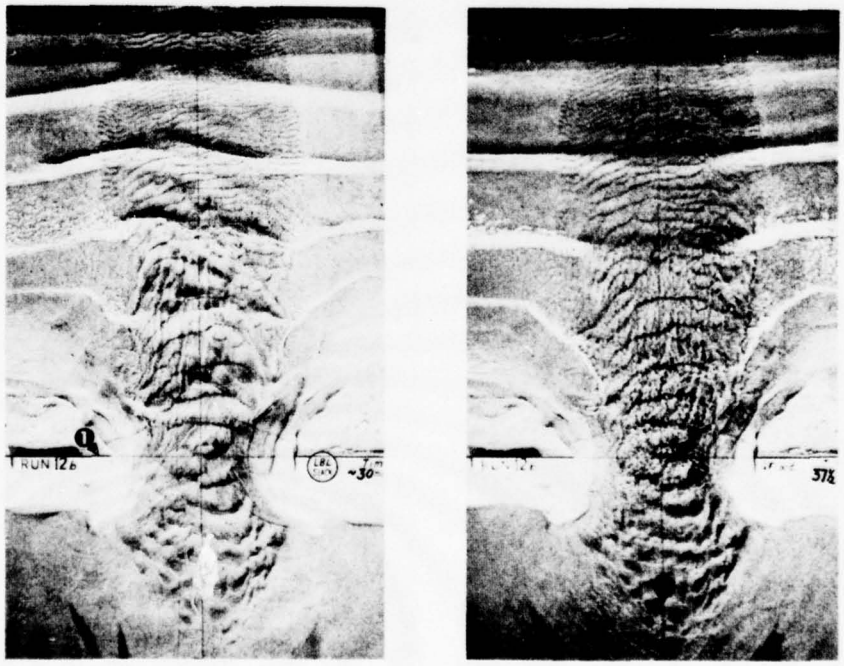

t: 30 minutes
Low water slack

t: 37.5 minutes

Figure 17. Time-lapse photos showing a short inlet under tidal and wave actions.--Continued

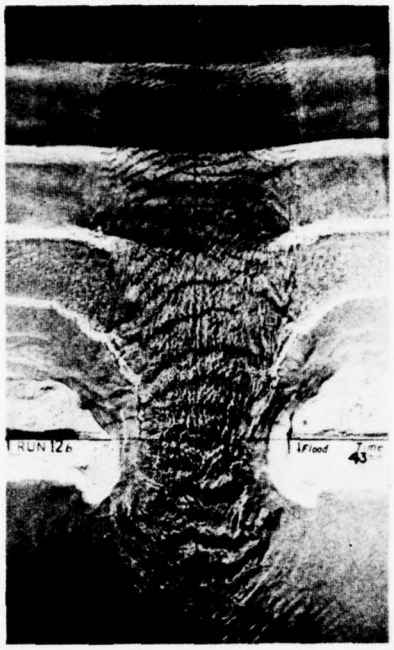

t: 43 minutes

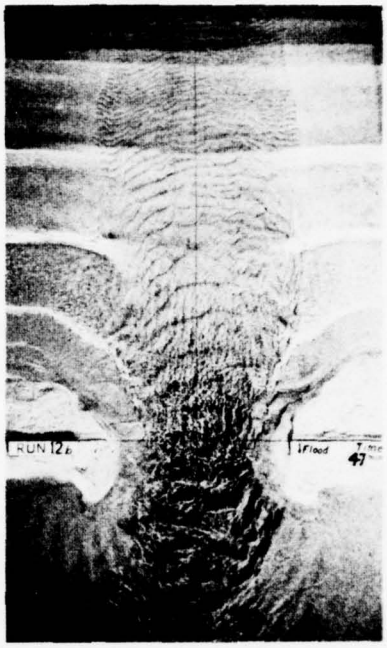

t: 47 minutes

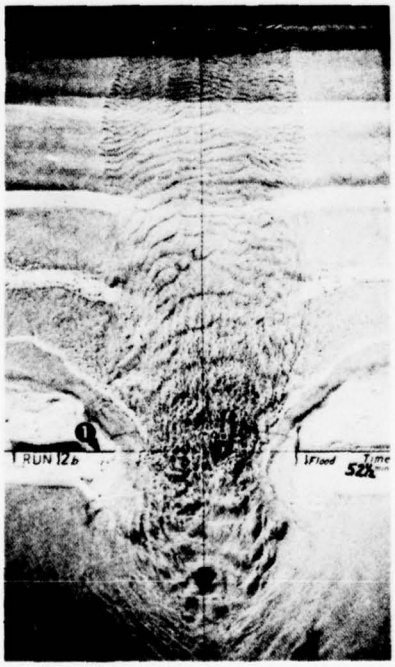

t: 52.5 minutes

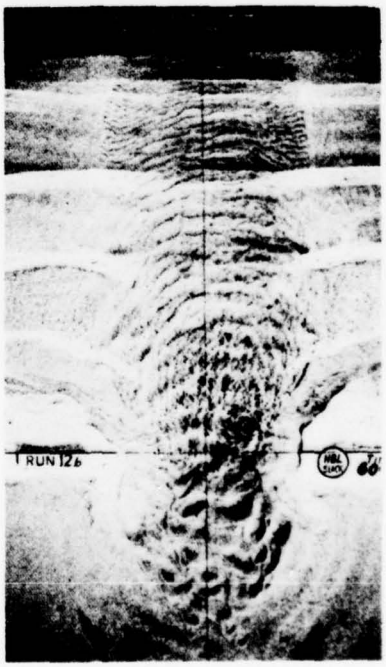

t: 60 minutes
(high water slack)

Figure 17. Time-lapse photos showing a short inlet under tidal and wave actions.--Continued

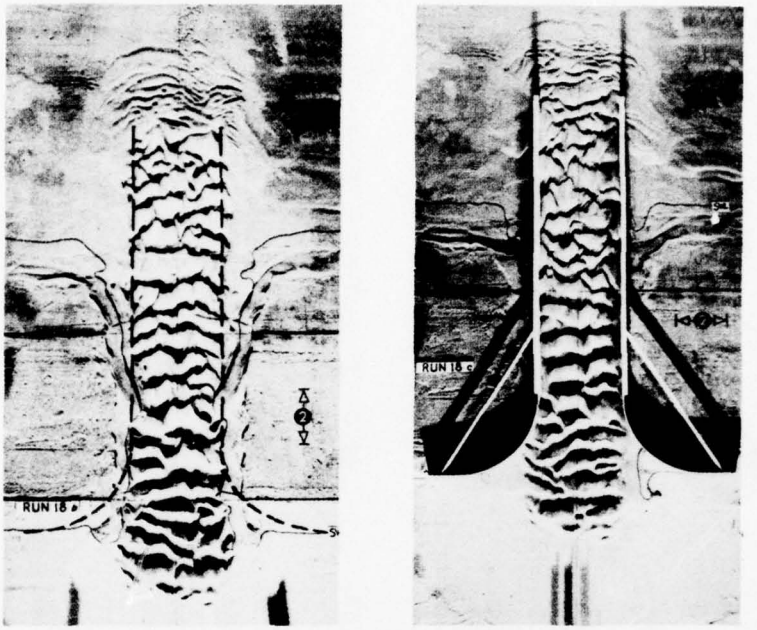

Bed before run | Bed after test completed

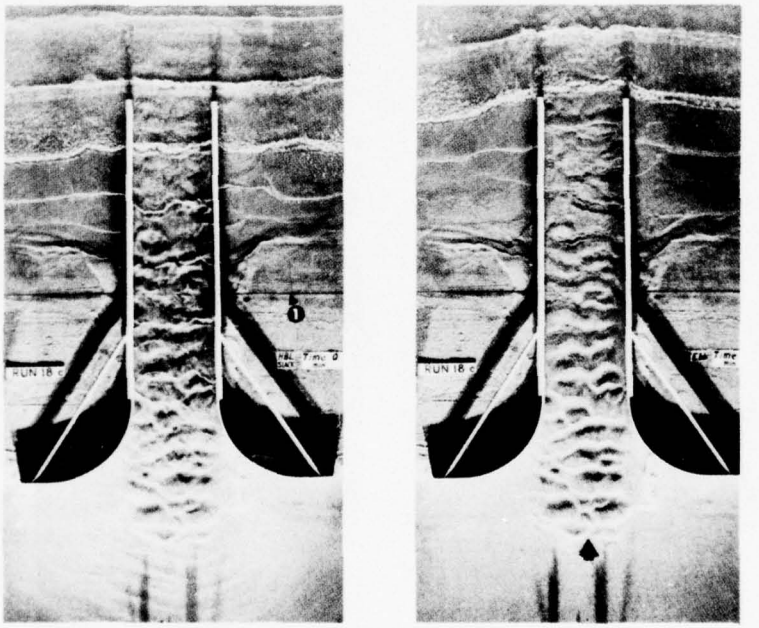

t: 0 (high water slack) | t: 5 minutes

Figure 18. Time-lapse photos showing an inlet controlled by smooth vertical jetties (18C, cycle 7) under tidal and wave actions. Tidal period is 45 minutes; wave period is 0.75 second. Numbers are: (1) start of ocean beach; (2) 1-foot length to show model size.

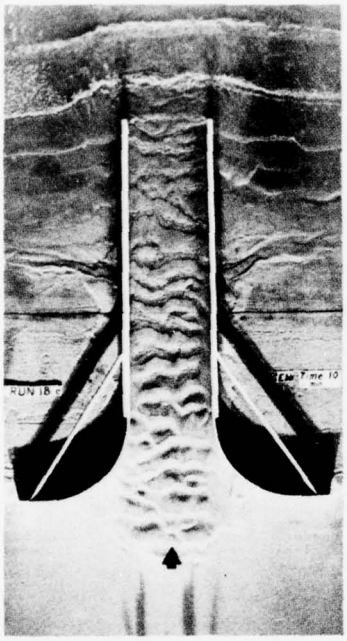

t: 10 minutes

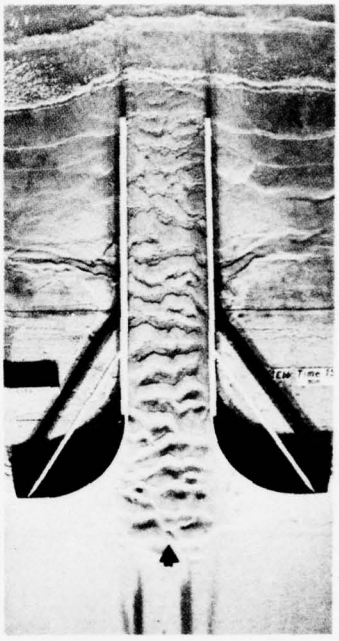

t: 15 minutes

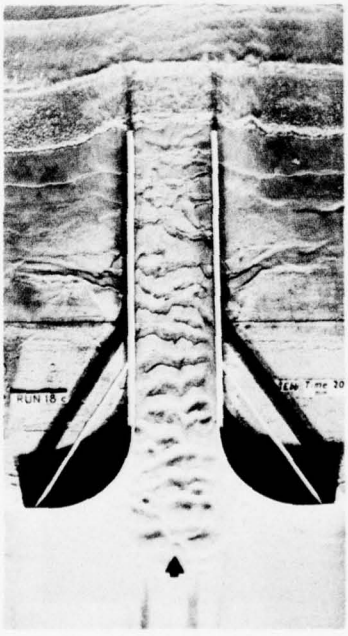

t: 20 minutes

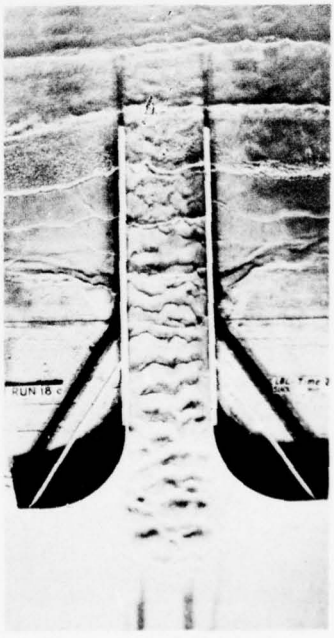

t: 25.5 minutes
(low water slack)

Figure 18. Time-lapse photos showing an inlet controlled by smooth vertical jetties under tidal and wave actions (ebbtide). --Continued

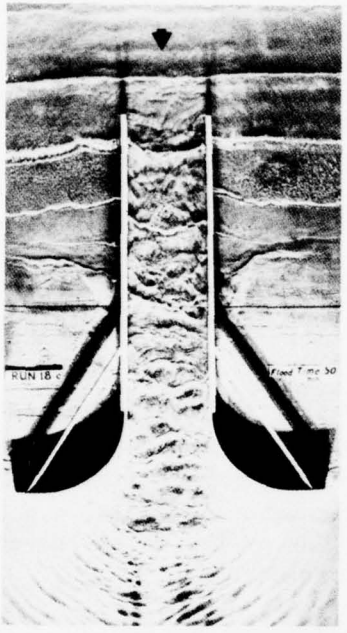

t: 30 minutes

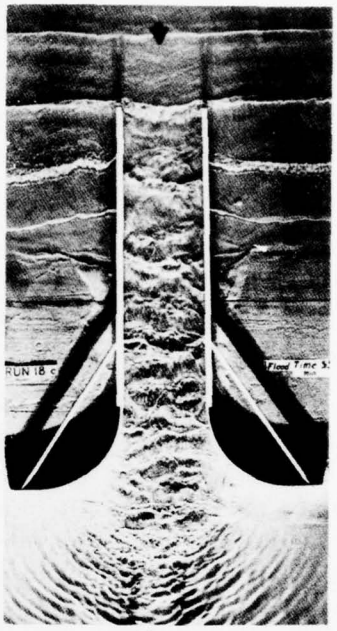

t: 35 minutes

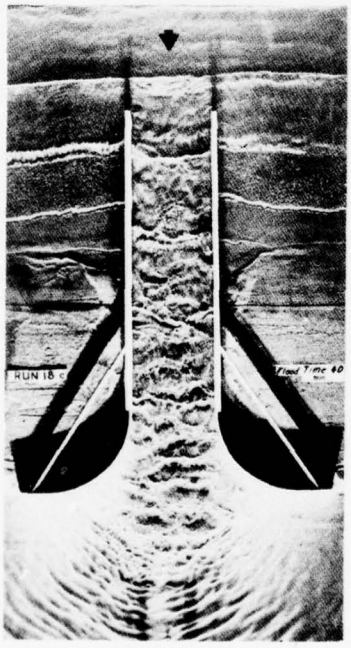

t: 40 minutes

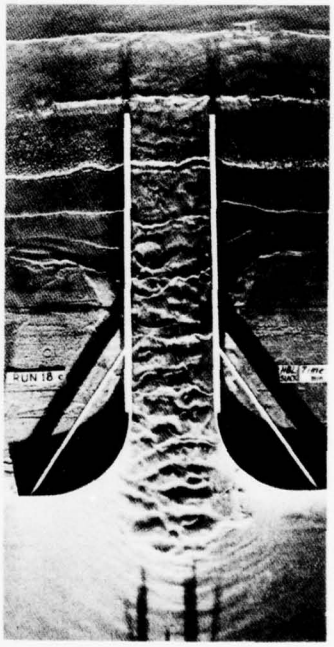

t: 45 minutes
High water slack

Figure 18. Time-lapse photos showing an inlet controlled by smooth vertical jetties under tidal and wave actions (floodtide). --Continued

the channel from the previous run. The vertical walls were parallel in the straight section and alined to the initial pilot channel. The jetties extended into the ocean offshore of the low water level mark on the beach. The bed between the walls was undisturbed. Lengths of the jetty straight sections were 12 and 6 feet, and width of the channels 2 and 1.6 feet, respectively.

Before the start of the run the superelevation measured in part B was introduced in the bay, separated from the ocean by a semicircular barrier placed on the bay beach. Waves were introduced immediately after the floodtide flow started.

The first two photos in Figure 18 show the "uncontrolled" inlet bed (run 18B) before placement of the jetties and the channel bed at the end of the "controlled" inlet run. The photos in this figure illustrate the flow and wave patterns at the inlet throughout a cycle, e.g., the large amount of energy transmitted into the bay by the waves traveling along the channel (smooth walls) during floodtide.

Durations of these two runs were 24 hours for run 7C, and 7 hours for run 18C.

g. Freshwater Discharge into Bay (Run 16C). After cross-sectioning and profiling of the channel for run 16B, the test was resumed under the same wave and tide conditions. One and one-half cycles later a constant "freshwater" discharge, from the city water supply, was introduced into the bay (at the corner farthest from the inlet) until the end of the run. This discharge was measured by a rotameter. The constant rate of flow was 10.2 gallons per minute which corresponded to about 9 percent of the maximum discharge through the inlet at strength of ebbtide for run 16B.

A comparison of the configuration of the channel bed before the start and after the end of this run which lasted 4.5 hours, is shown in Figure 19. The main difference is the shape and size of the ripples close to the throat, probably caused by the increase in duration of the ebbtide flow and the superelevation and the peak velocity at the throat. The minimum cross-sectional area below MSL was equal to that measured before the start of the run.

h. Fixed Ripple Bed under Tidal Action (Runs 12E and 12F). Two similar runs (12A and -12A) were conducted as described for runs nA to determine the variation of the friction characteristics of a short inlet resulting from the orientation of the bed ripples. The resulting channel beds were fixed after the end of ebbtide and floodtide flows. Tidal action was resumed afterwards. Fixing of the channel bed was done by sprinkling fast-setting plaster on the wet ripples and beach; thus, a 0.004-foot-thick fixed plaster layer covered the entire inlet region. Figure 20 shows the two fixed channels; run 12E is on the ebbtide ripple bed and run 12F is on the floodtide ripple bed. The pilot channel trace

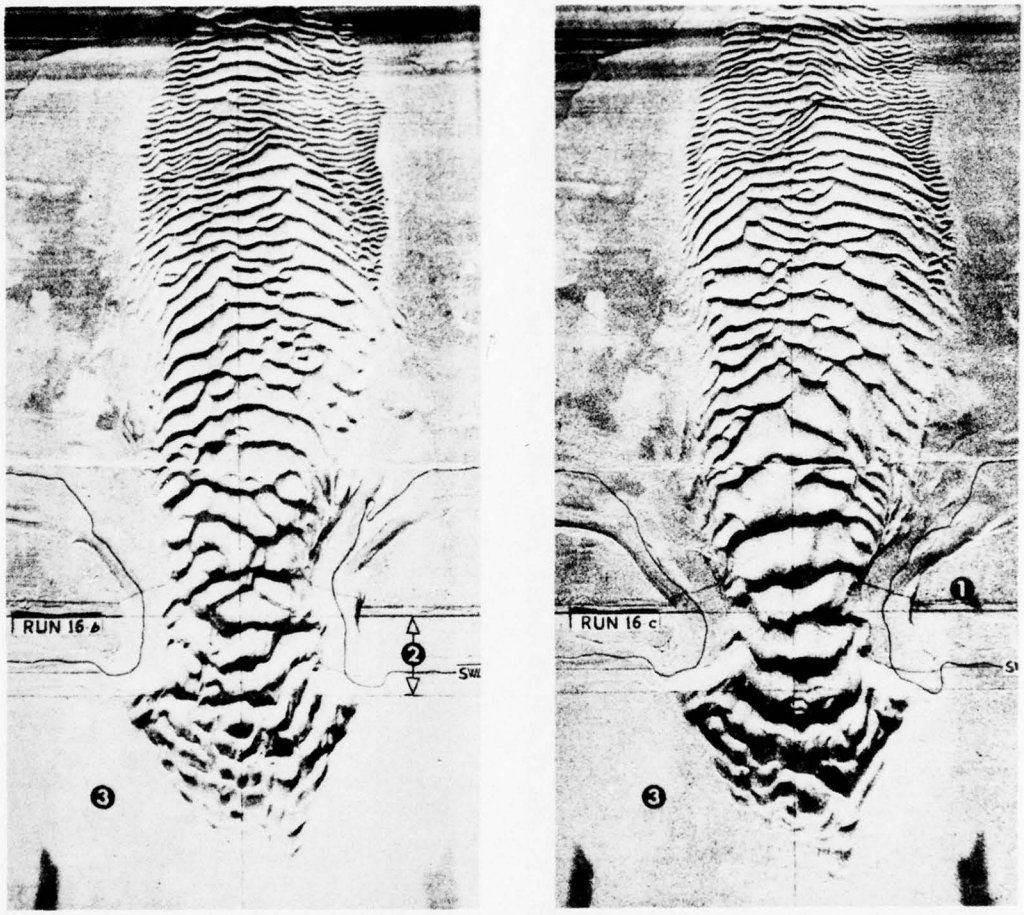

Before run 16C

After last ebbtide

Figure 19. Photos showing a short inlet bed after last ebbtide in a bay with "freshwater" discharge and before start of run 16C. Numbers are: (1) sand barrier crest; (2) 1 foot; (3) bay side of barrier.

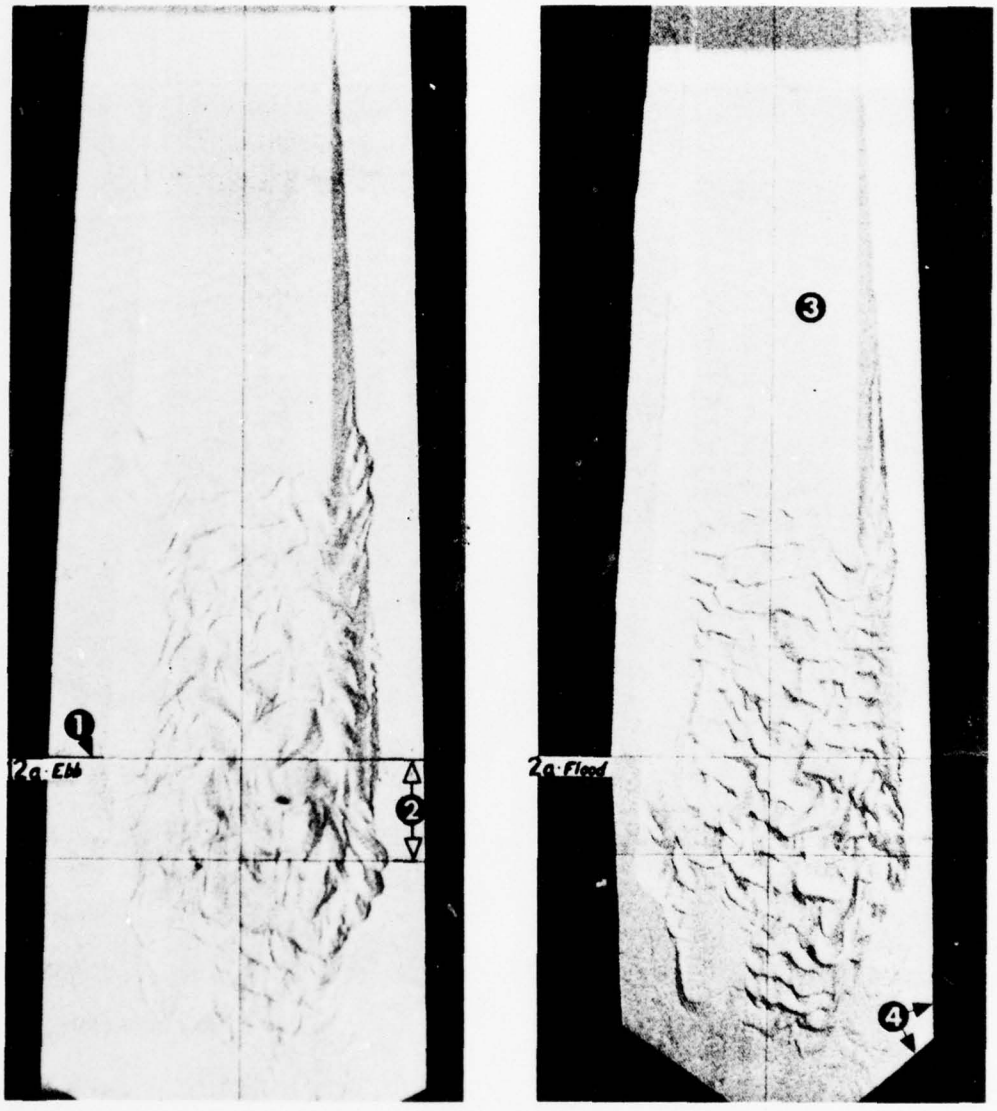

Bed after ebbtide (Run 12E)

Bed after floodtide (Run 12F)

Figure 20. Photos showing short and deep inlet beds "fixed" with plaster after last ebbtide and after last floodtide, under tidal action only. Numbers are: (1) sand barrier crest; (2) distance equals 1 foot for photo scale; (3) ocean section of pilot channel unaffected by currents; (4) edge of plaster layer.

on the oceanside is still visible in the figure because the cross-sectional area of the channel is large (channel depth large compared to tidal range), and the currents are not strong enough to move sediment in this region. The plaster layer thickness was considered in the computation of areas, widths, and perimeters.

Duration of each run was 4 hours. The plaster layer in run 12F was carefully removed, and the initial movable bed preserved as the pilot channel for run 12B with wave action.

i. Fixed-Bed Prismatic Channel (Run 11). A special test was conducted on a trapezoidal inlet (1.70-foot base; 30° banks) cut in a narrow sand barrier (bottom length 7 feet) and fixed with plaster to contrast the results from the movable-bed studies with those of idealized fixed prismatic channels.

The test involved only tidal action (run 11A) during a 3-hour period, followed by 4 hours of simultaneous tidal and low wave action (run 11B). Run 11C used tidal and steep wave actions for 2 hours. In each run, the time required to establish a periodic bay tide was considerably shorter with the fixed-bed model than the previous movable-bed tests.

IV. EXPERIMENTAL DATA

1. Measurements.

a. Ocean and Bay Tides and Current Velocities. Samples of the charts used to record tides in the ocean, inlet channel and bay (resistance gages), and flow velocities (current meter at about 60 percent of the depth) at the throat or at midchannel for runs A, are shown in Figure 21. Tide scales were not necessarily the same for the three tide gages--the signal from the bay was amplified two times for better interpretation, especially in the runs with small bay ranges. The figure shows slack watermarks at the bottom of the chart. Chart speed was 5 millimeters per minute and the galvanometer error ±0.25 millimeters over the central 4 centimeters.

In runs B and C, the wave action at the throat was sometimes so high during floodtide that the water level gage recorded the wave spectrum. These high-frequency signals were eliminated for the remaining tests by installing filters in the electronic circuits (300-microfarad capacitors) that allowed recording of the mean water elevations during the run.

Ocean and bay tides were also recorded by separate float recorders. A pen was mounted on a rod attached to a float to give a scale of 1:1 and a chart speed of 15 millimeters per minute. A comparison of readings made with the micromanometers and the float recorders showed a difference of less than 4 percent of the average reading.

b. Water Surface Slope at the Inlet. The remaining tests included recording of the water elevations and determination of the water slope

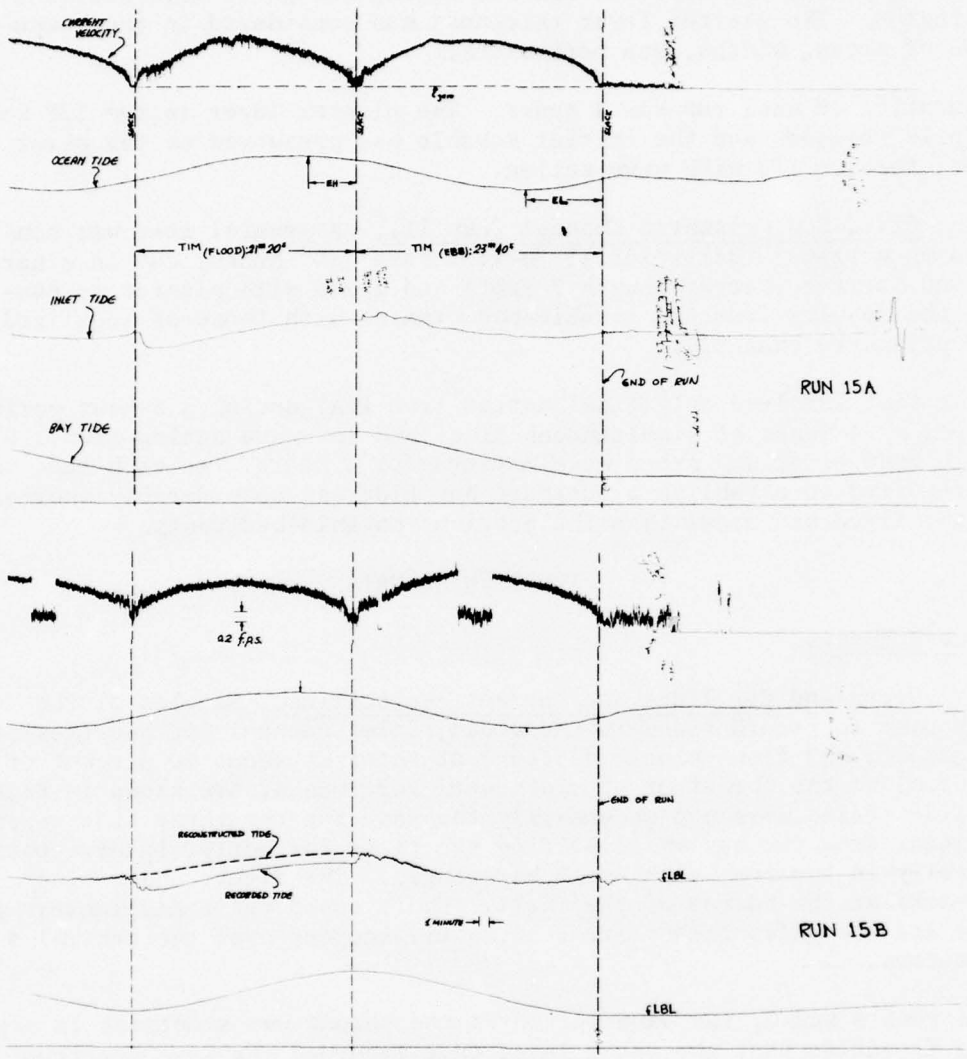

Figure 21. Samples of current velocity and ocean, inlet, and bay tide recordings by resistance gages. Last cycles of tidal action (run 15A) and tidal and wave actions (run 15B).

in the inlet throat region. Typical records are shown in Figure 22; traces in the lower part of the figure (run 15B) are the water surface difference in elevation between the locations of the two resistance gages (separated 3 to 4 feet along the channel centerline), and the piezometric difference of the same points obtained by placing normal resistance gages each inside two 1-inch diameter stilling wells connected by thin plastic tubing to intakes placed in the sand about 3 inches above the basin bottom and directly below the resistance gages. The stilling wells were 4 inches apart and always surrounded by bay water so that any change in water temperature was the same for both, and the signal was not affected by temperature change. Water stage at the throat (located midway between the slope-measuring gages) was also recorded on the same chart. The upper part of Figure 22 shows the traces corresponding to the tide-only condition.

c. Surface Waves. The two wave gages were installed along the beach centerline, one at the beach toe and the other 3 to 4 feet oceanward. Waves were modified by the currents and water depths (tide), and by reflections and uncontrolled vibrations from the wave machine. Chart speeds were 5 and 0.5 millimeters per second.

d. Flow Cross Sections. Typical sections for a short and deep channel, and location of the current meter propeller, are shown in Figure 23. The trace of the channel bed surface at different stations was obtained from the planigraph used to reproduce the cross sections.

e. Overhead Photography. Vertical photography was taken to document all inlet runs. Photos in Figure 24 show the channel bed (long channel) at the end of a run under tidal action only, at the end of the run that followed (tidal and wave action) and at the end of a run extension. Runs shown in the figure ended at slack water after ebbtide flow, as indicated by orientation of the sand ripples. In a few cases, the channel was contoured.

f. Inlet Channel Profile. The profile along the centerline of a pilot channel (Fig. 25) was obtained by computing depths below MSL from readings (to the thousandth of a foot) of the bed taken with a point gage mounted on the carriage. It covered the distance from the bay delta to the small ripples found on the original beach. Care was taken to record the lowest and highest points of the channel ripples as well as their shapes.

g. Logbook. High and low water and SWL readings from the micromanometers, water temperatures, hook gage readings, inflow manometer readings, current meter locations, and all other pertinent information (including visual observations) were registered in a logbook during the experiments.

2. Measurement Problems.

Temperature variations between the bay and ocean occasionally caused significant jumps in electronically measured water levels; these records

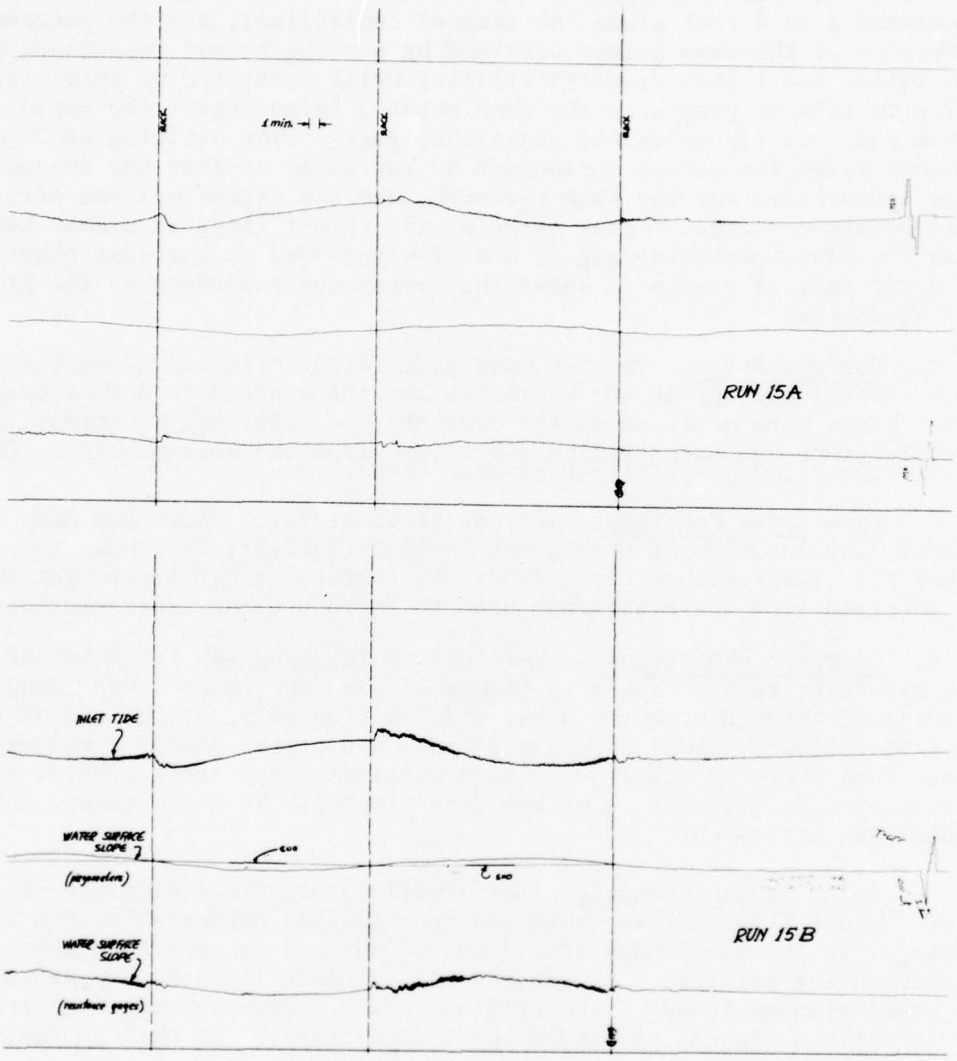

Figure 22. Sample recordings of water surface slopes at midchannel (run 15A) and at the throat (run 15B). Curve at center is proportional to the slope given by piezometers.

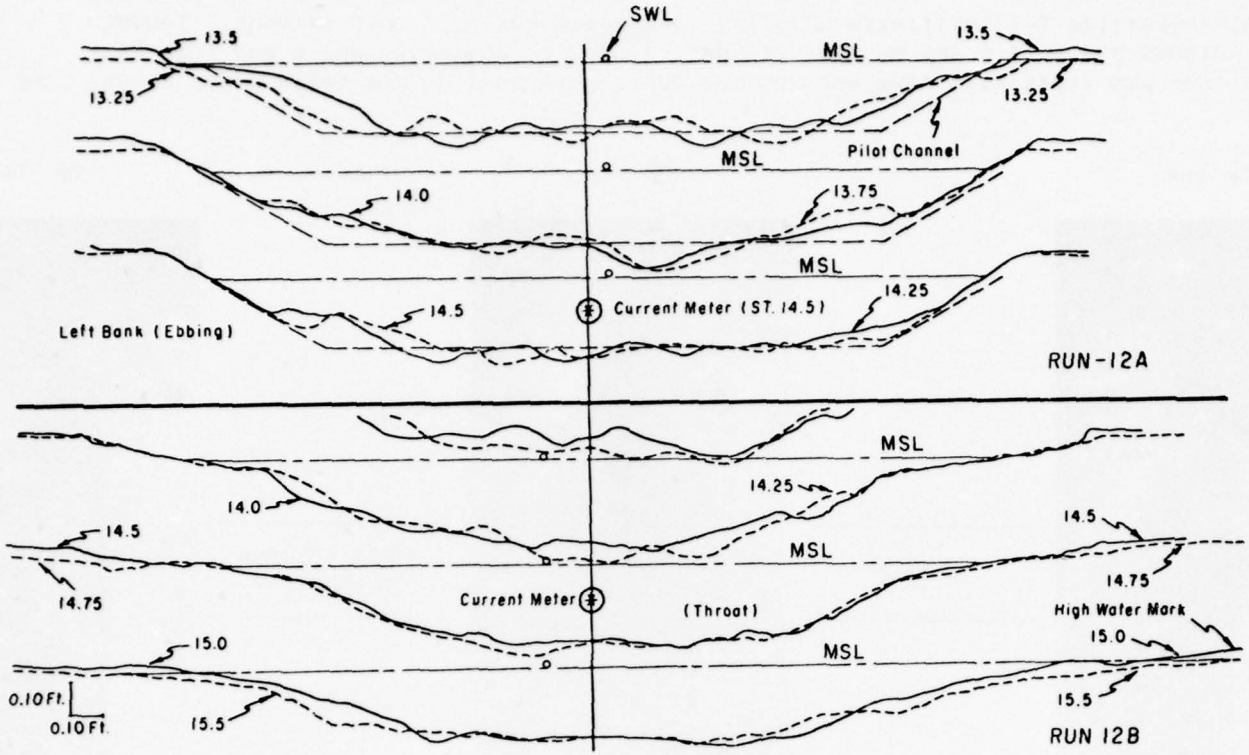

Figure 23. Sample flow cross-sectional records showing the pilot channel and sections at end of runs under tidal action (run 12A); and under tidal and wave actions (run 12B). Typical section for a short and deep channel.

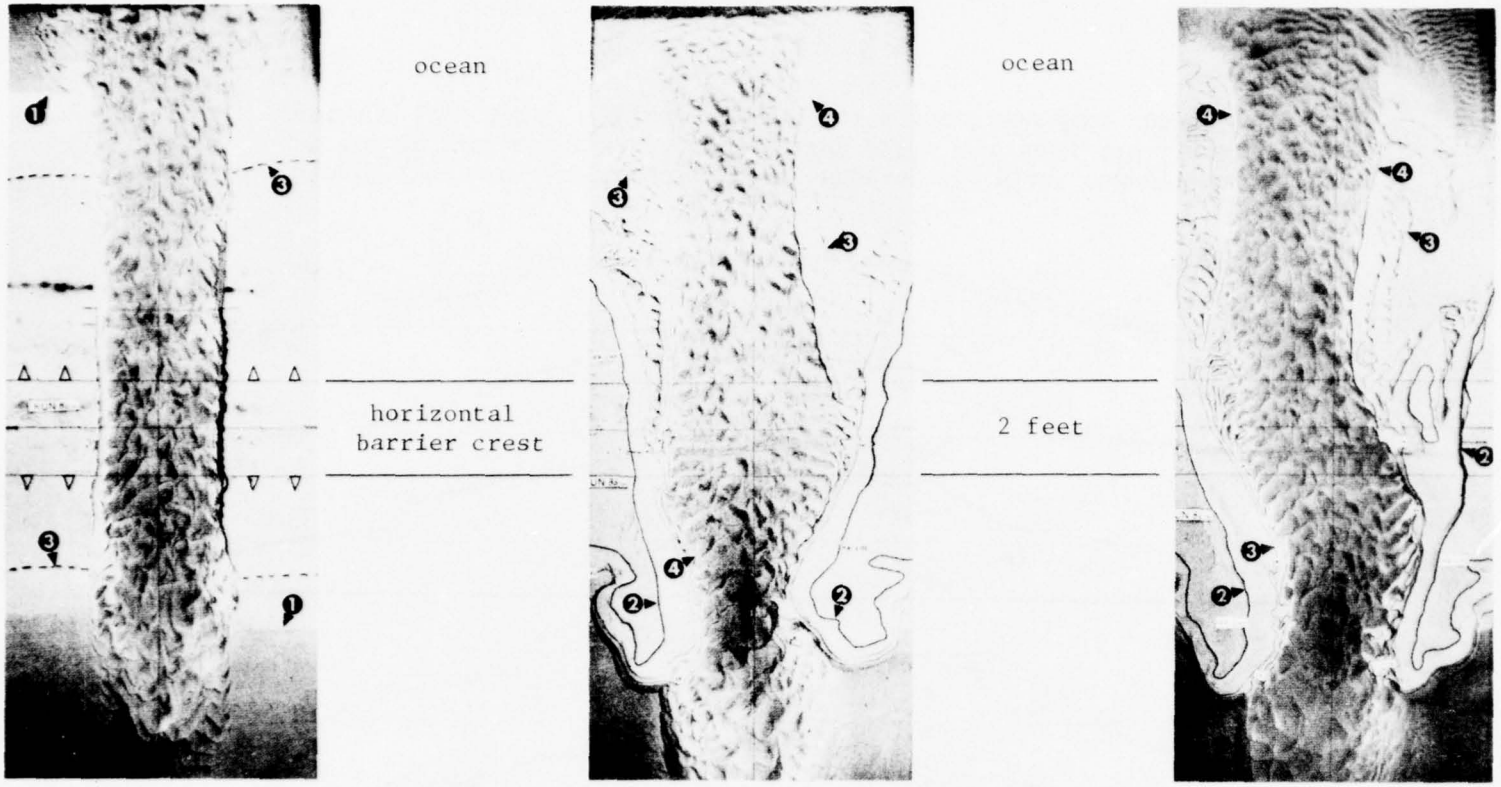

Figure 24. Photos taken after end of runs with tidal action (run 8A), with tidal and wave actions (run 8B), and a run extension (run 8C). Typical section for a long and shallow inlet channel. Numbers are: (1) low waterline; (2) high waterline; (3) stillwater level; (4) 0.04 foot below SWL.

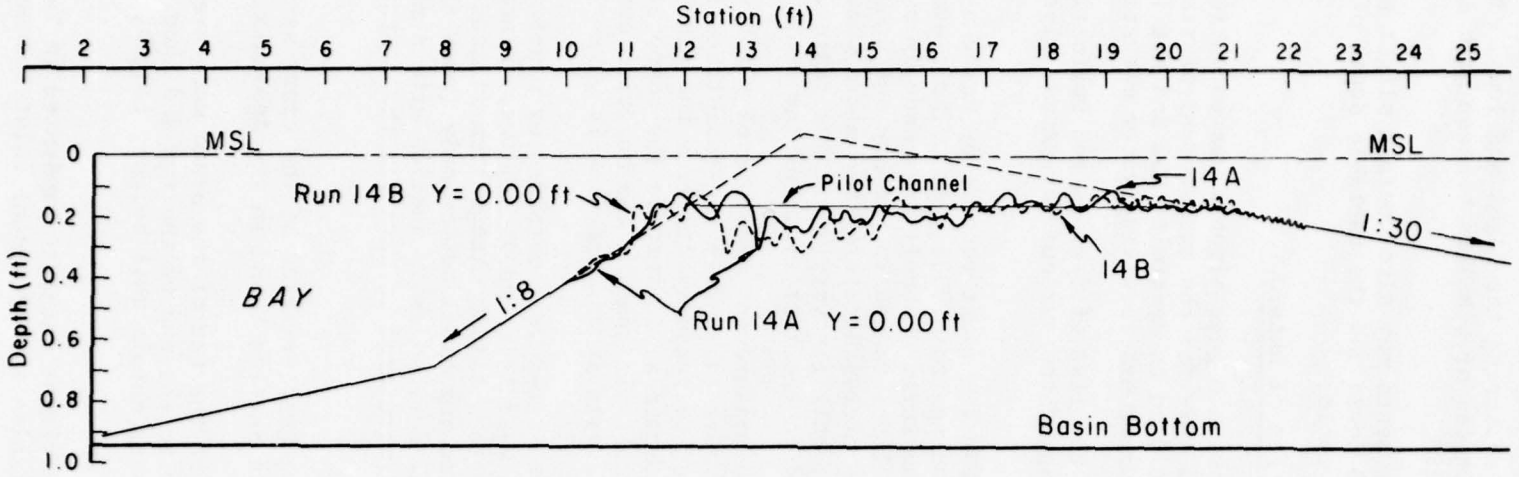

Figure 25. Sample records of vertical profiles along channel centerline (runs 14A and 14B). Typical case for narrow sand barrier.

were corrected by manually measuring the highs and lows. Therefore, some slope measurements and estimates of timelags between high and low waters are only approximate (run 15B).

Current velocity measurements may also contain slight errors due to complex flow induced by bed forms and the variable depth of the current meter throughout the tidal cycle.

3. Reduction and Presentation of Data.

Since drift of the resistance gage signals was uncontrollable, the resulting records were used only for the measurement of time durations and lags. Float gages were used to determine MSL and MBL (mean bay level), as well as other parameters involving water elevations.

Figures 26 and 27, and the list of Symbols and Definitions assist in understanding the meaning of the various parameters given in the tabulation of data.

Elevations were read from the float records by using a special eyepiece that permitted readings to 0.0005 foot. The elevations from the resistance gages (at the inlet channel) were made by using the appropriate calibrations. Tidal ranges in the bay and ocean were compared to those given by the micromanometers; the micromanometers were taken as the most accurate, only for very small bay ranges. All of these readings corresponded to the last cycle of the run.

Lags, duration, and the measurement of slope of the bay tide curve at maximum flow (dh_b/dt) were taken from the resistance gage charts. The slope was often compared to measurements from the float charts and, at times, the charts were chosen as definitive for computations because of irregularities or difficulty in reading the bay tide curve. Justification for compilation of data at maximum flow is given in Section V.

The flow cross-sectional areas were obtained by planimetering. The A_c, W_{MSL}, and p values were selected as follows. Since the shapes and areas of the cross sections seldom change from station to station, average values were computed for tidal action only (runs A). Whereas, for runs with waves (a well defined cross section with a minimum area) the throat characteristics were used as data for the computations in Section VI.

Data on the geometric characteristics of the cross sections are given in normalized form in Section V and in the Appendix.

Wave heights measured at the toe of the beach were averaged over several tidal cycles close to the end of the run and then transferred to deep water (linear theory) to obtain wave height, length, steepness, and wave power.

Hydraulic and other pertinent data are presented in Tables 1 to 4, and includes the main variables in the ocean, inlet channel, and bay.

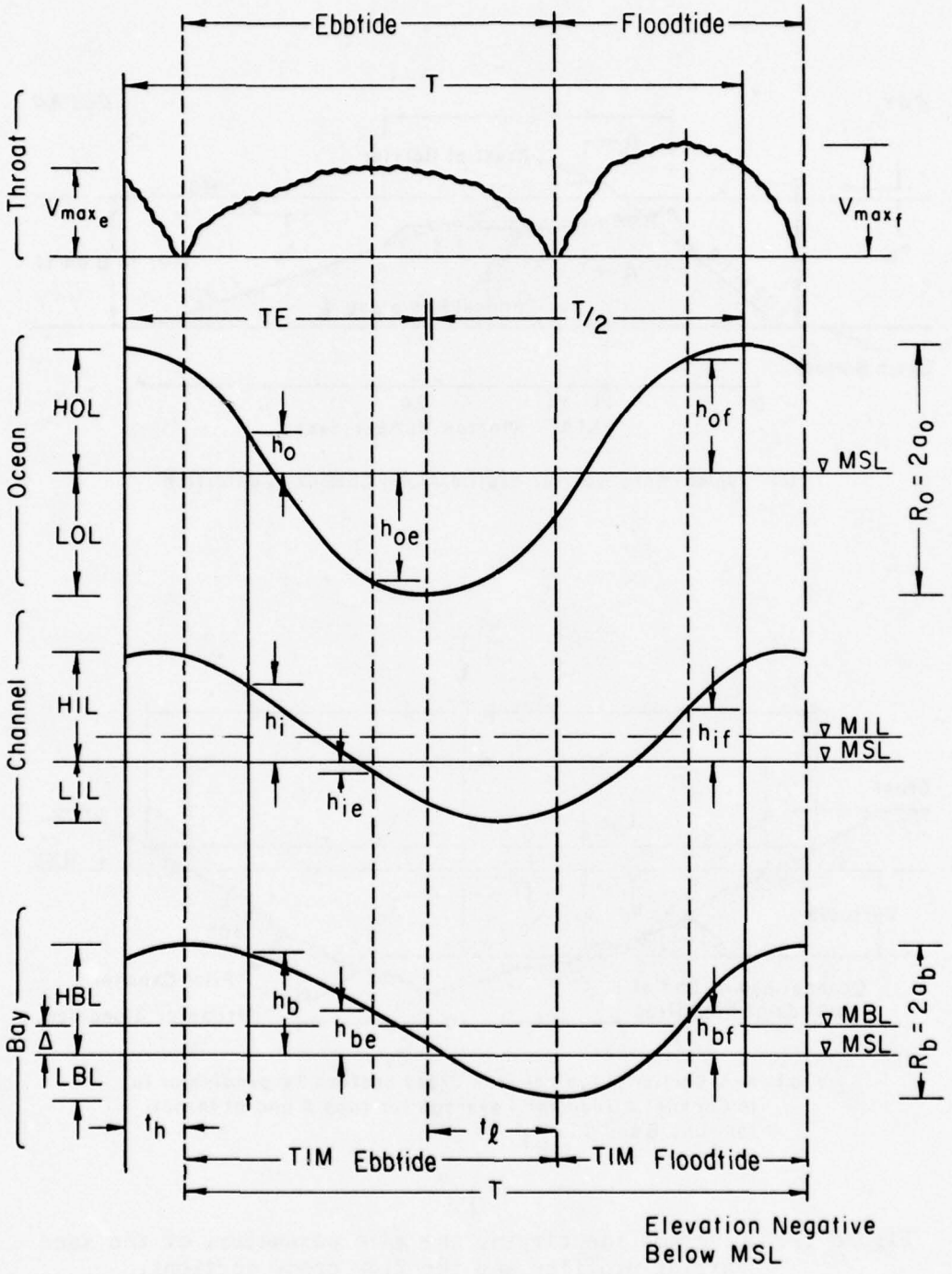

Figure 26. Schematic representation of simultaneous water elevations in the ocean, inlet, and bay; lags and durations; and the velocity at the inlet throat over a tidal cycle.

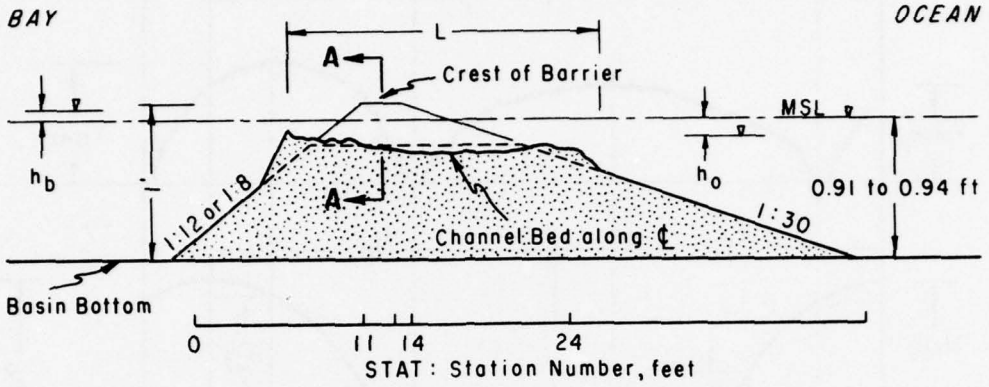

a) Typical Sand Barrier Profile Along Channel Centerline

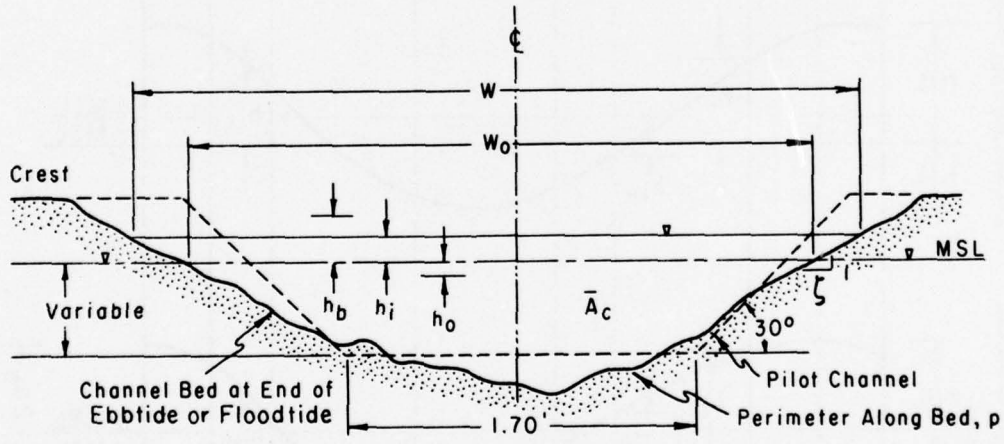

b) A-A Section: Typical Flow Cross Section Perpendicular to to Channel Alinement (average for runs A and at throat for runs B and C)

Figure 27. Diagrams identifying the main parameters of the sand barrier profiles and the flow cross sections.

Table 3. Bay experimental variables.

Run	A_b (ft^2)	Water temperature (°F)	Bay tide				Variables at maximum discharge						Remarks
							Tide level		Rate of bay water level change		Tide		
			R_b (ft)	High (ft)	Low (ft)	Mean bay level (ft)	Ebb (ft)	Flood (ft)	Ebb (10^{-5} ft/s)	Flood (10^{-5} ft/s)	Ebb h_f, h_c	Flood h_c, h_f	
2	5930	.....[1]	0.0530	.....	.....	.....	.....	.....	.....	.....	.....	.....	Preliminary run
3	5930	.....	0.0100	0.0230	0.0130	0.0180	0.0180	0.0160	2.91	4.58	0.0840	0.0500	Preliminary run
4	5930	.....	0.0060	0.0555	0.0495	0.0525	0.0525	0.0525	1.45	2.84	0.1200	0.0165	
5	5930	54.5	0.0055	0.0465	0.0410	0.0440	0.0440	0.0440	1.29	2.00	0.1145	0.0230	MSL for R4 adopted
6A	5950	71.0	0.0040	0.0305	0.0265	0.0285	.....	.....	0.80	1.60	.....	.....	
6B	5950	66.0	0.0110	0.0375	0.0275	0.0320	0.0320	0.0320	2.39	3.44	0.1030	0.0350	
7A	5950	70.0	0.0120	0.0355	0.0235	0.0295	0.0310	0.0275	1.67	3.58	0.1045	0.0500	
7B	5950	72.0	0.0300	0.0470	0.0170	0.0320	0.0330	0.0300	4.06	7.30	0.1015	0.0330	
7C	5950	66.0	0.0297	0.0369	0.0071	0.0220	0.0220	0.0220	3.92	5.50	0.0890	0.0435	High wave action in bay
8A	5950	69.0	0.0300	0.0320	0.0020	0.0170	0.0165	0.0130	4.09	6.55	0.0840	0.0465	
8B	5950	68.0	0.0335	0.0463	0.0127	0.0295	0.0300	0.0275	5.08	7.36	0.0970	0.0350	
8C	5950	68.0	0.0357	0.0434	0.0076	0.0255	0.0250	0.0245	4.89	8.10	0.0910	0.0365	
9A	5950	69.0	0.0315	0.0343	0.0027	0.0185	0.0180	0.0170	4.06	7.34	0.0865	0.0480	
9B	5950	69.0	0.0410	0.0455	0.0045	0.0250	0.0225	0.0205	5.70	9.00	0.0875	0.0370	Run follows R9A without interruption
10A	6120	70.0	0.0785	0.0505	−0.0280	.....	0.0045	0.0000	5.17	6.84	0.0605	0.0450	Equilibrium not reached
10B	6120	69.0	0.0840	0.0632	−0.0208	.....	0.0095	0.0095	6.44	8.28	0.0665	0.0310	Equilibrium not reached
11A[2]	6120	68.0	0.0340	0.0210	−0.0130	0.0035	0.0050	0.0010	2.42	2.46	0.0315	0.0225	
11B[2]	6120	66.5	0.0325	0.0215	−0.0110	0.0050	0.0040	0.0080	2.15	2.48	0.0330	0.0190	
11C[2]	6120	67.0	0.0300	0.0245	−0.0055	0.0095	0.0100	0.0040	2.18	2.19	0.0390	0.0200	Follows R11B uninterrupted
12A	6120	68.0	0.0555	0.0290	−0.0265	0.0000	−0.0020	−0.0065	4.21	4.47	0.0195	0.0180	
12E[2]	6120	68.0	0.0530	0.0285	−0.0245	0.0010	0.0005	−0.0040	4.13	4.67	0.0195	0.0175	
12A	6120	68.0	0.0530	0.0250	−0.0280	0.0000	−0.0020	−0.0100	4.09	4.24	0.0135	0.0185	
12F[2]	6120	68.0	0.0520	0.0265	−0.0255	0.0000	−0.0025	−0.0105	4.13	4.74	0.0170	0.0180	
12B	6120	65.0	0.0530	0.0295	−0.0235	0.0025	0.0010	−0.0025	4.30	4.25	0.0225	0.0165	
12C	6120	64.0	0.0495	.....	.....	.....	.....	.....	3.96	4.46	.....	.....	MSL for R12B adopted
14A	6120	61.0	0.0222	0.0130	−0.0100	0.0023	0.0030	0.0015	3.12	3.75	0.0295	0.0225	MBL by micromanometer
14B	6120	61.5	0.0223	0.0163	−0.0060	0.0038	0.0055	0.0040	3.19	3.38	0.0335	0.0205	
15A	6120	62.0	0.0335	0.0195	−0.0140	0.0027	0.0020	−0.0025	3.09	3.49	0.0270	0.0250	
15B	6120	62.0	0.0335	0.0220	−0.0115	0.0040	0.0045	0.0015	3.28	3.42	0.0310	0.0210	
16A	6120	60.5	0.0445	0.0235	−0.0210	0.0012	−0.0005	−0.0025	4.24	4.75	0.0210	0.0185	
16B	6120	61.0	0.0420	0.0235	−0.0185	0.0027	0.0000	−0.0005	4.23	4.65	0.0235	0.0185	
16C	6120	60.0	0.0410	0.0255	−0.0155	0.0050	0.0040	0.0030	4.50	4.75	0.0260	0.0150	10.2 gal/min freshwater inflow into bay
17A	5950	57.0	0.0060	0.0130	0.0070	0.0105	0.0105	0.0085	0.76	1.16	0.0475	0.0240	R_b, MBL by micromanometer
17B	5950	56.5	0.0052	0.0188	0.0136	0.0162	0.0175	0.0150	0.72	1.06	0.0545	0.0170	R_b, MBL by micromanometer
18B	5950	53.0	0.0079	0.0200	0.0120	0.0162	0.0130	0.0145	0.63	0.94	0.0505	0.0195	R_b, MBL by micromanometer
18C	5950	52.0	0.0090	0.0175	0.0085	0.0130	0.0130	0.0130	0.60	1.04	0.0520	0.0210	6-foot parallel jetties

[1]Not determined.
[2]Fixed bed.

Table 4. Experimental and computed parameters for tide-only runs.

Run	a_b/a_o	Bay superelevation		Measured tidal prism	Channel geometry at MSL			Dimensionless duration of tide	Tidal timelag					Inlet velocities				Tide
														V_{max}		V_{max}	Q_{max}	
		Δ/R_o	Δ/R_b	Ω (ft^3)	A_c (ft^2)	R_h (ft)	D (ft)		ϵ_h	ϵ_f	K	F	$K\sqrt{F}$	Theoretical (ft/s)	Measured (ft/s)	(ft/s)	(ft^3/s)	
3	0.075	0.135	1.800	59.3	0.197	0.0961	0.1021	0.600	0.179	0.288	0.081	5.88	0.197	0.96	1.24	0.0833	0.173	Ebb
								0.400			0.108	3.36	0.197	0.98	1.15	0.1310	0.272	Flood
6A	0.027	0.195	7.125	23.8	0.128	0.0610	0.0640	0.633	0.184	0.315	.....[1]	.....	0.123	.....	0.71	0.0210	0.048	Ebb
								0.370			.....	.....	0.123	.....	0.94	0.0420	0.095	Flood
7A	0.080	0.197	2.458	71.4	0.179	0.0740	0.0778	0.616	0.167	0.296	0.049	26.32	0.253	0.51	0.93	0.0638	0.099	Ebb
								0.385			0.098	6.62	0.253	0.70	1.31	0.1367	0.213	Flood
8A	0.219	0.124	0.567	178.5	0.331	0.1195	0.1273	0.581	0.157	0.262	0.179	7.55	0.491	0.85	0.98	0.1716	0.243	Ebb
								0.422			0.261	3.55	0.491	0.92	1.18	0.2748	0.390	Flood
9A	0.227	0.133	0.587	187.4	0.318	0.1156	0.1233	0.585	0.168	0.260	0.160	8.53	0.469	0.81	1.10	0.1681	0.242	Ebb
								0.420			0.289	2.62	0.469	1.09	1.20	0.3039	0.437	Flood
10A	0.628	-----	-----	480.4	0.412	0.1421	0.1543	0.562	0.082	0.182	0.533	5.40	1.239	0.85	1.06	0.4739	0.316	Ebb
								0.438			0.720	2.96	1.239	0.99	1.49	0.6270	0.419	Flood
11A[2]	0.576	0.059	0.103	208.1	0.187	0.0890	0.0917	0.530	0.137	0.175	0.603	1.84	0.819	1.05	1.18	0.4700	0.148	Ebb
								0.470			0.541	2.29	0.819	0.80	1.15	0.4778	0.151	Flood
12A	0.937	0.000	0.000	339.7	0.415	0.1590	0.1722	0.502	0.030	0.095	1.090	2.71	1.794	0.68	0.75	0.7974	0.258	Ebb
								0.498			1.098	2.67	1.794	0.66	0.79	0.8466	0.274	Flood
12F[2]	0.898	0.017	0.019	324.4	0.402	0.1546	0.1675	0.506	0.025	0.103	1.059	2.76	1.760	0.67	0.92	0.8021	0.253	Ebb
								0.494			1.178	2.23	1.760	0.71	0.72	0.9070	0.286	Flood
12A	0.946	0.000	0.000	324.4	0.417	0.1616	0.1752	0.502	0.017	0.095	1.321	2.02	1.880	0.66	0.88	0.8397	0.250	Ebb
								0.498			1.102	2.91	1.880	0.64	0.88	0.8705	0.259	Flood
12F[2]	0.920	0.000	0.000	318.2	0.406	0.1580	0.1713	0.501	0.033	0.108	1.177	2.41	1.826	0.68	0.90	0.8418	0.253	Ebb
								0.499			1.211	2.27	1.826	0.71	0.86	0.9662	0.290	Flood
14A	0.404	0.042	0.104	135.9	0.324	0.1296	0.1415	0.535	0.100	0.200	0.366	4.06	0.737	0.68	1.02	0.3261	0.191	Ebb
								0.465			0.409	3.25	0.737	0.67	1.04	0.3920	0.229	Flood
15A	0.615	0.050	0.081	205.0	0.331	0.1319	0.1409	0.526	0.100	0.164	0.556	4.14	1.131	0.65	1.02	0.4873	0.189	Ebb
								0.474			0.545	4.30	1.131	0.61	1.00	0.5504	0.214	Flood
16A	0.824	0.022	0.027	272.3	0.430	0.1610	0.1734	0.512	0.081	0.130	0.858	2.96	1.476	0.68	0.88	0.6748	0.259	Ebb
								0.488			0.903	2.67	1.476	0.67	0.84	0.7560	0.291	Flood
17A	0.083	0.146	1.750	35.7	0.102	0.0518	0.0540	0.595	0.197	0.300	0.059	12.33	0.208	0.50	0.56	0.0605	0.045	Ebb
								0.405			0.083	6.23	0.208	0.50	0.64	0.0923	0.069	Flood

[1]Not determined.
[2]Fixed bed.

V. CORRELATION OF HYDRAULIC VARIABLES

1. Summary of Computations.

Using the data in Tables 1, 2, and 3, each experimental run was identified by its characteristic coefficients of repletion (different for ebbtide and floodtide) as defined by Keulegan (1967, equation 4) to obtain a direct comparison with his theory. Corresponding values of the energy losses coefficient, F, were also computed.

Subsequently, and based on measurements, computations were made of the tidal-damping ratio (a_b/a_o); superelevation (Δ/R_o) where Δ is mean bay level above MSL; timelag between high waters (ε_h); dimensionless maximum mean flow velocities (V'_{max}); absolute values of tidal prisms, Ω; inlet channel geometric and hydraulic characteristics (A_c, R_{MSL}, D_H); maximum mean flow velocities at ebbtide and floodtide (V_{maxe}, V_{maxf}); and maximum discharge (Q_{max}).

The results are given in Tables 4, 5, and 6.

2. Computations of Parameters from Experimental Data.

a. Computations of K. The Keulegan (1967) assumptions of a vertical bay wall and uniform bay level motion were observed to hold for the inlet conditions tested; therefore, the Keulegan repletion coefficient is computed using ebbtide and floodtide conditions separately to determine K_e and K_f.

Since the bay basin walls are vertical ($\beta = 0$), the instantaneous rate of filling (floodtide flow) or emptying (ebbtide flow) of the bay is given by:

$$Q = A_b \cdot \frac{dh_b}{dt} , \tag{12}$$

dh_b/dt being the slope of the bay tide curve (values in Table 3 are the maximum values of these slopes). This rate is equal to the flow discharge through the inlet channel (conservation of mass).

At maximum discharge the acceleration term $\partial V/\partial t$ in equation (7) is assumed to be negligible. Therefore, equation (3) can be used to compute the corresponding values of K, i.e.,

$$K_f = \frac{T}{\pi\sqrt{2R_o}\,\sqrt{(h_o - h_b)_f}} \cdot \frac{1}{A'_{cf}} \cdot \left[\frac{dh_b}{dt}\right]_f^{max} , \tag{13}$$

Table 5. Experimental and computed parameters for simultaneous wave and tide runs.

Run	a_b/s_o	Bay superelevation Δ/R_o	Bay superelevation Δ/R_b	Measured tidal prism Ω (ft^3)	Channel geometry at MSL A_c (ft^2)	Channel geometry at MSL R_h (ft)	Channel geometry at MSL D (ft)	Dimensionless duration of tide	Tidal timelag ϕ_h	Tidal timelag ϕ_q	K	F	$K\sqrt{F}$	Inlet velocities V_{max} Theoretical (ft/s)	Inlet velocities V_{max} Measured (ft/s)	Inlet velocities V'_{max} (ft/s)	Inlet velocities Q_{max} (ft^3/s)	Tide
4	0.044	0.385	8.750	35.6	0.089	0.0549	0.0567	0.607	0.188	0.313	0.014	37.75	0.088	0.45	0.71	0.0406	0.086	Ebb
								0.393			0.067	1.75	0.088	0.78	1.01	0.0795	0.168	Flood
5	0.040	0.320	8.000	32.6	0.076	0.0481	0.0497	0.609	0.189	0.314	0.022	11.70	0.075	0.79	0.77	0.0358	0.076	Ebb
								0.391			0.032	5.66	0.075	0.51	0.97	0.0556	0.119	Flood
6B	0.080	0.232	2.909	65.4	0.124	0.0629	0.0656	0.578	0.177	0.287	0.042	8.42	0.120	0.89	0.91	0.0655	0.142	Ebb
								0.412			0.066	3.30	0.120	0.83	1.04	0.0943	0.205	Flood
7B	0.221	0.235	1.067	178.5	0.246	0.0911	0.0946	0.576	0.165	0.260	0.119	9.39	0.365	0.84	1.03	0.1710	0.242	Ebb
								0.424			0.307	1.42	0.365	1.23	1.44	0.3075	0.434	Flood
8B	0.249	0.219	0.881	199.3	0.276	0.1255	0.1333	0.571	0.162	0.259	0.158	6.83	0.412	0.96	1.02	0.2164	0.302	Ebb
								0.429			0.331	1.55	0.412	1.21	1.86	0.3135	0.438	Flood
8C	0.268	0.192	0.714	212.4	0.341	0.1353	0.1445	0.577	0.166	0.244	0.164	9.79	0.514	0.77	0.84	0.2116	0.291	Ebb
								0.437			0.395	1.69	0.514	1.18	1.22	0.3505	0.482	Flood
9B	0.315	0.192	0.610	243.9	0.392	0.0871	0.0885	0.573	0.157	0.242	0.199	8.98	0.596	0.79	0.86	0.2518	0.339	Ebb
								0.429			0.358	2.77	0.596	0.93	0.90	0.3975	0.535	Flood
10B	0.680	—[1]	—	514.1	0.462	0.1018	0.1065	0.552	0.061	0.160	0.616	5.15	1.398	0.91	0.92	0.5975	0.394	Ebb
								0.448			0.820	2.90	1.398	0.83	1.25	0.7683	0.507	Flood
11B[2]	0.537	0.083	0.154	198.9	0.183	0.0871	0.0897	0.527	0.129	0.156	0.418	3.59	0.791	0.77	1.21	0.4072	0.132	Ebb
								0.473			0.522	2.30	0.791	0.73	1.07	0.4697	0.152	Flood
11C[2]	0.496	0.157	0.317	183.6	0.183	0.0871	0.0897	0.500	0.133	0.165	0.372	4.52	0.791	0.75	1.17	0.4129	0.133	Ebb
								0.500			0.432	3.35	0.791	0.62	1.10	0.4148	0.134	Flood
12B	0.891	0.042	0.047	324.4	0.356	0.1402	0.1477	0.517	0.025	0.103	1.030	2.29	1.557	0.80	0.88	0.8309	0.263	Ebb
								0.483			1.103	1.99	1.557	0.73	0.90	0.8212	0.260	Flood
12C	0.861	—	—	302.9	0.336	0.1388	0.1480	0.503	—	0.125	—	—	1.495	—	—	0.7918	0.242	Ebb
								0.497			—	—	1.495	—	—	0.8918	0.273	Flood
14B	0.391	0.067	0.170	136.5	0.286	0.1135	0.1207	0.538	0.138	0.190	0.336	3.61	0.639	0.77	1.06	0.3217	0.195	Ebb
								0.462			0.354	3.26	0.639	0.64	1.00	0.3409	0.207	Flood
15B	0.558	0.067	0.119	205.0	0.264	0.1109	0.1163	0.527	0.111	0.156	0.532	2.61	0.860	0.88	1.04	0.4698	0.201	Ebb
								0.473			0.543	2.51	0.860	0.73	0.94	0.4899	0.209	Flood
16B	0.737	0.047	0.064	257.0	0.374	0.1375	0.1455	0.513	0.080	0.149	0.796	2.46	1.250	0.78	0.92	0.6378	0.259	Ebb
								0.487			0.847	2.18	1.250	0.74	0.88	0.7011	0.285	Flood
17B	0.072	0.225	3.115	30.9	0.083	0.0503	0.0522	0.558	0.182	0.247	0.047	13.20	0.169	0.52	0.54	0.0573	0.043	Ebb
								0.442			0.080	4.45	0.169	0.50	0.60	0.0844	0.063	Flood
18B	0.110	0.227	2.051	47.0	0.074	0.0503	0.0536	0.564	0.199	0.263	0.070	10.50	0.228	0.56	0.60	0.0761	0.037	Ebb
								0.436			0.102	5.02	0.228	0.50	0.54	0.1135	0.056	Flood

[1]Not determined.

[2]Fixed bed.

Table 6. Experimental and computed parameters for special runs, and simultaneous wave and tidal action.

Run	a_b/a_o	Bay superelevation		Measured tidal prism	Channel geometry at MSL			Dimensionless duration of tide	Tidal timelag					Inlet velocities				Tide	Remarks
														V_{max}		V'_{max}	Q_{max}		
		Δ/R_o	Δ/R_b	Ω (ft^3)	A_c (ft^2)	R_h (ft)	D (ft)		ϵ_h	ϵ_f	K	F	$K\sqrt{F}$	Theoretical (ft/s)	Measured (ft/s)	(ft/s)	(ft^3/s)		
7C	0.217	0.161	0.741	176.7	0.283	0.1241	0.1437	0.558	0.169	0.248	0.161	6.78	0.418	0.92	0.90	0.1639	0.233	Ebb	Jetties
								0.442			0.233	3.21	0.418	0.94	0.99	0.2300	0.327	Flood	
18C	0.122	0.177	1.444	53.5	0.094	0.0503	0.0538	0.564	0.200	0.248	0.063	16.23	0.254	0.45	0.66	0.0702	0.036	Ebb	Jetties
								0.436			0.111	5.28	0.254	0.51	0.62	0.1216	0.062	Flood	
16C	0.726	0.088	0.122	250.9	0.375	0.1431	0.1512	0.548	0.073	0.149	0.773	2.65	1.258	0.80	0.92	0.6845	0.275	Ebb	Freshwater inflow
								0.452			0.928	1.84	1.258	0.73	0.86	0.7225	0.291	Flood	

for floodtide, and

$$K_e = \frac{T}{\pi\sqrt{2R_o}\ \sqrt{(h_b - h_o)_e}} \cdot \frac{1}{A'_{ce}} \cdot \left[\frac{dh_b}{dt}\right]_e^{max} , \qquad (14)$$

for ebbtide, where subscript f is for floodtide and e is for ebbtide. A'_c is the dimensionless cross-sectional area (A_c/A_c at MSL) used in these two equations to account for the varying cross-sectional area with tide stage.

Values of K_f and K_e for each run were computed with equations (13) and (14), by using all the respective measured parameters T, R_o, h_b, h_o, $[dh_b/dt]$ max (from bay tide curves) and where the ratio of the actual channel cross-sectional area at maximum discharge (e.g., at maximum floodtide discharge) to the area at MSL is:

$$A'_{cf} = \frac{\bar{A}_c + (W_{MSL} + \zeta\, h_{if})\, h_{if}}{\bar{A}_c} , \qquad (15)$$

with $\bar{A}_c$ the average area at MSL, W_{MSL} the width at MSL, ζ the bank slope (horizontal distance per unit of vertical distance) and h_{if} the inlet water level above MSL at maximum floodtide discharge.

b. Computation of F. The coefficient, F, accounts for the unit energy losses at maximum inlet discharge due to friction (fL/4R), flow contraction into the inlet channel (entrance losses, k_{en}), flow expansion into the bay or ocean (exit losses, k_{ex}), and other minor losses (included in $k_{en} + k_{ex}$). Values of F may be computed both at maximum ebbtide and floodtide discharges using Keulegan's definition of K:

$$F_f = \left(\frac{\sqrt{g}}{\pi\sqrt{R_o}} \cdot \frac{\bar{A}_c}{A_b} \cdot \frac{T}{K_f}\right)^2 , \qquad (16)$$

and

$$F_e = \left(\frac{\sqrt{g}}{\pi\sqrt{R_o}}\ \frac{\bar{A}_c}{A_b}\ \frac{T}{K_e}\right)^2 . \qquad (17)$$

c. Computation of $K\sqrt{F}$. The product $K\sqrt{F}$ is a dimensionless number, constant throughout a tidal cycle for a given inlet, where:

$$K\sqrt{F} = K_f\sqrt{F_f} = K_e\sqrt{F_e} = \frac{\sqrt{gT}}{\pi\sqrt{R_o}} \cdot \frac{\bar{A}_c}{A_b} . \qquad (18)$$

$K\sqrt{F}$ is a useful variable since its computation is based only on non-friction terms, measurable both in the laboratory and in the field. For this parameter it is unnecessary to estimate the friction coefficient, f, the exit and entrance energy loss coefficients and the inlet length, and the effect of the ocean tide on the channel is reflected in the value of the inlet cross-sectional area for an inlet that has reached an "equilibrium" (for these tests, values of $K\sqrt{F}$ were computed when the bay tide became periodic).

d. Computation of Dimensionless Current Velocity and Discharge. The maximum discharge through the inlet channel is given by:

$$Q_{max} = A_b \cdot \left(\frac{dh_b}{dt}\right)_{max} . \tag{19}$$

The maximum slope of the bay tide lasts long enough to validate the assumption that, for all practical purposes, the maximum mean velocity across a section is given by:

$$V_{max} = \frac{Q_{max}}{A_c} . \tag{20}$$

From O'Brien and Dean (1972), dimensionless values of maximum mean current velocities at the selected cross section were determined from experimental results for both ebbtide and floodtide using the definition:

$$V'_{max} = \frac{Q_{max} T}{\pi A_b R_o} , \tag{21}$$

or using equation (18):

$$V'_{max} = V_{max} \frac{K\sqrt{F}}{\sqrt{gR_o}} A'_c . \tag{22}$$

Dimensionless values of maximum discharge were also computed from the definition:

$$Q_{max} = CD \cdot \bar{A}_c \cdot \sqrt{gR_o} \tag{23}$$

which yields, combined with equation (20), the "discharge coefficient,"

$$CD = \frac{V_{max}}{\sqrt{gR_o}} , \tag{24}$$

and, using equation (22),

$$CD = \frac{V'_{max}}{K\sqrt{F}\ A'_c} \cdot \tag{25}$$

The absolute theoretical velocity is, from equation (24),

$$V^T_{max} = CD \cdot \sqrt{gR_o} \ , \tag{26}$$

which may differ from the experimental values computed in equation (20).

e. Computation of Friction Factor (f) and Roughness Coefficient (n). Estimations of friction factors at maximum discharge were made using the channel length, L, and the cross section as shown by the measurements in Table 2, with the friction factors for ebbtide and floodtide flow defined by:

$$f = \frac{4R}{L}\left(F - \left(k_{en} + k_{ex}\right)\right) \cdot \tag{27}$$

For these calculations, it is assumed that $k_{en} + k_{ex} = 1.0$ (Huval and Wintergerst, in preparation, 1977).

Since the relationship between f and the Manning roughness coefficient, n, is given by equation (11), estimates of n may be obtained by:

$$n = 0.185 \cdot R^{2/3} \cdot \sqrt{(F-1)/L} \ . \tag{28}$$

Experimental values of f range from about 0.01 to 0.65, but most range from 0.05 to 0.20 (Tables 4, 5, and 6).

Computed values of n range from about 0.006 to 0.049, but most range from 0.013 to 0.030.

3. Computation of Theoretical Parameters by the Lumped Parameter Approach.

The computer program in Huval and Wintergerst (in preparation, 1977) was modified to use the experimental data collected in this investigation. The input to the new program (DATATHE) included:

(a) All measured data necessary to compute K and F at the maximum ebbtide and floodtide discharge;

(b) a sinusoidal ocean tide with range, R_o, and period, T,

(c) initial values of mean flow velocity and bay water elevation,

(d) coefficients indicating the time interval selected for integration of the differential equations and the number of tidal cycles necessary for the solution to reach a periodic bay tide, and

(e) $\beta = 0$ (vertical bay walls).

The program determines n for ebbtide and floodtide flows; then, two different integrations are made, one for each of the n values. It is assumed that the roughness coefficient at maximum ebbtide or floodtide discharge is unchanged throughout the process of integration. Therefore, for each run two similar prismatic channels of length and cross-section characteristics are used (Table 2), but with different roughnesses.

The integration procedure is explained by the description of program INLET (Huval and Wintergerst, in preparation, 1977). Program output includes the bay tide, the mean current velocity, the discharge at the inlet as a function of time, the net discharge for a tidal cycle, maximum and minimum water levels, timelags and durations, elevations, etc. (Table 7). These results constitute the theoretical values (lumped parameter approach) that will be compared to the experimental values in Tables 4, 5, and 6. Figures at the bottom of Table 7 correspond to theoretical values of the parameters used for comparison to experimental results. Therefore, two sets of solutions, one for each of the two roughness coefficients computed, are obtained.

After a thorough study of the results, it was decided that a representative lumped parameter approach would be the solution for the ebbtide flow roughness coefficient, which implies that theoretical results correspond to values of F and K at maximum ebbtide flow only. The K values covered a range wider than that corresponding to the floodtide flow and yielded more consistent results.

Computer programs used in the calculations are listed in Mayor-Mora (1973).

4. Comparison of Measured and Theoretical Tides and Currents.

The theoretical values obtained by the lumped parameter approach of ocean and bay elevations, the mean current velocity at the inlet, and the rate of discharge using the coefficient of repletion defined by ebbtide flow (run 8A) are shown in Figure 28. The difference in bay level when K is defined by floodtide is shown in Figure 29 (run 8A); the figure includes theoretical bay levels defined by ebbtide flow when waves and tides are present (run 8B).

A comparison of measured data and lumped parameter theoretical results gave the best agreement for a coefficient of repletion defined for ebbtide flow, K_e; therefore, this parameter was used in analysis. Figures 30 and 31 show the agreement between measured and predicted hydraulic parameters for ebbtide flow prediction with tides only and for

Table 7. Samples of program "DATATHE" output (lumped parameter approach).

Results using K_f (Run 8B)						Results using K_w (Run 8B)					
T (min)	HO (ft)	QF (ft^3/s)	HB (ft)	V (ft/s)	Q (ft^3/s)	T (min)	HO (ft)	QF (ft^3/s)	HB (ft)	V (ft/s)	Q (ft^3/s)
0.00	0.000	0.0	−0.013	0.26	0.07	0.00	0.000	0.0	0.004	−0.24	−0.07
1.00	0.014	0.0	−0.011	0.95	0.26	0.68	0.010	0.0	0.003[2]	0.01	0.00
2.00	0.027	0.0	−0.008	1.19	0.35	1.00	0.014	0.0	0.003	0.21	0.06
3.00	0.040	0.0	−0.004	1.35	0.43	2.00	0.027	0.0	0.005	0.48	0.15
4.00	0.050	0.0	0.000	1.47	0.49	3.00	0.040	0.0	0.006	0.60	0.20
5.00	0.058	0.0	0.005	1.53	0.54	4.00	0.050	0.0	0.008	0.69	0.24
5.92	0.064	0.0	0.011	1.55[1]	0.56	5.00	0.058	0.0	0.011	0.75	0.27
6.00	0.064	0.0	0.011	1.55	0.57	6.00	0.064	0.0	0.014	0.79	0.29
6.84	0.067	0.0	0.016	1.53	0.57[1]	6.84	0.087	0.0	0.016	0.80[2]	0.30
7.00	0.067	0.0	0.017	1.53	0.57	7.00	0.067	0.0	0.017	0.80	0.30
7.48	0.067[1]	0.0	0.020	1.50	0.57	7.24	0.067	0.0	0.018	0.80	0.30[2]
8.00	0.067	0.0	0.022	1.45	0.56	7.48	0.067[2]	0.0	0.018	0.79	0.30
9.00	0.064	0.0	0.028	1.32	0.51	8.00	0.067	0.0	0.020	0.78	0.30
10.00	0.058	0.0	0.033	1.14	0.44	9.00	0.064	0.0	0.023	0.73	0.28
11.00	0.050	0.0	0.037	0.88	0.33	10.00	0.058	0.0	0.025	0.66	0.25
12.00	0.040	0.0	0.039	0.49	0.18	11.00	0.050	0.0	0.028	0.54	0.20
12.76	0.030	0.0	0.040[1]	0.00	0.00	12.00	0.040	0.0	0.029	0.38	0.14
13.00	0.027	0.0	0.040	−0.24	−0.08	13.00	0.027	0.0	0.030	0.12	0.04
14.00	0.014	0.0	0.038	−0.95	−0.32	13.24	0.024	0.0	0.030[2]	0.00	0.00
15.00	−0.000	0.0	0.034	−1.18	−0.37	14.00	0.014	0.0	0.030	−0.39	−0.13
16.00	−0.014	0.0	0.030	−1.34	−0.39	15.00	−0.000	0.0	0.028	−0.53	−0.16
17.00	−0.027	0.0	0.026	−1.46	−0.40	16.00	−0.014	0.0	0.027	−0.62	−0.18
17.32	−0.031	0.0	0.025	−1.49	−0.40[1]	17.00	−0.027	0.0	0.025	−0.69	−0.19
18.00	−0.040	0.0	0.022	−1.55	−0.40	17.76	−0.037	0.0	0.023	−0.72	−0.19[2]
19.00	−0.050	0.0	0.018	−1.60	−0.39	18.00	−0.040	0.0	0.023	−0.73	−0.19
20.00	−0.058	0.0	0.014	−1.63	−0.38	19.00	−0.050	0.0	0.021	−0.75	−0.19
20.56	−0.062	0.0	0.012	−1.63[1]	−0.37	20.00	−0.058	0.0	0.019	−0.77	−0.18
21.00	−0.064	0.0	0.011	−1.63	−0.37	20.84	−0.063	0.0	0.018	−0.77[2]	−0.18
22.00	−0.067	0.0	0.007	−1.61	−0.36	21.00	−0.064	0.0	0.017	−0.77	−0.18
22.48	−0.067[1]	0.0	0.005	−1.59	−0.35	22.00	−0.067	0.0	0.015	−0.76	−0.17
23.00	−0.067	0.0	0.003	−1.57	−0.34	22.48	−0.067[2]	0.0	0.015	−0.76	−0.17
24.00	−0.064	0.0	0.000	−1.50	−0.33	23.00	−0.067	0.0	0.014	−0.75	−0.17
25.00	−0.058	0.0	−0.003	−1.40	−0.31	24.00	−0.064	0.0	0.012	−0.73	−0.17
26.00	−0.050	0.0	−0.006	−1.27	−0.28	25.00	−0.058	0.0	0.010	−0.71	−0.16
27.00	−0.040	0.0	−0.009	−1.09	−0.25	26.00	−0.050	0.0	0.009	−0.67	−0.16
28.00	−0.027	0.0	−0.011	−0.85	−0.20	27.00	−0.040	0.0	0.007	−0.61	−0.15
29.00	−0.014	0.0	−0.013	−0.48	−0.12	28.00	−0.027	0.0	0.006	−0.53	−0.14
29.76	−0.003	0.0	−0.013[1]	0.01	0.00	29.00	−0.014	0.0	0.004	−0.42	−0.11
30.00	0.000	0.0	−0.013	0.26	0.07	30.00	0.000	0.0	0.004	−0.24	−0.07

[1]DHB = 0.0119 foot.

[2]DHB = 0.0164 foot.

Values of variables on punch cards (Floodtide)

Run
8B 0.397 0.088 0.223 317.6 329.4 0.276 0.1255 0.1333 0.567 0.176 0.243
8B 0.331 1.55 0.412 1.63 0.0078 0.2877 0.402 0.014 0.0061 0.699 0.302 0.98
8B 0.433 0.331 1.55 0.412 1.55 0.0078 0.4109 0.574 0.014 0.998 0.98

Values of variables on punch cards (Ebbtide)

Run
8B 0.202 0.122 0.605 161.4 329.4 0.276 0.1255 0.1333 0.581 0.192 0.273
8B 0.158 6.83 0.412 0.77 0.0250 0.1353 0.189 0.145 0.0061 0.329 0.312 0.95
8B 0.419 0.158 6.83 0.412 0.80 0.0250 0.2152 0.301 0.145 0.523 0.95

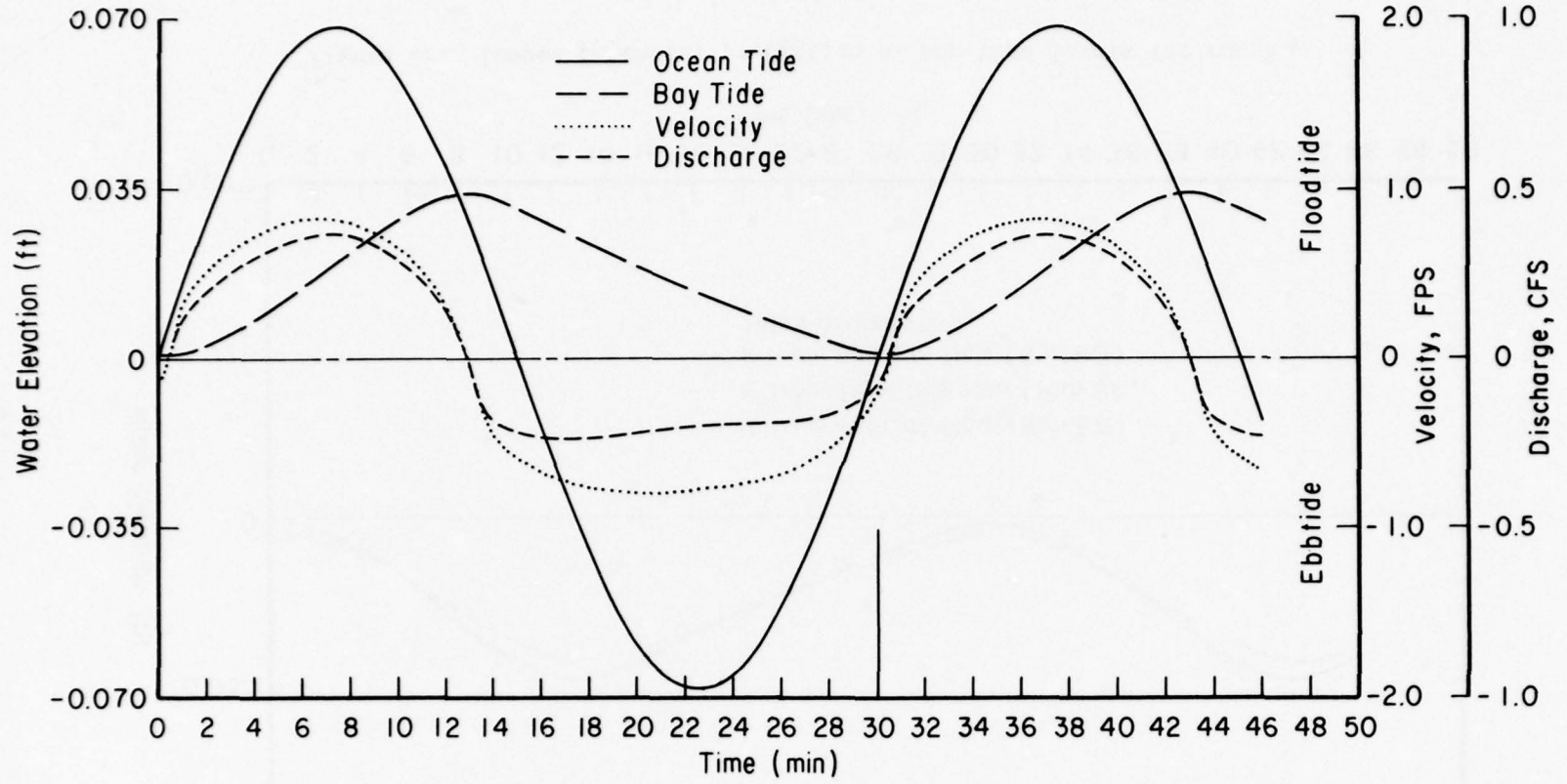

Figure 28. Tidal elevations, mean current velocity at midchannel, and discharge as functions of time computed by the lumped parameter approach (tidal action only and ebbtide flow coefficient of repletion, K=0.179).

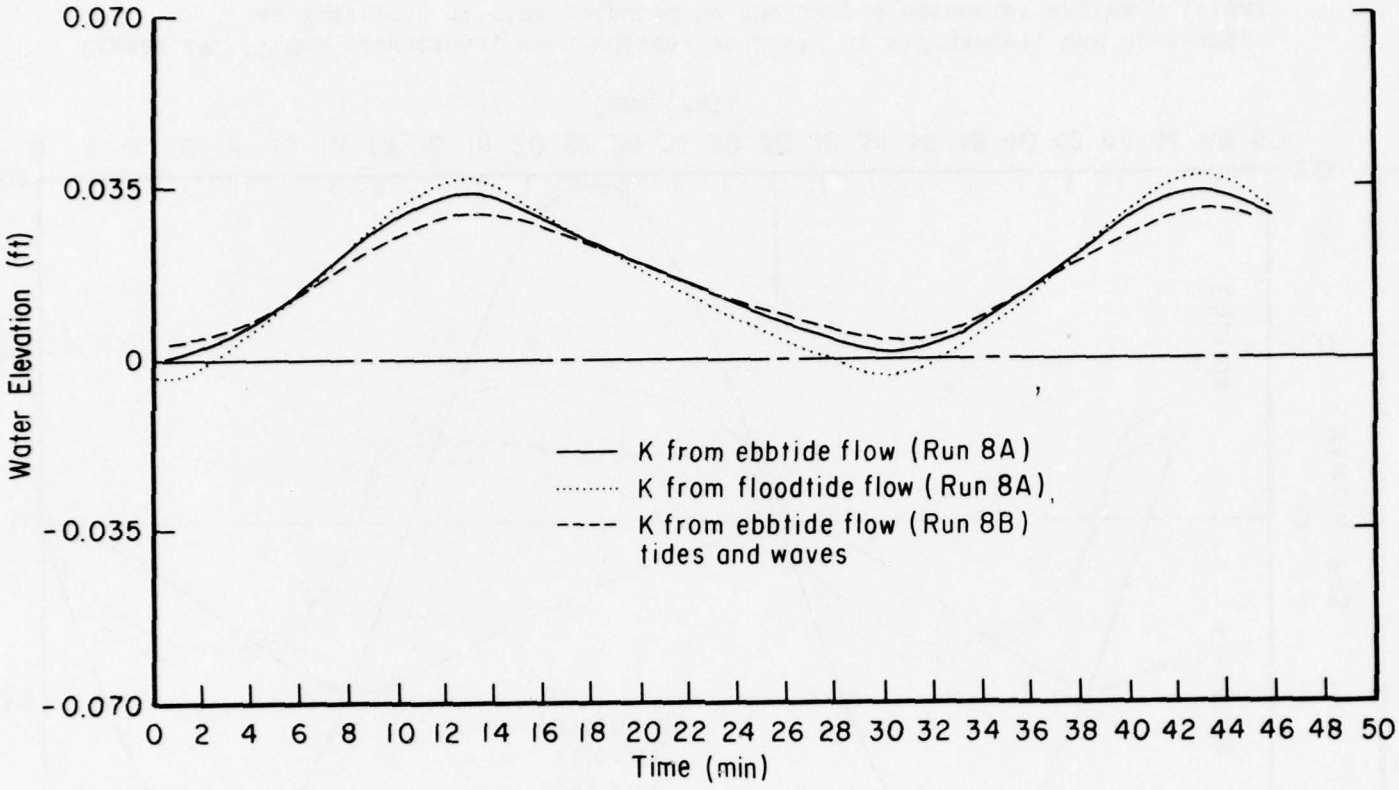

Figure 29. Lumped parameter prediction of bay tide levels for run 8.

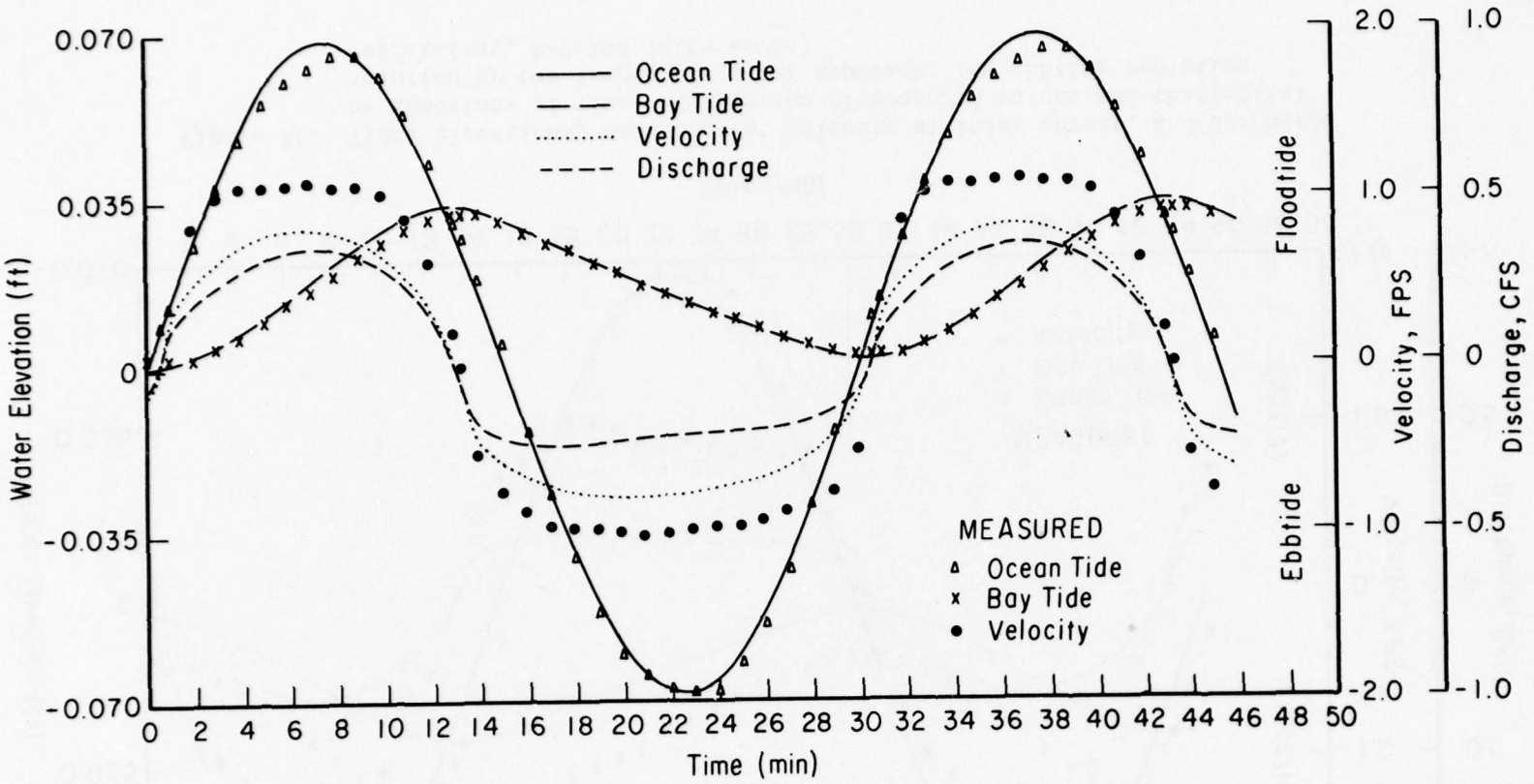

Figure 30. Tidal elevations, mean current velocity at midchannel, and discharge as functions of time. Comparison of measured values and theoretical solution by the lumped parameter approach; low ebbtide repletion coefficient, K=0.179 (no waves).

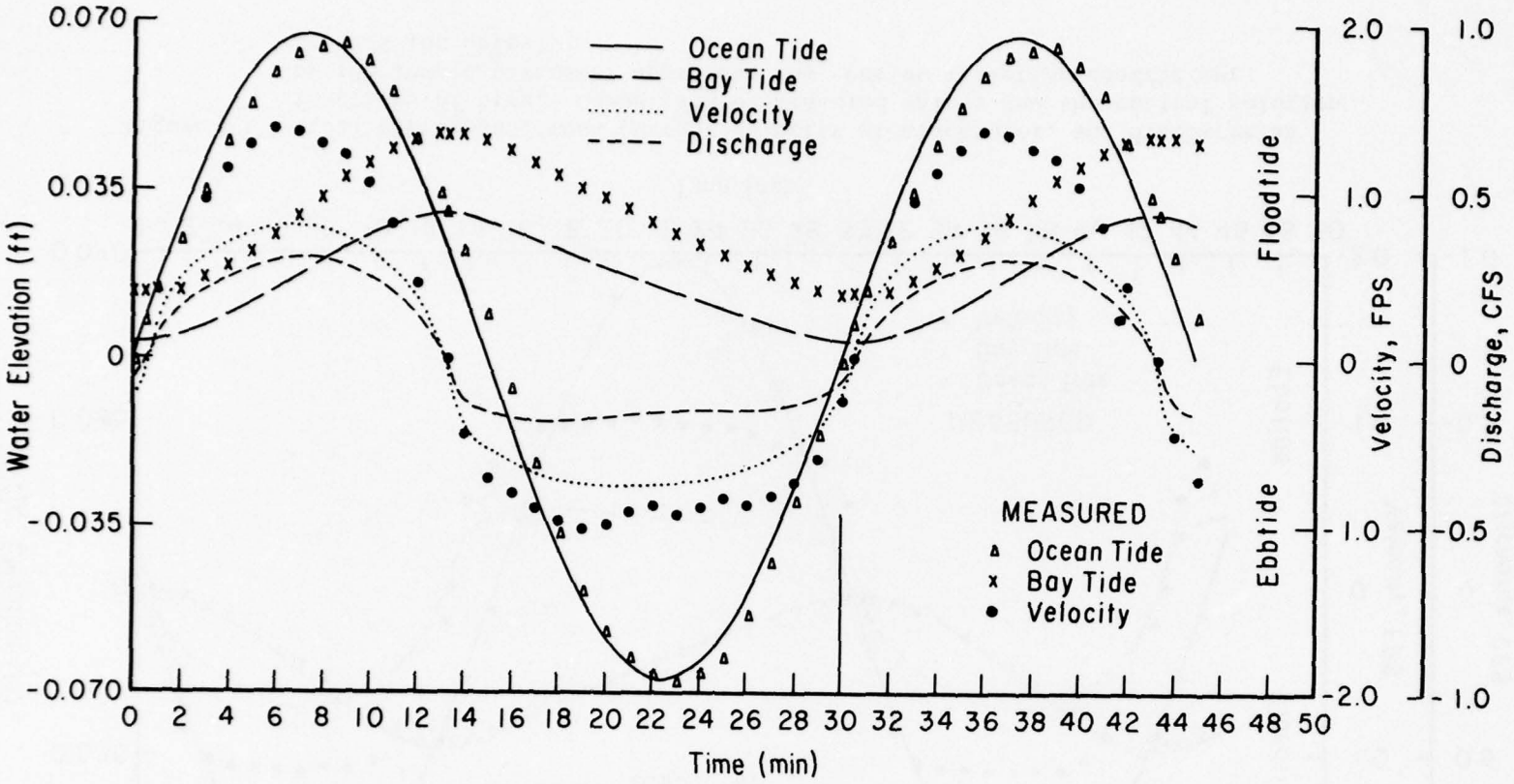

Figure 31. Tidal elevations, mean current velocity at inlet throat, and discharge as functions of time. Comparison of measured values and theoretical solution by the lumped parameter approach; low ebbtide repletion coefficient, K=0.158 (with waves).

tide and wave conditions for small values of K_e (runs 8A and 8B, respectively). Experimental and theoretical results for relatively large values of K_e are compared in Figures 32 and 33 (runs 12A and 12B, respectively).

A possible reason for the better agreement between observed and predicted parameters for K defined at ebbtide is that during ebbtide the Keulegan assumption of open channel flow is better approximated than during floodtide when the inlet acts more as an orifice.

It was also found that wave action in addition to tides reduces agreement between predicted and measured water levels and velocities (Figs. 30 to 33). This may be due to wave-induced velocities or a change in the effective geometric characteristics of the inlet.

5. Dimensionless Parameters as Functions of K_e.

Five dimensionless inlet hydraulic parameters are presented as functions of inlet repletion coefficients (Figs. 34 to 39). The parameters are plotted using open symbols for tide only experimental tests, and closed symbols for experimental results from tests with tides and waves. Keulegan's (1967) results are shown by a solid line, and results from the lumped parameter techniques (Huval and Wintergerst, in preparation, 1977) by a dashline.

The tidal damping coefficient, a_b/a_o, is plotted as a function of Keulegan's repletion coefficient for ebbtide, K_e, in both experimental results and from theory (Fig. 34). All results are similar and lead to the following conclusions for the parameter a_b/a_o: (a) Inertia is not important in bay tide levels for these conditions because Keulegan (no inertia) and lumped parameters (inertia) techniques give similar results, (b) a_b/a_o is the same for tests with and without waves, and (c) there is excellent agreement between theoretical and experimental results.

An alternate method of presenting the tidal damping coefficient is to plot the variable against the inlet parameter, $K_e\sqrt{F}$ (Fig. 35). The same trends and good agreement are found between a_b/a_o and $K_e\sqrt{F}$ as with the repletion coefficient; therefore, either inlet parameter may be used. Since this was found for other dimensionless hydraulic variables as well, only plots of K_e are presented.

Dimensionless lags between high and low waters, equal to the timelag divided by the tidal period, show deviations from the Keulegan predictions and best agreement with the lumped parameter solution (Figs. 36 and 37). Experiments show that lags between high water are shorter and lags between low water are longer than Keulegan's predictions. This may be due to the change in the cross-sectional area and the size of the friction and inertia terms over a tidal cycle.

The dimensionless maximum inlet velocity, V'_{max}, from experiments shows good agreement with Keulegan's theory (Fig. 38).

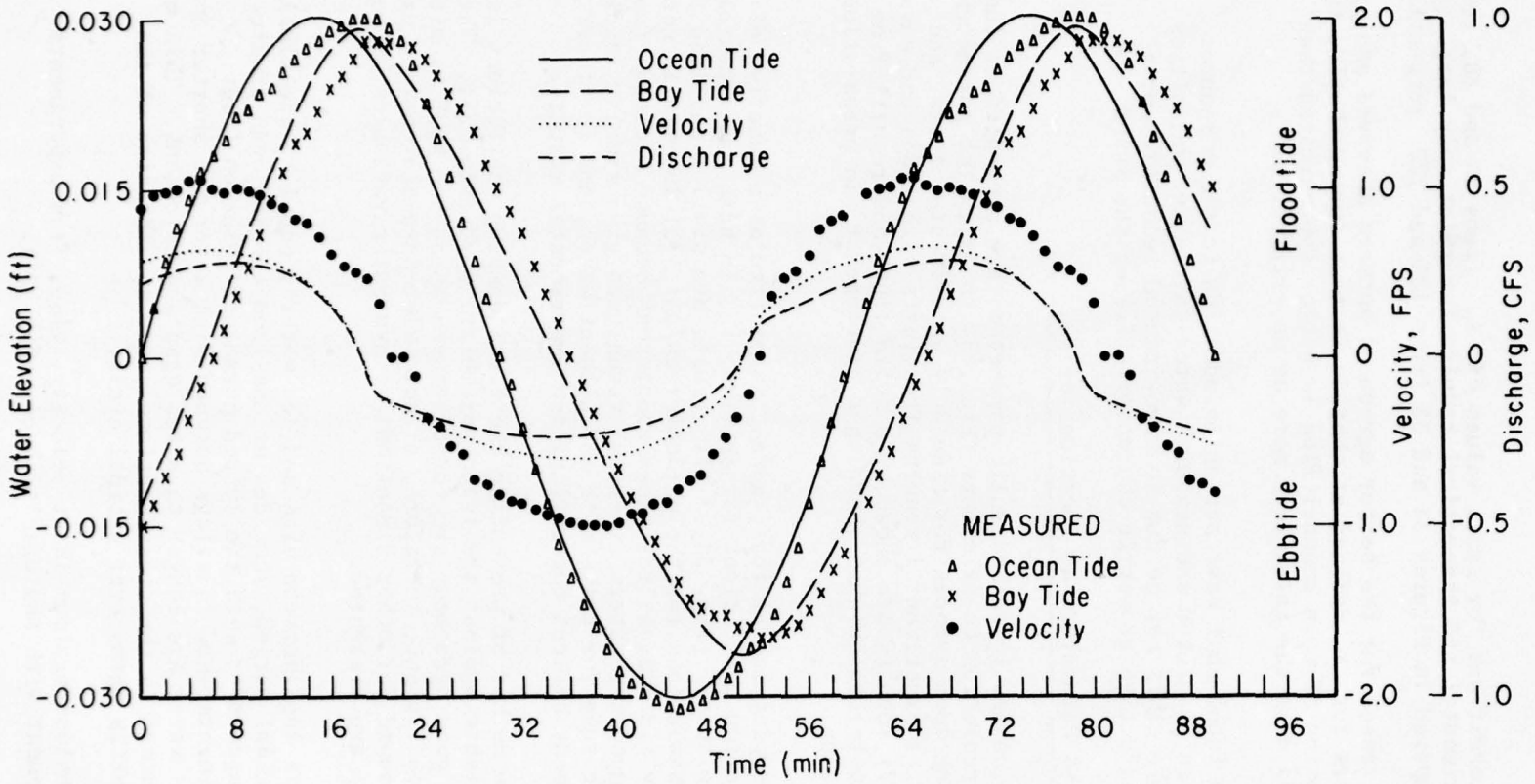

Figure 32. Tidal elevations, mean current velocity at midinlet, and discharge as functions of time. Comparison of measured values and theoretical solution by the lumped parameter approach; high ebbtide repletion coefficient, K=1.09 (no waves).

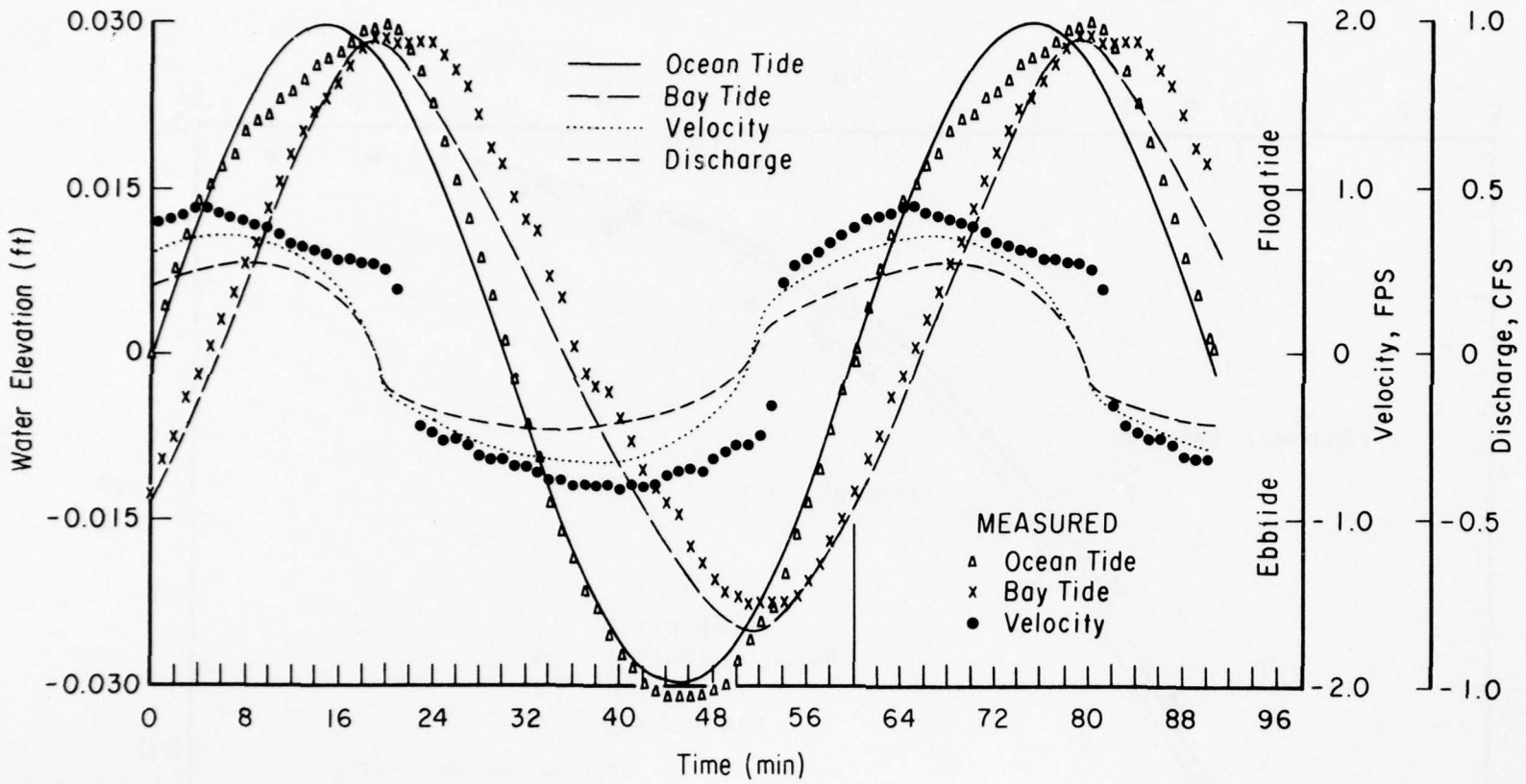

Figure 33. Tidal elevations, mean current velocity at inlet throat, and discharge as functions of time. Comparison of measured values and theoretical solution by the lumped parameter approach; high ebbtide repletion coefficient, K=1.03 (with waves).

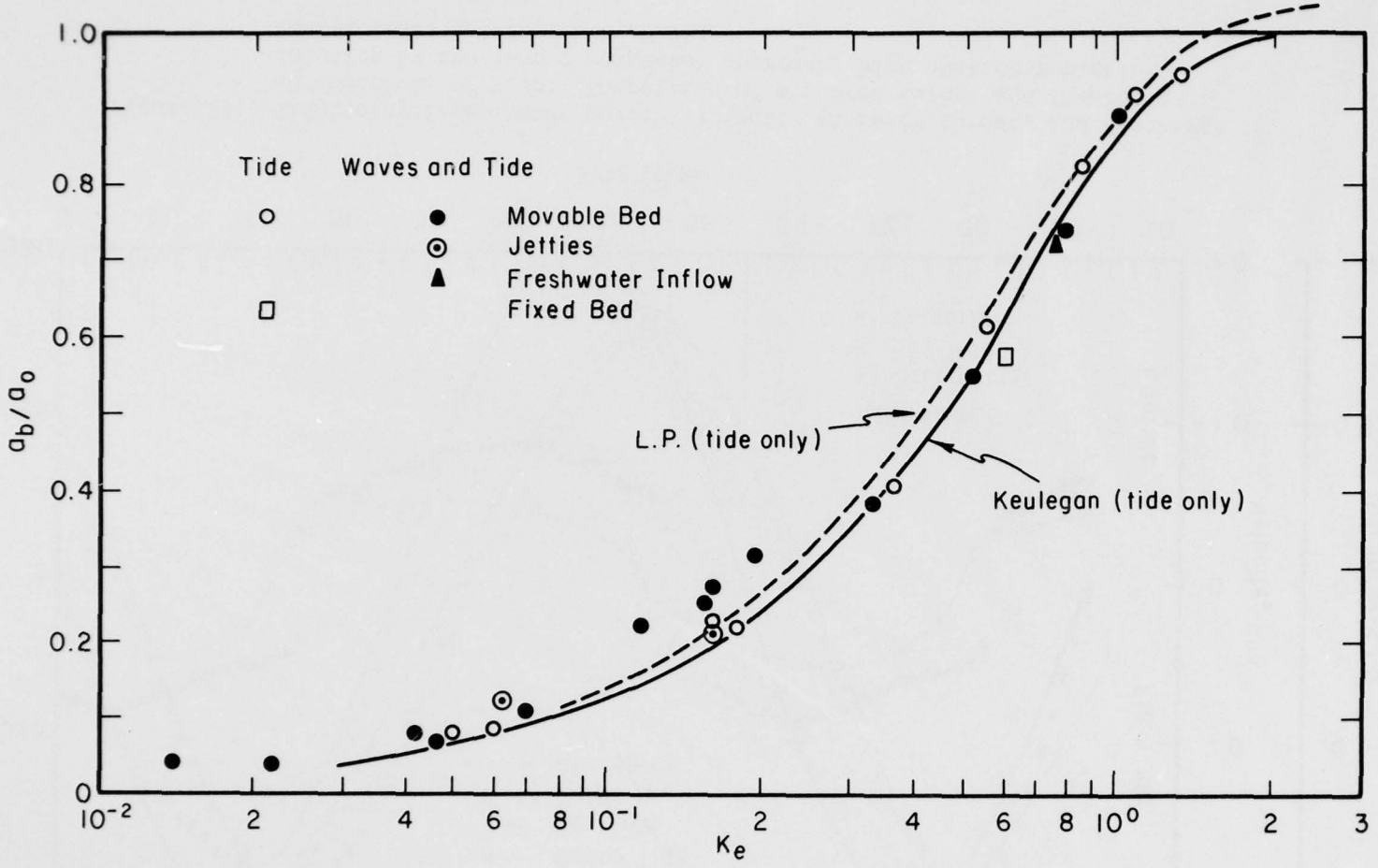

Figure 34. Tidal damping as a function of Keulegan's repletion coefficient for ebbtide.

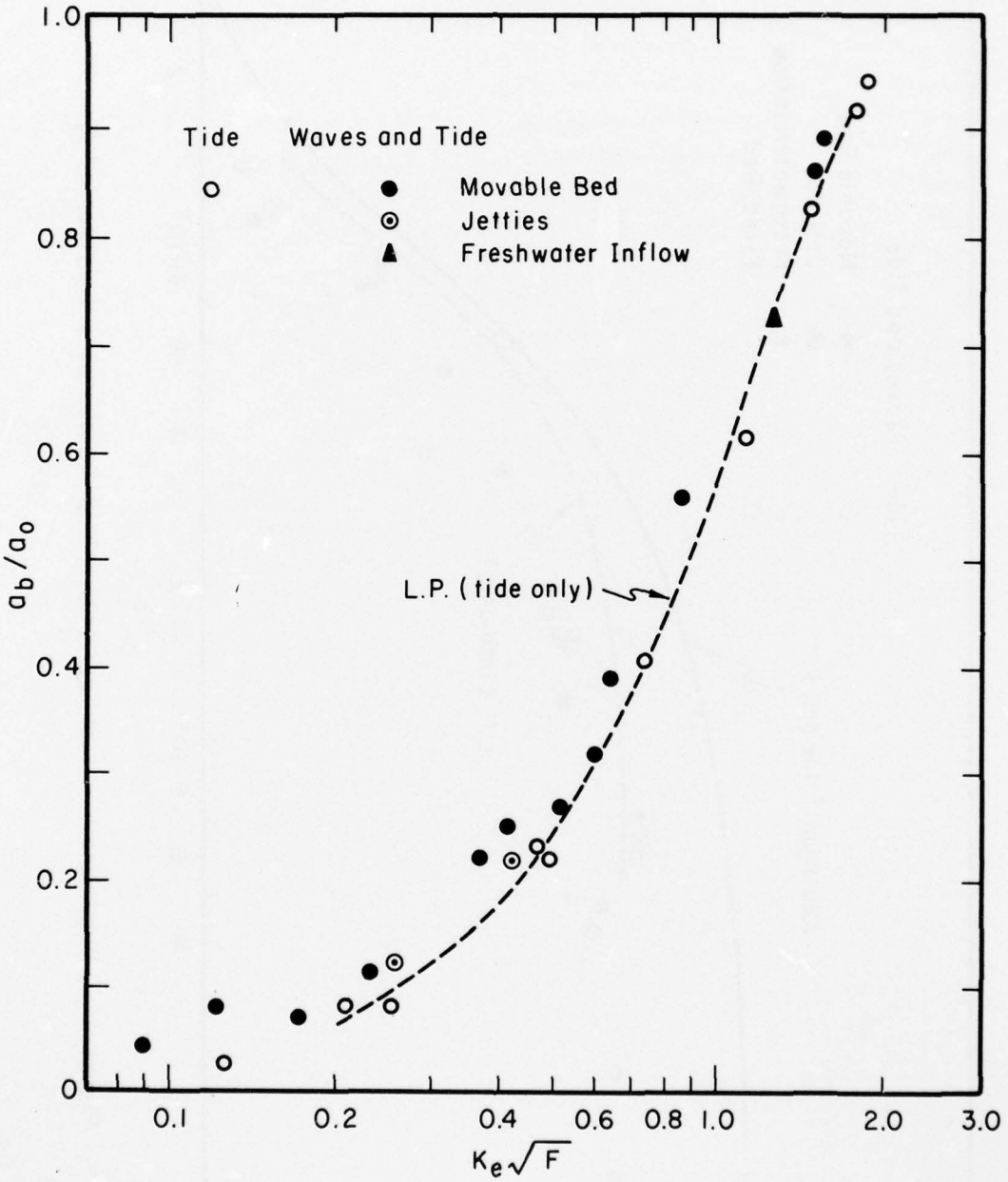

Figure 35. Tidal damping as a function of $K_e\sqrt{F}$.

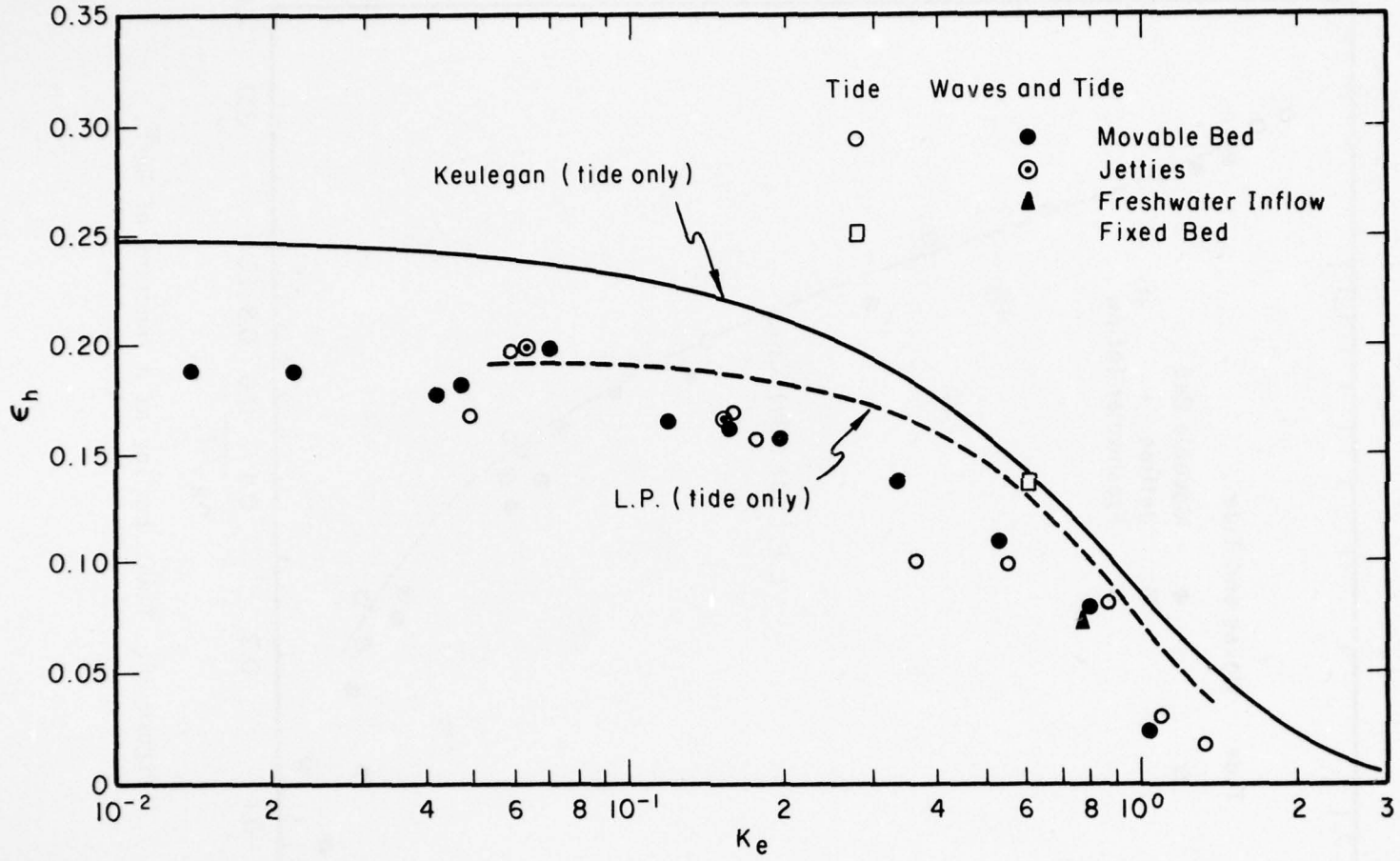

Figure 36. Dimensionless timelag between high waters as a function of K_e.

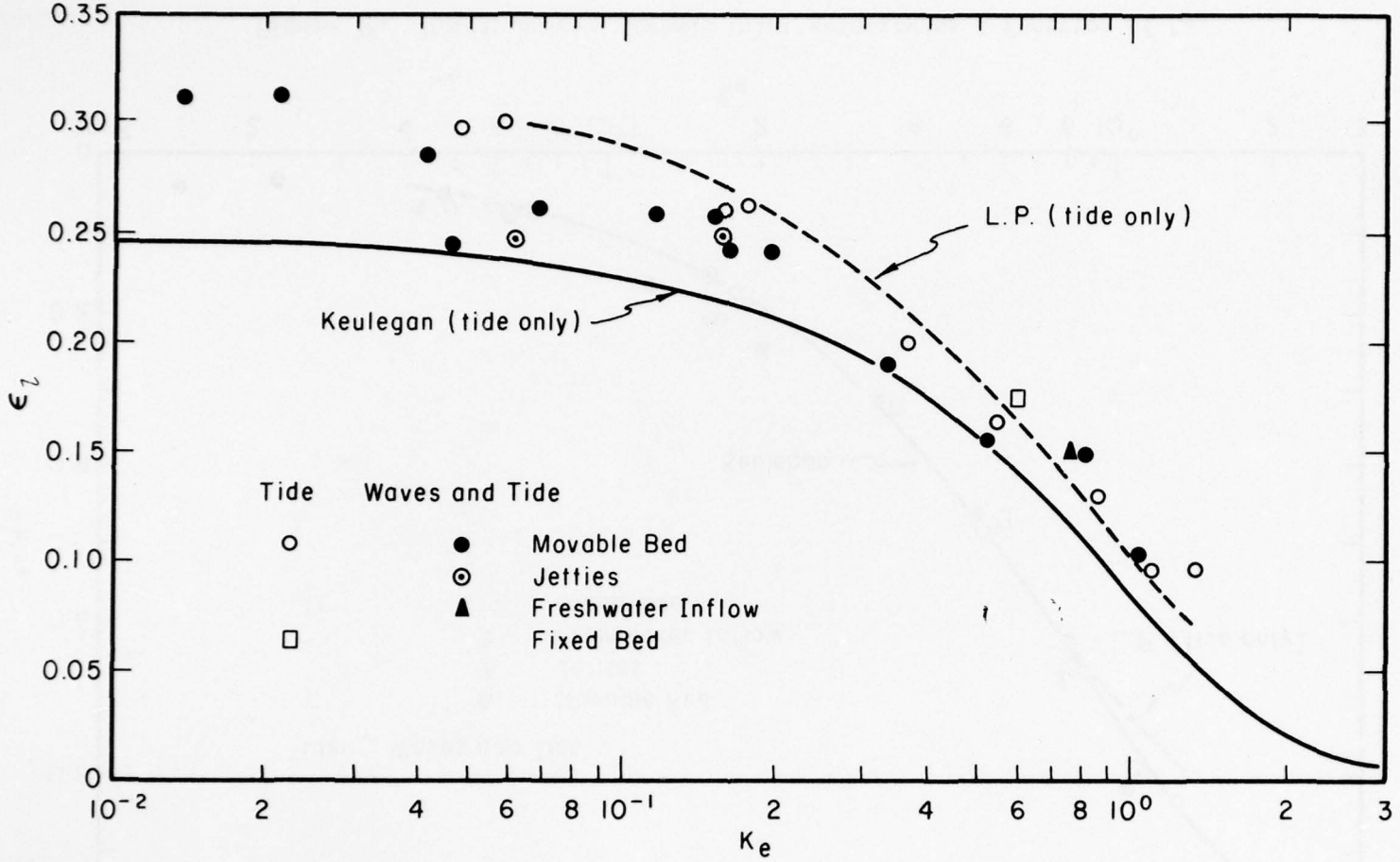

Figure 37. Dimensionless timelag between low waters as a function of K_e.

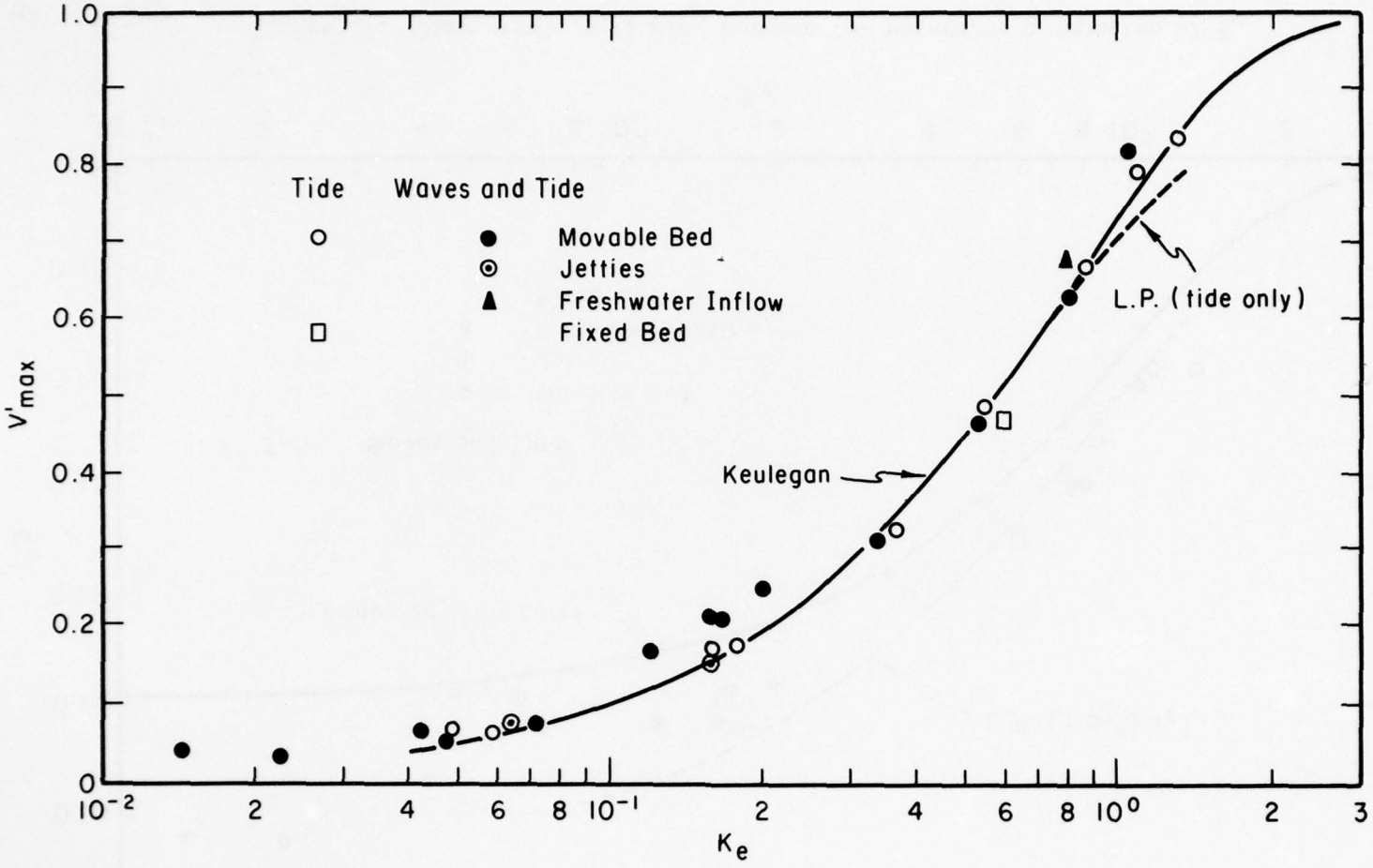

Figure 38. Dimensionless maximum inlet velocity as a function of K_e.

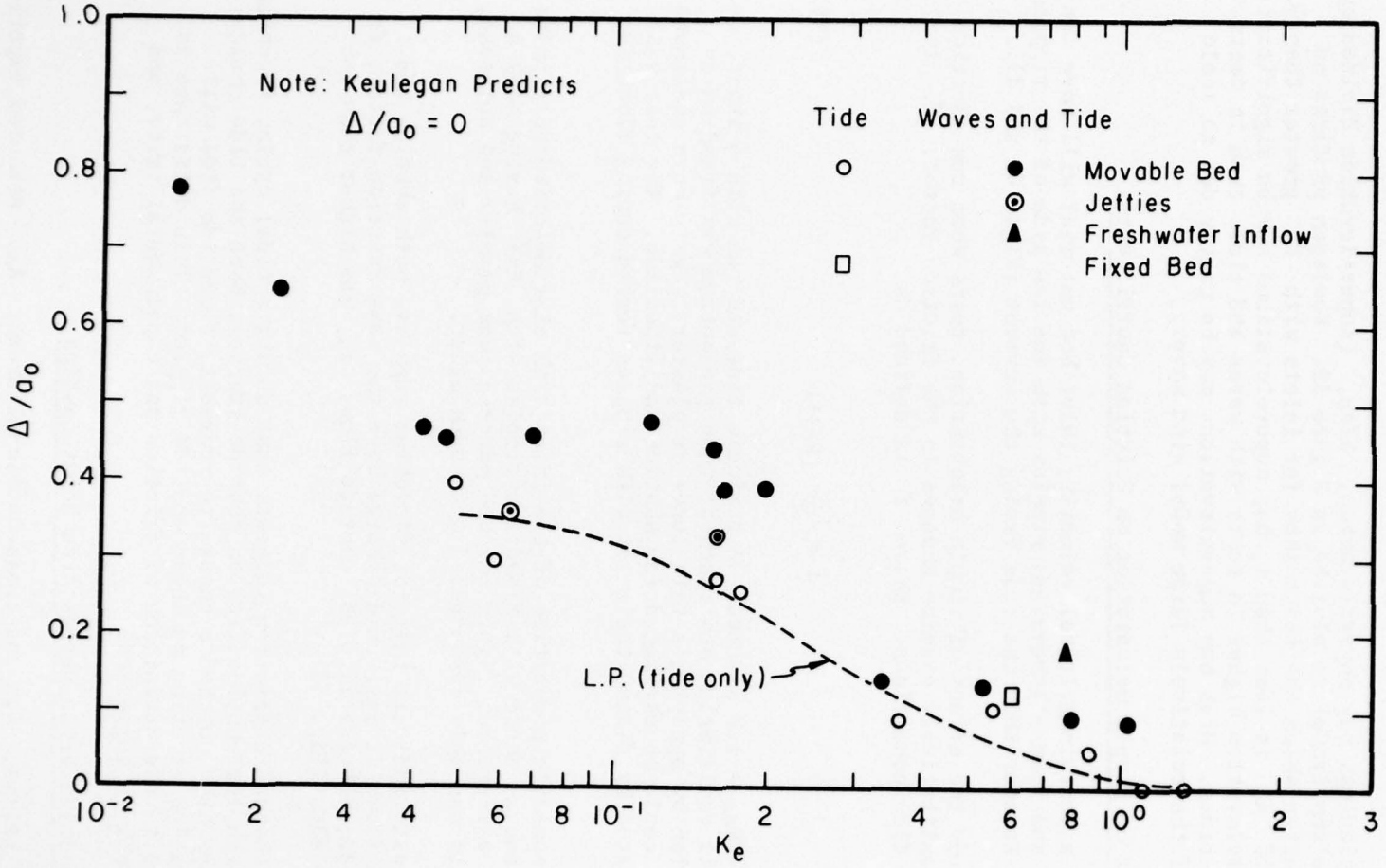

Figure 39. Dimensionless bay superelevation as a function of K_e.

Dimensionless bay superelevation, Δ/a_o, (superelevation divided by ocean tide amplitude) is plotted in Figure 39. Keulegan predicts no superelevation which the tests show for inlets with K_e greater than 1. However, if K_e is less than 1, bay superelevations may be significant with superelevation higher in tests with waves and tides than in tests with only tides. High bay superelevations may be partly due to scale effects of the relatively large model wind waves.

6. Effect of Ripple Orientation on Friction Coefficients.

Above a certain critical velocity, inlet bed material will move continuously and form asymmetrical ripples with the lee side of the ripples generally steeper than the side facing the current (Figs. 40 and 41).

To study the effect of ripple orientation, tests were run (Section III) to qualitatively examine changes in the friction factor, f, for different flow conditions. Where f is defined as:

$$f = \frac{4R}{L} (F'-1), \tag{29}$$

with $k_{en} + k_{ex} = 1.0$ assumed. A periodic tide was run with a short, deep inlet until equilibrium was reached; then the bottom was fixed on an ebbtide plan by applying a thin layer of plaster. Tests were continued until f could be estimated for ebbtide and floodtide. The test was then repeated by fixing the inlet with ripples formed during floodtide flow.

The geometric properties of the inlet with ebbtide-oriented ripples are the same as those with floodtide ripples with $K\sqrt{F}$ having only a 4 percent difference. Since the bed material was plaster and not sand, these tests can only be compared with each other.

The tests indicate that for floodtide ripples, both ebbtide and floodtide flows at maximum discharge have the same friction factor, f; however, for ebbtide ripples, ebbtide flow, f, was higher than for floodtide flow (Fig. 42).

This change in friction suggests that during a tidal cycle, friction will be high for ebbtide flow on ebbtide ripples. When the tide changes and ripples have not had a change to reorient, floodtide flow will experience low friction on these ebbtide ripples. This difference is partly due to the definition of friction and experimental error, and further work is suggested.

7. Tidal Inlet Prism versus Area Relationships.

Tidal prisms, Ω, and cross-sectional areas, A_c, measured experimentally in these tests are plotted in Figure 43 on log-log paper. A best-fit regression analysis shows that the logarithms of prism and

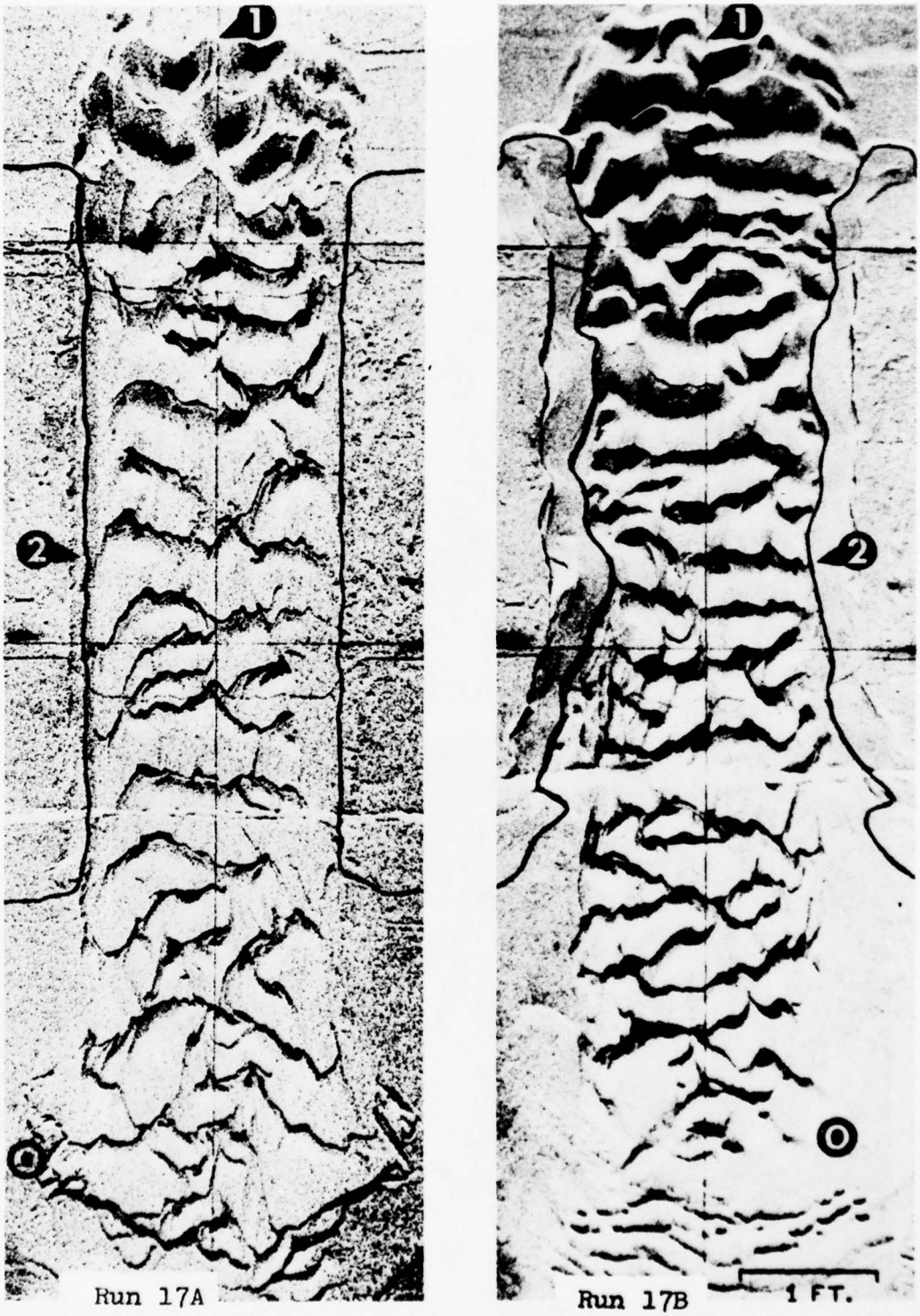

Figure 40. Typical rippled beds after ebbtide flow for high (F) inlets. Numbers are: (θ) oceanside; (1) channel centerline; (2) stillwater level.

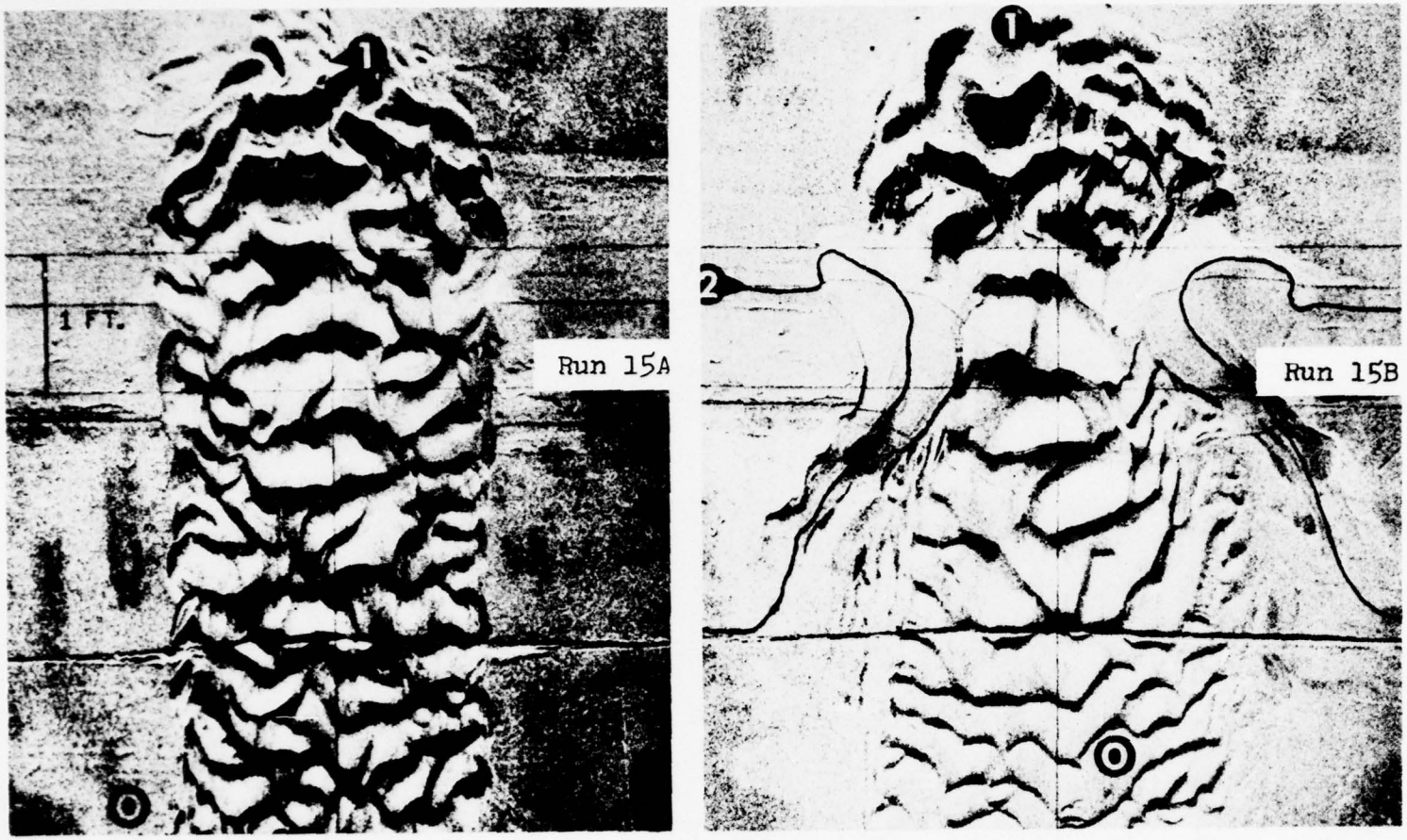

Figure 41. Examples of typical rippled beds after ebbtide flow for low (F) model inlets. Numbers are: (0) oceanside; (1) channel centerline; (2) stillwater level.

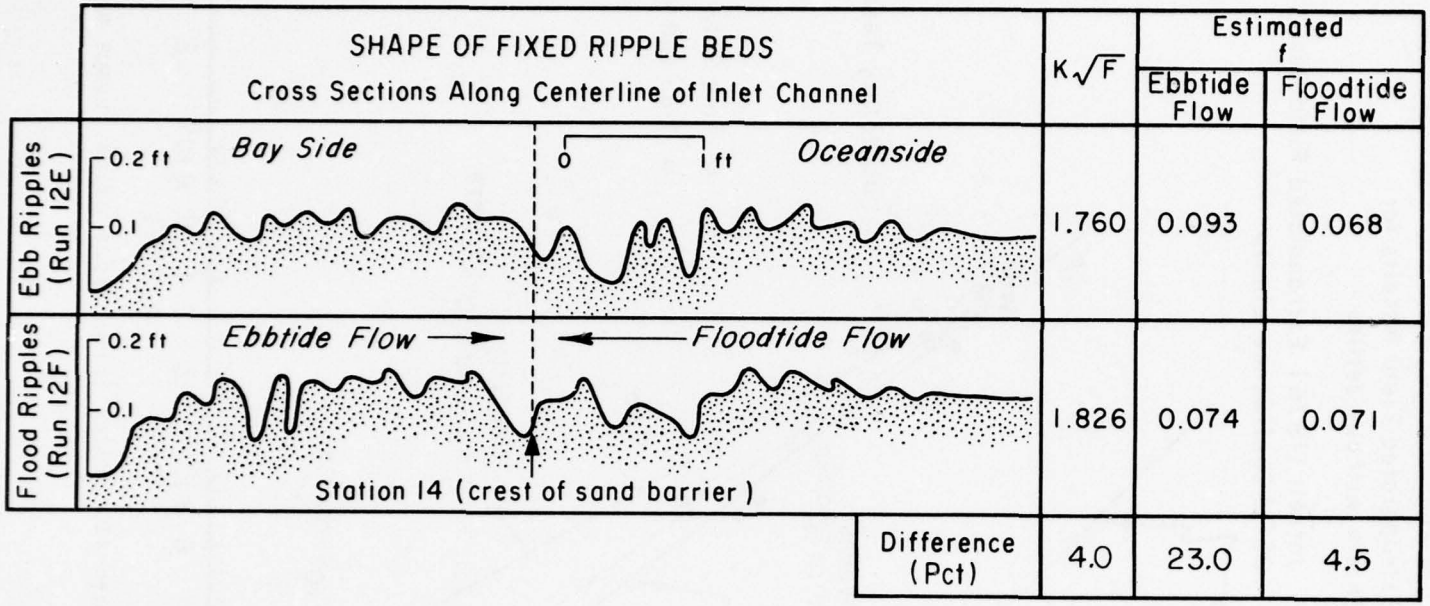

Figure 42. Fixed ripple beds and estimated friction coefficients at maximum discharge.

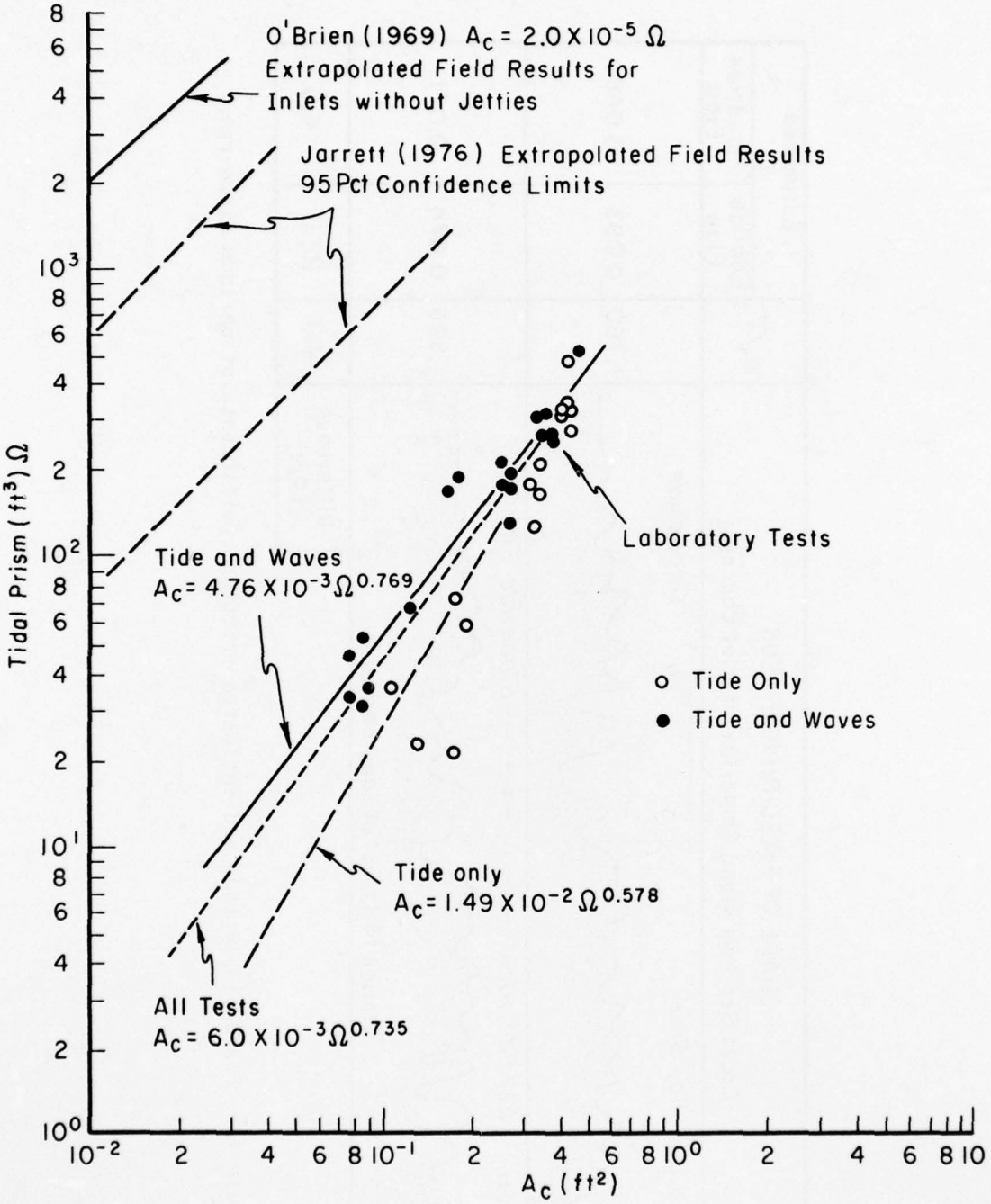

Figure 43. Model inlet tidal prism versus area.

area are linearly related with correlation coefficients greater than 0.90 for tests with tides and tests with both waves and tides (Table 8).

Table 8. Experimental relations between inlet prisms and areas.

Type of tests	Relation
Tide only (15 runs)	$\Omega = 1400\ A_c^{1.73}$ or $A_c = 1.49 \times 10^{-2}\ \Omega^{0.578}$
Tide and waves (20 runs)	$\Omega = 1050\ A_c^{1.30}$ or $A_c = 4.76 \times 10^{-3}\ \Omega^{0.769}$
All tests (35 runs)	$\Omega = 1050\ A_c^{1.36}$ or $A_c = 6.0 \times 10^{-3}\ \Omega^{0.735}$

Model tests show that for a given tidal prism, a model inlet will have a smaller cross-sectional area for a test with waves and tides, than an inlet with tides only. This suggests that waves carry sand to the inlet and reduce the inlet area.

Comparison of these model tests with results from models by McNair (in preparation, 1977) shows that the two sets of tests had similar ranges of experimental conditions and results of tidal area versus prism.

Comparison of model results with field data from the east, west, and gulf coasts (Jarrett, 1976) shows that for a given tidal prism, model tests predict an inlet area an order of magnitude higher than the 95-percent confidence limit of extrapolated field data (Fig. 43). This suggests that either the inlet area versus prism relationship may not be an exponential relation for the entire range of conditions from model to prototype or that scale effects are important. A possible scale effect in the tests is the use of typical size quartz sand which does not model prototype barrier sediment conditions.

VI. SUMMARY AND CONCLUSIONS

A series of 36 tests were conducted in an idealized movable-bed tidal inlet model. Sinusoidal tides and model waves were run continuously at the model inlet until a periodic tide was established in the bay. Parameters measured included ocean and bay hydraulic conditions, inlet velocities, and the inlet geometry.

Results of these tests show that two techniques accurately predicted idealized model inlet hydraulics. The Keulegan (1967) inlet repletion coefficient technique predicted the ratio of the bay to ocean tide amplitudes for a wide range of model conditions when the repletion coefficient was defined for ebbtide flow. The lumped parameter method (Huval and Wintergerst, in preparation, 1977) which extends the Keulegan method by considering inertia and variable inlet geometry, gave a good prediction of maximum inlet velocity, bay superelevation, and the time-lag for high and low waters.

Additional tests on a fixed-bed inlet with ripples showed that both ebbtide and floodtide flows had the same friction factor at maximum discharge for floodtide-oriented ripples, but higher friction over ebbtide ripples for ebbtide flow.

Analysis of model tidal prisms and inlet areas for movable-bed models shows that as the tidal prism increases the inlet area also increases for prototype inlets (O'Brien, 1969; Jarrett, 1976). However, the constants in this equation are not the same for model and prototype inlets. The reason for this difference between model and prototype constants is that forces were scaled, while sediment was not, so that scale effects become important.

Waves superimposed on tides reduced the inlet cross-sectional area for a given model tidal prism with a 40 percent reduction for the smaller areas tested. This suggests that waves cause a net transport of sediment to the inlet zone which reduces the inlet area.

LITERATURE CITED

BROWN, E.I., "Inlets on Sandy Coasts," *Proceedings of the American Society of Civil Engineers*, Vol. 54, No. 2, 1928, pp. 505-553.

CHAPMAN, M.A., "A Note on the Fluctuation of Water-Level in a Tidal-Power Reservoir," *Philosophical Magazine*, Vol. 46, Sixth Series, 1923, pp. 101-108.

CHOW, V.T., *Open Channel Hydraulics*, McGraw-Hill, New York, 1959.

HUVAL, C.J., and WINTERGERST, G.L., "Simplified Numerical (Lumped Parameter) Simulation," Comparison of Numerical and Physical Hydraulic Models, Masonboro Inlet, North Carolina, GITI Report 6, App. 4, U.S. Army, Corps of Engineers, Coastal Engineering Research Center, Fort Belvoir, Va., and U.S. Army Engineer Waterways Experiment Station, Vicksburg, Miss., (in preparation, 1977).

JARRETT, J.T., "Tidal Prism-Inlet Area Relationships," GITI Report 3, U.S. Army, Corps of Engineers, Coastal Engineering Research Center, Fort Belvoir, Va., and U.S. Army Engineer Waterways Experiment Station, Vicksburg, Miss., Feb. 1976.

KEULEGAN, G.H., "Tidal Flow in Entrances - Water Level Fluctuations of Basins in Communication with Seas," Technical Bulletin No. 14, U.S. Army, Corps of Engineers, Committee on Tidal Hydraulics, Vicksburg, Miss., July 1967.

MAYOR-MORA, R.E., "Hydraulics of Tidal Inlets on Sandy Coasts," HEL 24-16, Hydraulic Engineering Laboratory Report, University of California, Berkeley, Calif., Aug. 1973.

McNAIR, E.C. "Reanalysis of Beach Erosion Board Technical Memorandum No. 94," GITI Report, U.S. Army, Corps of Engineers, Coastal Engineering Research Center, Fort Belvoir, Va., and U.S. Army Engineer Waterways Experiment Station, Vicksburg, Miss., (in preparation, 1977).

MOTA OLIVEIRA, I.B., "Natural Flushing Ability in Tidal Inlets," Memorandum No. 395, Laboratorio Nacional de Engenharia Civil, Lisbon, 1971.

O'BRIEN, M.P., "The Lag and Reduction Range in Tide Gage Wells," Technical Memorandum No. 14, U.S. Tidal Laboratory, Berkeley, Calif., 1937.

O'BRIEN, M.P., "Equilibrium Flow Areas of Inlets on Sandy Coasts," *Journal of Waterways and Harbors Division*, ASCE, Vol. 95, No. WW1, Feb. 1969, pp. 43-52.

O'BRIEN, M.P. and DEAN, R.G., "Hydraulics and Sedimentary Stability of Coastal Inlets," *Proceedings of the 13th Coastal Engineering Conference*, Vancouver, Canada, July 1972, pp. 761-780.

AD-A040 021 CALIFORNIA UNIV BERKELEY HYDRAULIC ENGINEERING LAB F/G 8/3
LABORATORY INVESTIGATION OF TIDAL INLETS ON SANDY COASTS.(U)
APR 77 R E MAYOR-MORA DACW72-71-C-0005
UNCLASSIFIED WES-GITI-11 NL

2 OF 2
AD A040021

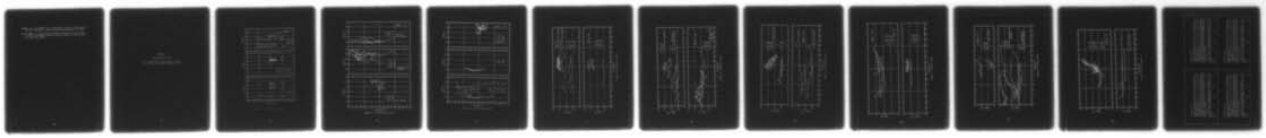

END

DATE FILMED
6-77

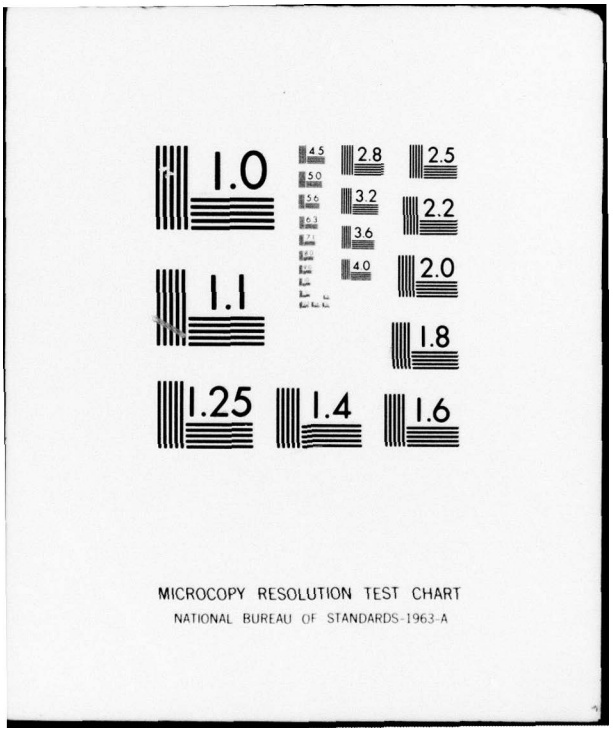
1.0
1.1
1.25
1.4
1.6
1.8
2.0
2.2
2.5
2.8
3.2
3.6
4.0
4.5
5.0
5.6
6.3
7.1
MICROCOPY RESOLUTION TEST CHART
NATIONAL BUREAU OF STANDARDS-1963-A

SHEMDIN, O.H., and FORNEY, R.M., "Tidal Motion in Bays," *Proceedings of the 12th Conference on Coastal Engineering*, Washington, D.C; 1970.

VAN DE KREEKE, J., "Water-Level Fluctuations and Flow in Tidal Inlets," *Journal of Waterways and Harbors Division*, ASCE, Vol. 93, No. WW4, Nov. 1967, pp. 97-106.

APPENDIX

MODEL GEOMETRIC DATA

Plots showing model data at mean sea level as a function of stations along the inlet.

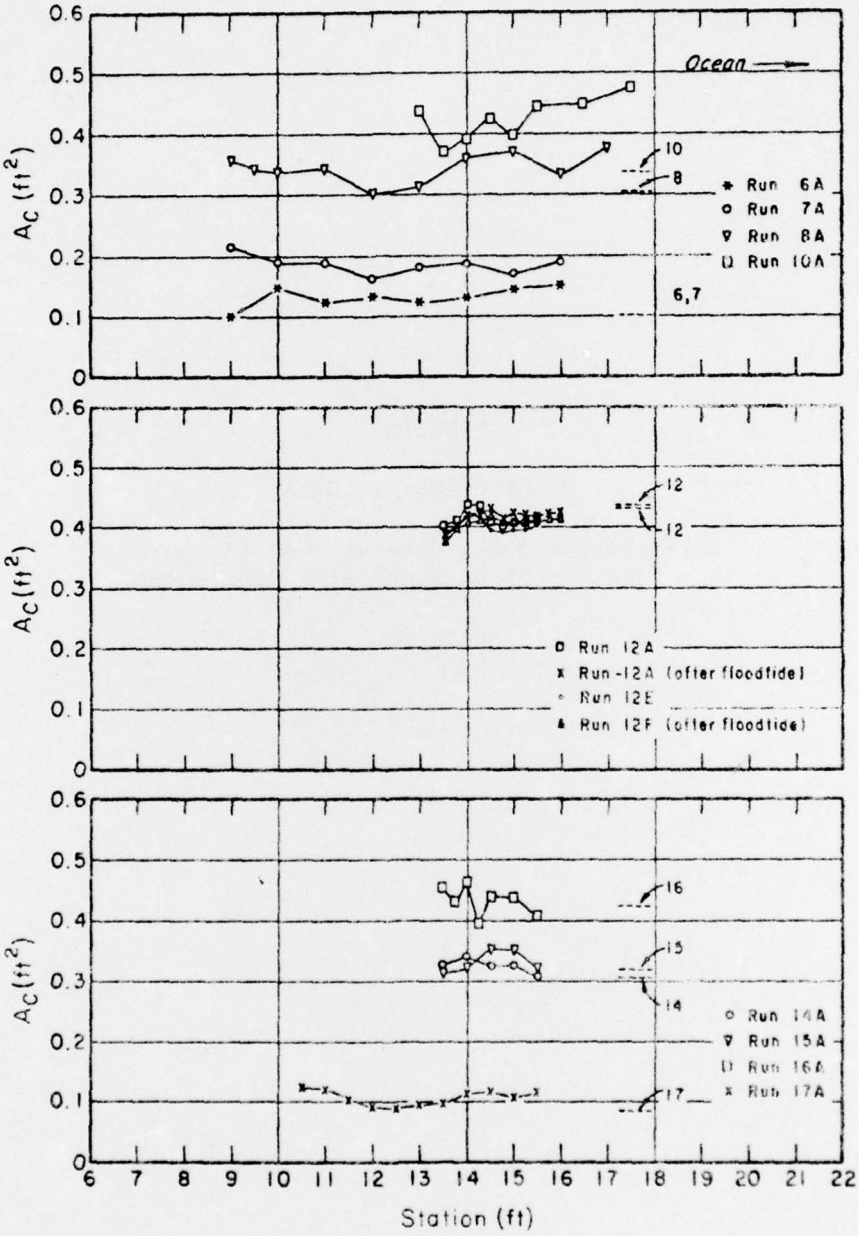

Figure A-1. Cross-sectional area.

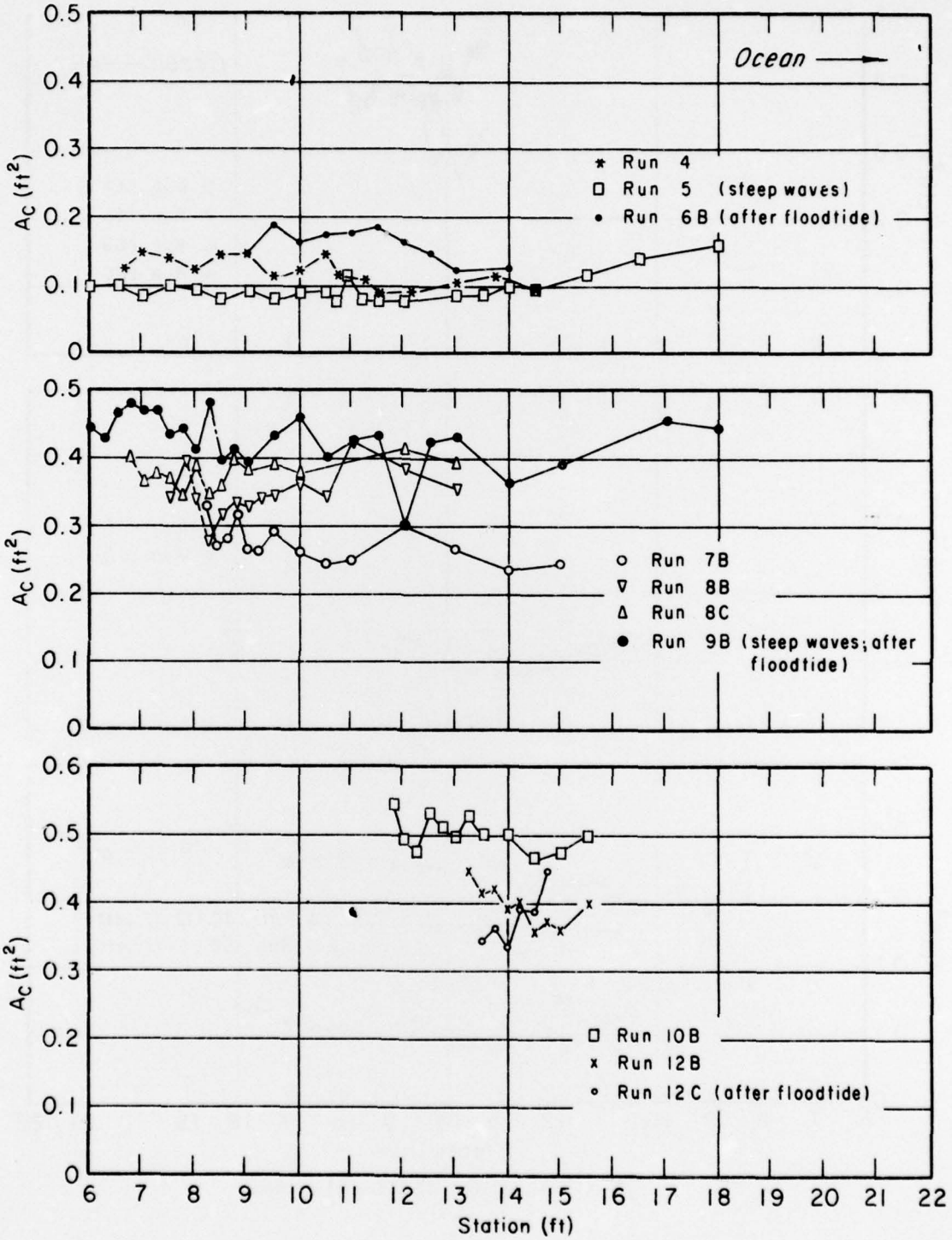

Figure A-2. Cross-sectional area.

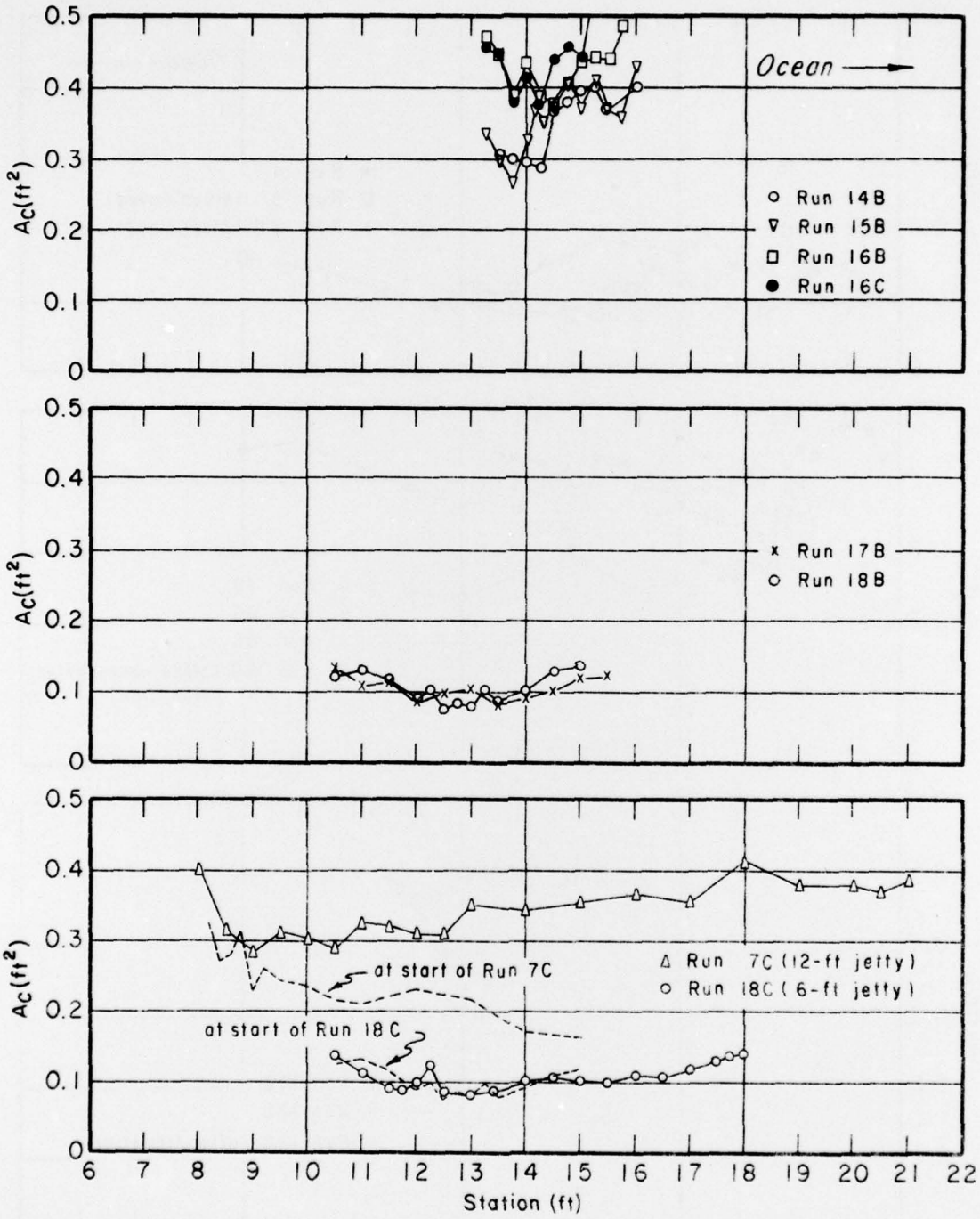

Figure A-3. Cross-sectional area.

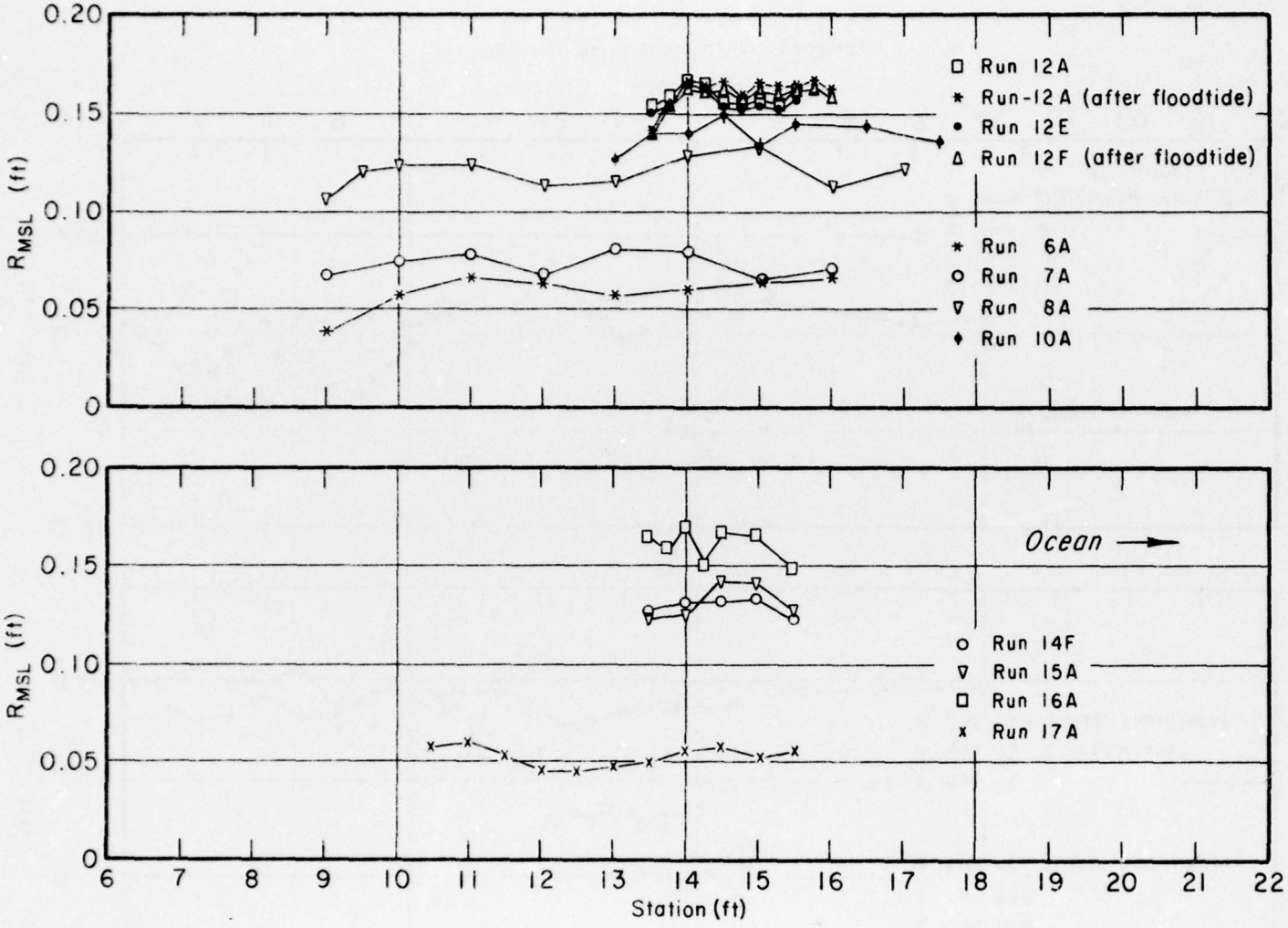

Figure A-4. Hydraulic radius.

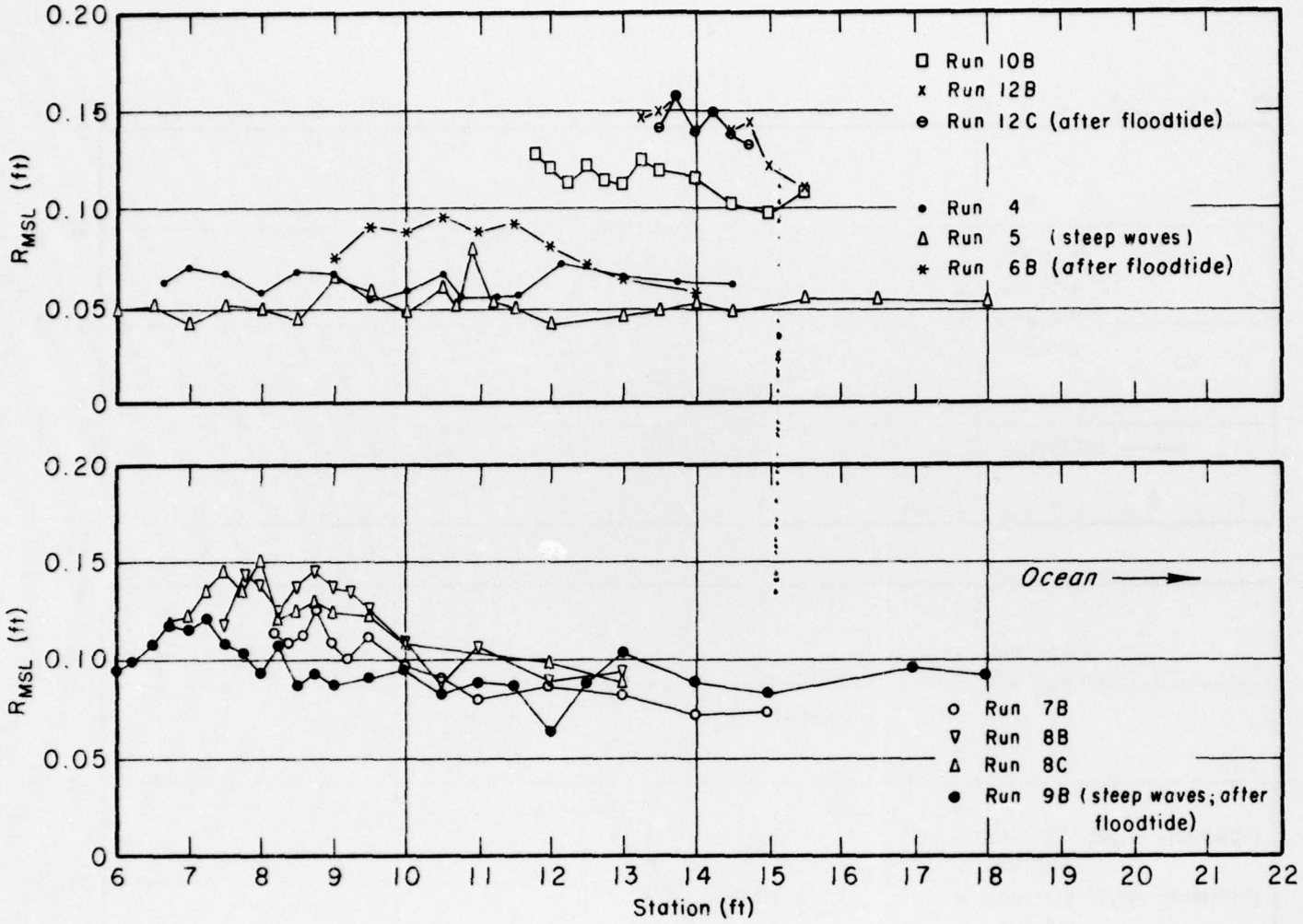

Figure A-5. Hydraulic radius.

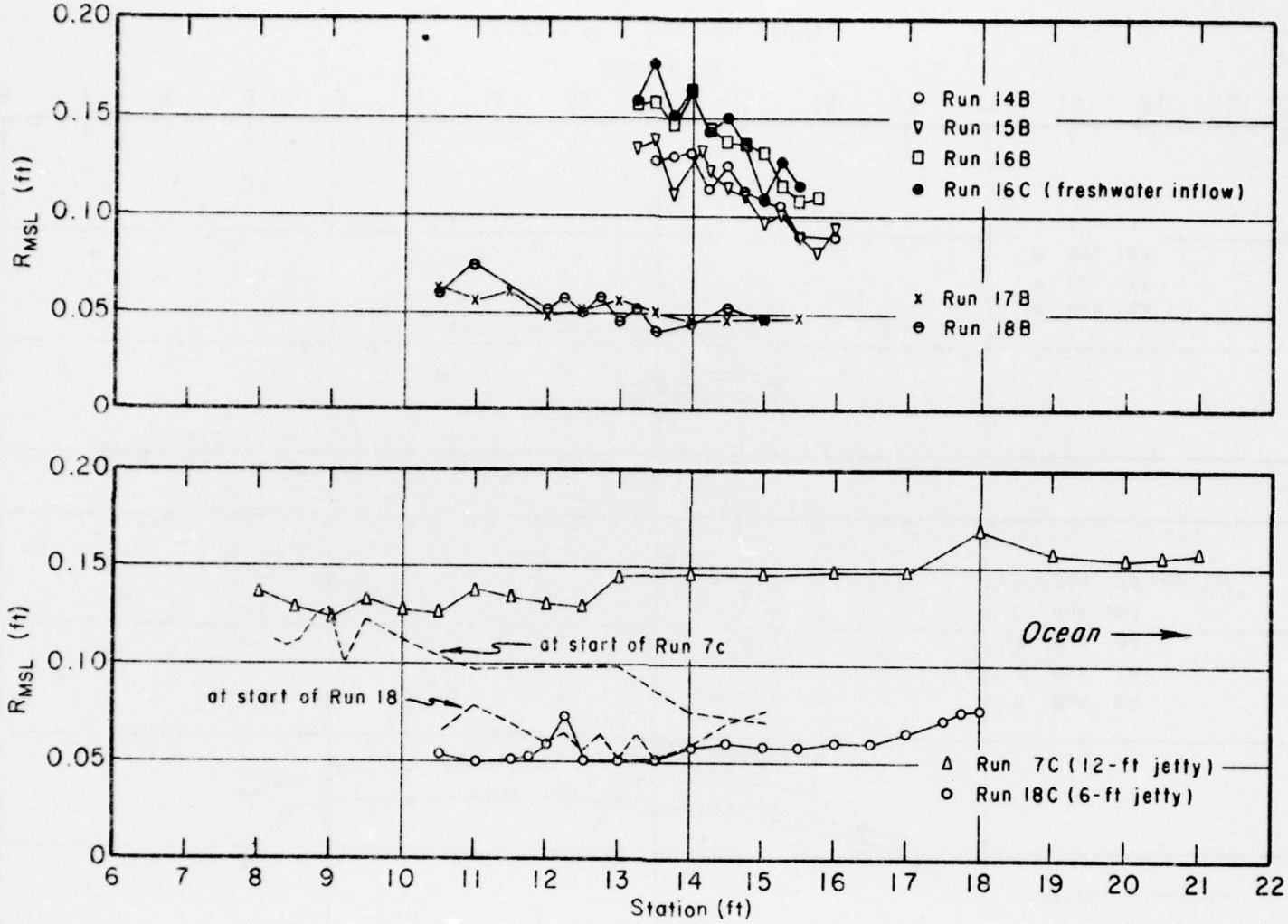

Figure A-6. Hydraulic radius.

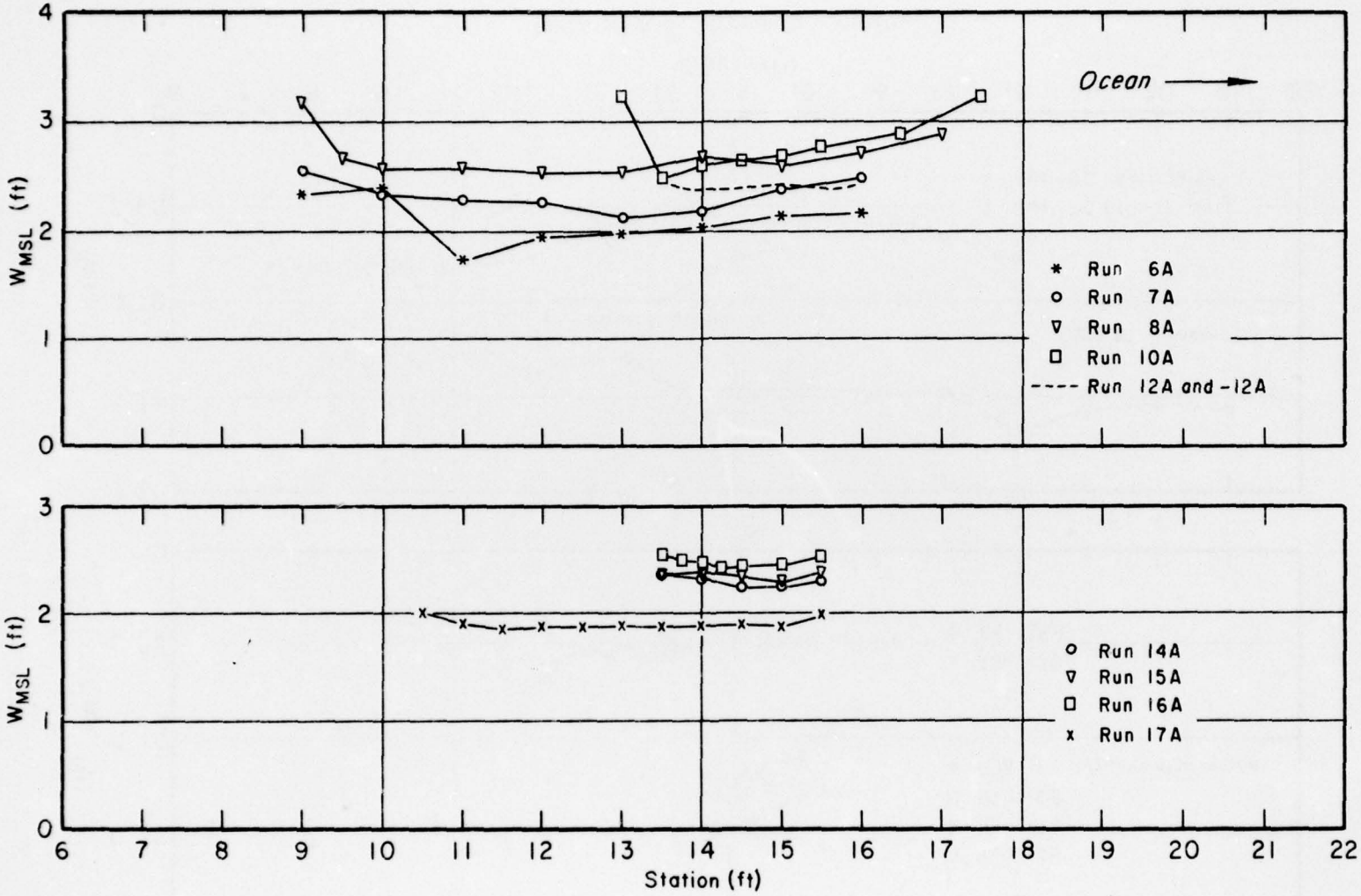

Figure A-7. Section width.

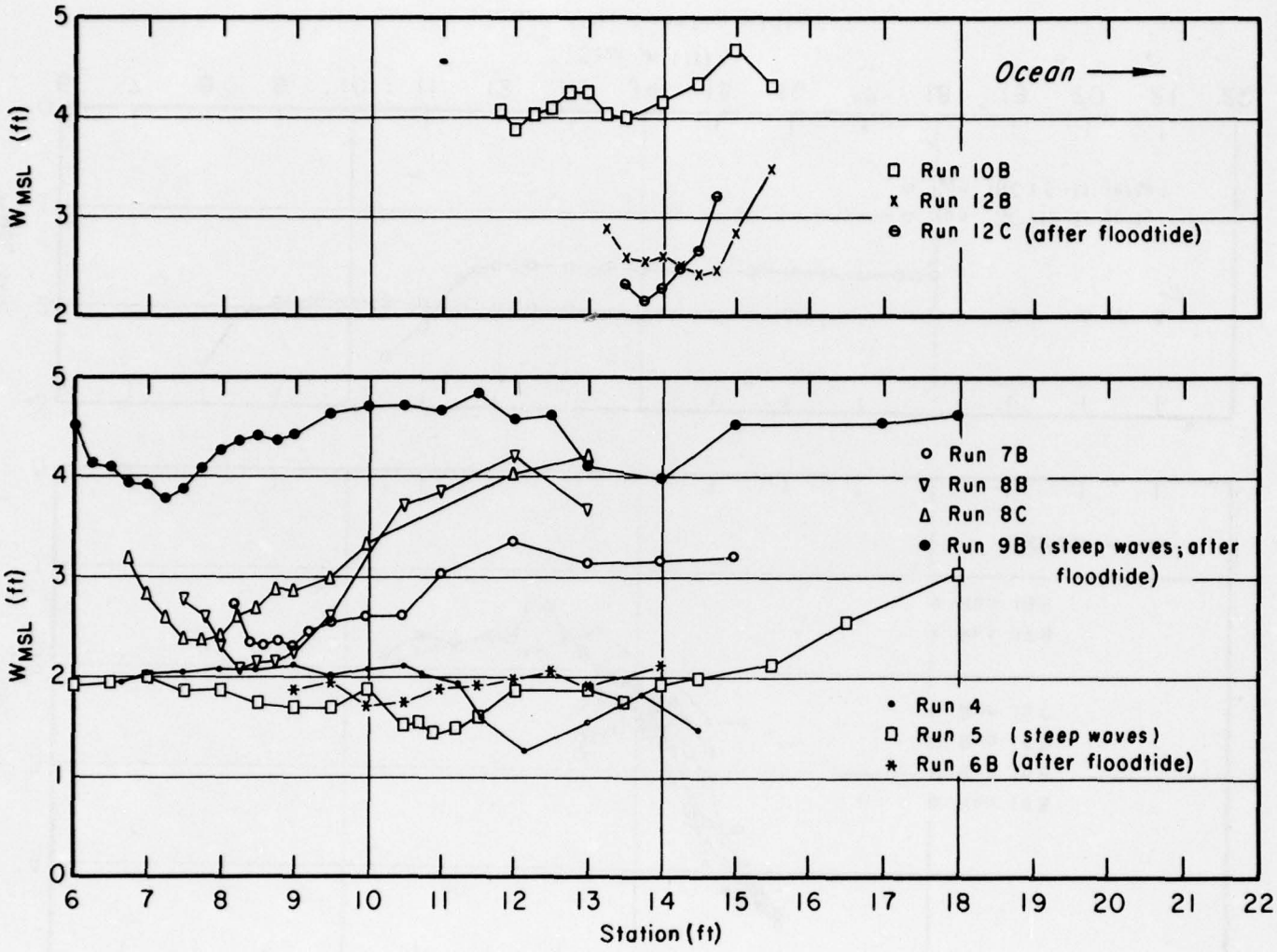

Figure A-8. Section width.

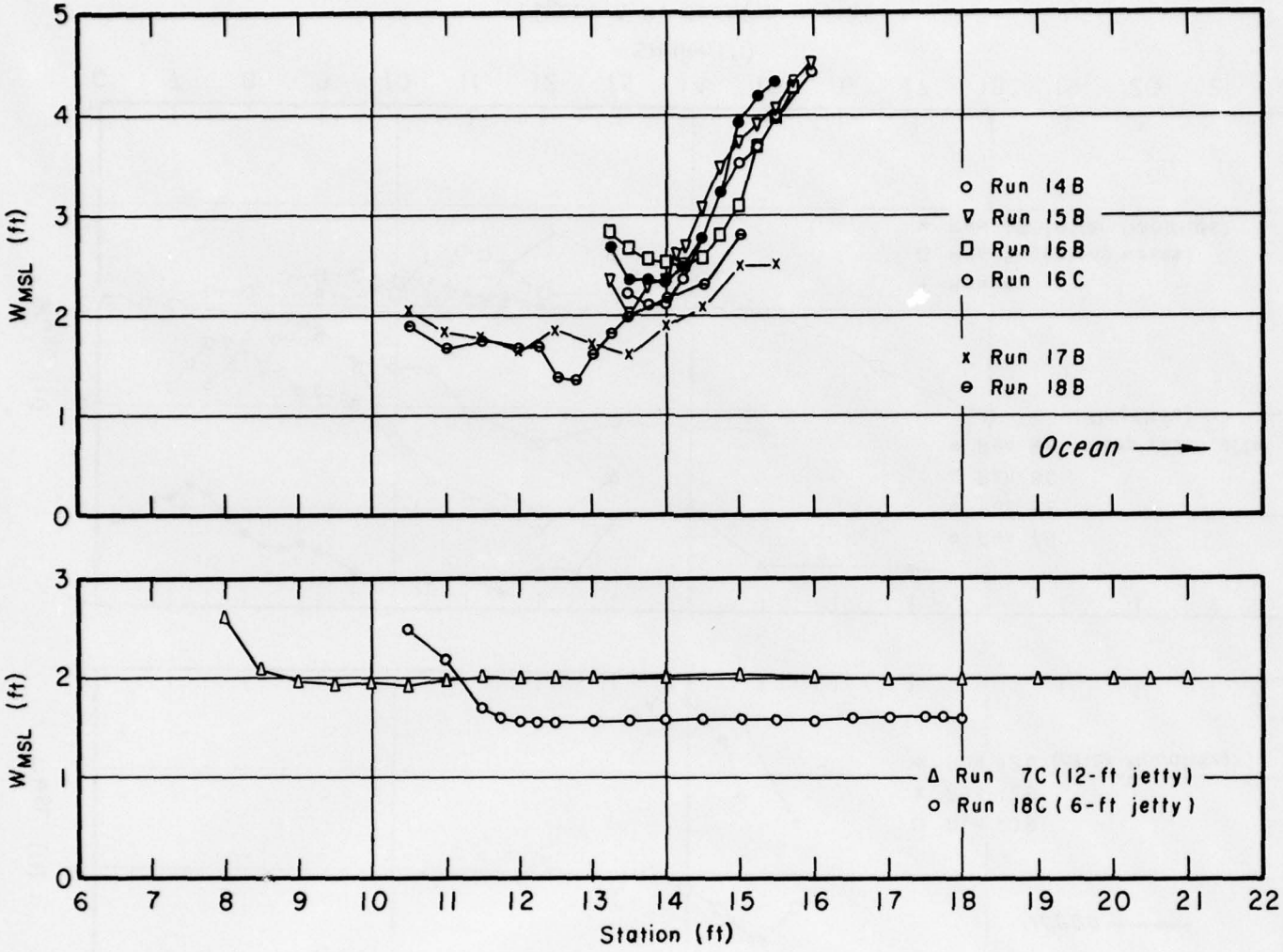

Figure A-9. Section width.

Mayor-Mora, Ramiro E.

Laboratory investigation of tidal inlets on sandy coasts / by Ramiro E. Mayor-Mora. Fort Belvoir, Va. : U.S. Coastal Engineering Research Center, 1977.
106 p. : ill. (GITI report 11) Also (Contract - DACW72-71-C-0005)
Bibliography : p. 95.
A movable-bed inlet model is used to study inlet hydraulics for a variety of inlet configurations and for various conditions. Parameters useful to classify inlet hydraulics are suggested, and inlet stability by re-examining the inlet cross-sectional area versus prism relationship is discussed.

1. Tidal inlets. 2. Hydraulic models. 3. Model basins. I. Title. II. Series: U.S. Army, Corps of Engineers. GITI report 11. III. Series: U.S. Coastal Engineering Research Center. Contract DACW72-71-C-0005.

BG454 .I5 U581r no. 11 551.4

Mayor-Mora, Ramiro E.

Laboratory investigation of tidal inlets on sandy coasts / by Ramiro E. Mayor-Mora. Fort Belvoir, Va. : U.S. Coastal Engineering Research Center, 1977.
106 p. : ill. (GITI report 11) Also (Contract - DACW72-71-C-0005)
Bibliography : p. 95.
A movable-bed inlet model is used to study inlet hydraulics for a variety of inlet configurations and for various conditions. Parameters useful to classify inlet hydraulics are suggested, and inlet stability by re-examining the inlet cross-sectional area versus prism relationship is discussed.

1. Tidal inlets. 2. Hydraulic models. 3. Model basins. I. Title. II. Series: U.S. Army, Corps of Engineers. GITI report 11. III. Series: U.S. Coastal Engineering Research Center. Contract DACW72-71-C-0005.

BG454 .I5 U581r no. 11 551.4

Mayor-Mora, Ramiro E.

Laboratory investigation of tidal inlets on sandy coasts / by Ramiro E. Mayor-Mora. Fort Belvoir, Va. : U.S. Coastal Engineering Research Center, 1977.
106 p. : ill. (GITI report 11) Also (Contract - DACW72-71-C-0005)
Bibliography : p. 95.
A movable-bed inlet model is used to study inlet hydraulics for a variety of inlet configurations and for various conditions. Parameters useful to classify inlet hydraulics are suggested, and inlet stability by re-examining the inlet cross-sectional area versus prism relationship is discussed.

1. Tidal inlets. 2. Hydraulic models. 3. Model basins. I. Title. II. Series: U.S. Army, Corps of Engineers. GITI report 11. III. Series: U.S. Coastal Engineering Research Center. Contract DACW72-71-C-0005.

BG454 .I5 U581r no. 11 551.4

Mayor-Mora, Ramiro E.

Laboratory investigation of tidal inlets on sandy coasts / by Ramiro E. Mayor-Mora. Fort Belvoir, Va. : U.S. Coastal Engineering Research Center, 1977.
106 p. : ill. (GITI report 11) Also (Contract - DACW72-71-C-0005)
Bibliography : p. 95.
A movable-bed inlet model is used to study inlet hydraulics for a variety of inlet configurations and for various conditions. Parameters useful to classify inlet hydraulics are suggested, and inlet stability by re-examining the inlet cross-sectional area versus prism relationship is discussed.

1. Tidal inlets. 2. Hydraulic models. 3. Model basins. I. Title. II. Series: U.S. Army, Corps of Engineers. GITI report 11. III. Series: U.S. Coastal Engineering Research Center. Contract DACW72-71-C-0005.

BG454 .I5 U581r no. 11 551.4

Mayor-Mora, Ramiro E.

Laboratory investigation of tidal inlets on sandy coasts / by Ramiro E. Mayor-Mora. Fort Belvoir, Va. : U.S. Coastal Engineering Research Center, 1977.

106 p. : ill. (GITI report 11) Also (Contract - DACW72-71-C-0005)

Bibliography : p. 95.

A movable-bed inlet model is used to study inlet hydraulics for a variety of inlet configurations and for various conditions. Parameters useful to classify inlet hydraulics are suggested, and inlet stability by re-examining the inlet cross-sectional area versus prism relationship is discussed.

1. Tidal inlets. 2. Hydraulic models. 3. Model basins. I. Title. II. Series: U.S. Army, Corps of Engineers. GITI report 11. III. Series: U.S. Coastal Engineering Research Center. Contract DACW72-71-C-0005.

BG454 .I5 U581r no. 11 551.4

Mayor-Mora, Ramiro E.

Laboratory investigation of tidal inlets on sandy coasts / by Ramiro E. Mayor-Mora. Fort Belvoir, Va. : U.S. Coastal Engineering Research Center, 1977.

106 p. : ill. (GITI report 11) Also (Contract - DACW72-71-C-0005)

Bibliography : p. 95.

A movable-bed inlet model is used to study inlet hydraulics for a variety of inlet configurations and for various conditions. Parameters useful to classify inlet hydraulics are suggested, and inlet stability by re-examining the inlet cross-sectional area versus prism relationship is discussed.

1. Tidal inlets. 2. Hydraulic models. 3. Model basins. I. Title. II. Series: U.S. Army, Corps of Engineers. GITI report 11. III. Series: U.S. Coastal Engineering Research Center. Contract DACW72-71-C-0005.

BG454 .I5 U581r no. 11 551.4

Mayor-Mora, Ramiro E.

Laboratory investigation of tidal inlets on sandy coasts / by Ramiro E. Mayor-Mora. Fort Belvoir, Va. : U.S. Coastal Engineering Research Center, 1977.

106 p. : ill. (GITI report 11) Also (Contract - DACW72-71-C-0005)

Bibliography : p. 95.

A movable-bed inlet model is used to study inlet hydraulics for a variety of inlet configurations and for various conditions. Parameters useful to classify inlet hydraulics are suggested, and inlet stability by re-examining the inlet cross-sectional area versus prism relationship is discussed.

1. Tidal inlets. 2. Hydraulic models. 3. Model basins. I. Title. II. Series: U.S. Army, Corps of Engineers. GITI report 11. III. Series: U.S. Coastal Engineering Research Center. Contract DACW72-71-C-0005.

BG454 .I5 U581r no. 11 551.4

Mayor-Mora, Ramiro E.

Laboratory investigation of tidal inlets on sandy coasts / by Ramiro E. Mayor-Mora. Fort Belvoir, Va. : U.S. Coastal Engineering Research Center, 1977.

106 p. : ill. (GITI report 11) Also (Contract - DACW72-71-C-0005)

Bibliography : p. 95.

A movable-bed inlet model is used to study inlet hydraulics for a variety of inlet configurations and for various conditions. Parameters useful to classify inlet hydraulics are suggested, and inlet stability by re-examining the inlet cross-sectional area versus prism relationship is discussed.

1. Tidal inlets. 2. Hydraulic models. 3. Model basins. I. Title. II. Series: U.S. Army, Corps of Engineers. GITI report 11. III. Series: U.S. Coastal Engineering Research Center. Contract DACW72-71-C-0005.

BG454 .I5 U581r no. 11 551.4